# Mathematical modeling of ephemeral gully erosion

by

Vladimir Rustemovich Karimov

B.S./M.S., Bauman Moscow State Technical University, 2010

AN ABSTRACT OF A DISSERTATION

submitted in partial fulfillment of the requirements for the degree

DOCTOR OF PHILOSOPHY

Department of Biological and Agricultural Engineering
College of Engineering

KANSAS STATE UNIVERSITY
Manhattan, Kansas

2017

# Abstract

As the world faces an increasing demand for food due to the growing global population and the pernicious effects of land degradation, there is a need to overcome this challenge by using sustainable management practices for agricultural productions. One of the problems, which sustainable agriculture seeks to address, is the loss of topsoil due to soil erosion. Changing weather patterns also contribute to the average annual rainfall across the globe with an excess precipitation, which creates runoff and causes soil erosion. One of the significant yet less studied types of soil erosion is ephemeral gully erosion. Formed by the concentrated overland flow during intensive rainfall events, ephemeral gullies are channels on agricultural fields that can be removed by tillage operations but appear at the same location every year. Even though simplified ephemeral gully models estimate soil losses, they do not account for complicated hydrological and soil erosion processes of channel formations. The purpose of this research work is to investigate sediment sources and develop tools that can predict ephemeral gully erosion more efficiently. To achieve this goal, an experimental study was conducted on an agricultural field in central Kansas by tracking channel development, monitoring soil moisture content, and recording the amount of rainfall. Runoff and sediment loads from contributing catchment and critical and actual shear stresses were estimated by the computer model, and conclusions were made on the effect of saturation dynamics on the erosion processes. Furthermore, a two-dimensional subsurface water flow and soil erosion model was developed with the variable soil erodibility parameters which account for the subsurface fluxes and the effects on the soil detachment process. The model was applied to study the impacts of variable soil erodibility parameters on the erosion process for different soils and various antecedent soil moisture conditions. Also developed to estimate the soil losses at the field scale was an integrated

spatially-distributed ephemeral gully model with dynamic time-dependent channel development. The model showed good fit by matching the experimental data. The results from this work can be used to advance the research of soil erosion prediction from concentrated flow channels and ephemeral gullies formed on agricultural fields.

# Mathematical modeling of ephemeral gully erosion

by

Vladimir Rustemovich Karimov

B.S./M.S., Bauman Moscow State Technical University, 2010

A DISSERTATION

submitted in partial fulfillment of the requirements for the degree

DOCTOR OF PHILOSOPHY

Department of Biological and Agricultural Engineering
College of Engineering

KANSAS STATE UNIVERSITY
Manhattan, Kansas

2017

Approved by:

Major Professor
Dr. Aleksey Y. Sheshukov

# Copyright

# Abstract

As the world faces an increasing demand for food due to the growing global population and the pernicious effects of land degradation, there is a need to overcome this challenge by using sustainable management practices for agricultural productions. One of the problems, which sustainable agriculture seeks to address, is the loss of topsoil due to soil erosion. Changing weather patterns also contribute to the average annual rainfall across the globe with an excess precipitation, which creates runoff and causes soil erosion. One of the significant yet less studied types of soil erosion is ephemeral gully erosion. Formed by the concentrated overland flow during intensive rainfall events, ephemeral gullies are channels on agricultural fields that can be removed by tillage operations but appear at the same location every year. Even though simplified ephemeral gully models estimate soil losses, they do not account for complicated hydrological and soil erosion processes of channel formations. The purpose of this research work is to investigate sediment sources and develop tools that can predict ephemeral gully erosion more efficiently. To achieve this goal, an experimental study was conducted on an agricultural field in central Kansas by tracking channel development, monitoring soil moisture content, and recording the amount of rainfall. Runoff and sediment loads from contributing catchment and critical and actual shear stresses were estimated by the computer model, and conclusions were made on the effect of saturation dynamics on the erosion processes. Furthermore, a two-dimensional subsurface water flow and soil erosion model was developed with the variable soil erodibility parameters which account for the subsurface fluxes and the effects on the soil detachment process. The model was applied to study the impacts of variable soil erodibility parameters on the erosion process for different soils and various antecedent soil moisture conditions. Also developed to estimate the soil losses at the field scale was an integrated

spatially-distributed ephemeral gully model with dynamic time-dependent channel development. The model showed good fit by matching the experimental data. The results from this work can be used to advance the research of soil erosion prediction from concentrated flow channels and ephemeral gullies formed on agricultural fields.

# Table of Contents

List of Figures ..... xi
List of Tables ..... xiv
Acknowledgements ..... xv
Chapter 1 - Introduction ..... 1
Soil Erosion ..... 1
Ephemeral Gully Erosion ..... 3
Goals and Objectives ..... 4
Chapter 2 - Literature Review ..... 7
Introduction ..... 7
Qualitative Description of the Ephemeral Gully Erosion Process and Reviews ..... 7
Modeling ..... 9
Topography-Based Assessment ..... 9
Physically Based Models ..... 14
Application of Models ..... 19
Field and Experimental Laboratory Studies ..... 22
Summary ..... 25
Chapter 3 - Effects of Intra-Storm Soil Moisture and Runoff Characteristics on Ephemeral Gully Development: Evidence from a No-Till Field Study ..... 26
Introduction ..... 26
Materials and Methods Study Area ..... 30
Field Equipment ..... 32
Measuring Channel Cross Sections ..... 34
Estimating Ephemeral Gully Erosion ..... 36
Estimating Sheet and Rill Erosion ..... 37
Results ..... 39
Soil Erosion and Accumulation between Soil Surveys ..... 39
Seasonal Changes in the Headcut Area ..... 41
Elevation Changes along Ephemeral Gully ..... 43
Daily Climate Dataseries ..... 45

Significant Runoff Events ..... 48
Discussion ..... 50
Characteristics of the Critical Shear Stress ..... 50
Applicability of the Critical Shear Stress Function to Field Experiment ..... 53
Factors Affecting Ephemeral Gully Erosion ..... 55
Conclusions ..... 56
Chapter 4 - Evaluating the Effects of Subsurface Seepage and Drainage on Channel Development with Two-Dimensional Numerical Modeling ..... 58
Introduction ..... 58
Physical Model ..... 61
Mathematical Model ..... 65
Numerical Scheme ..... 69
Channel Erosion ..... 71
Model Testing ..... 72
Mass Conservation Test ..... 73
Evaluating the Model with the Experiment Conducted by Huang et. al. ..... 73
Evaluating the Model with the Experiment Performed by Wells et al. ..... 78
Discussion ..... 81
Effect from the Change of Model Parameters ..... 81
Shear Stress and Soil Erodibility ..... 84
Summary ..... 87
Chapter 5 - Impacts of Subsurface Fluxes on Concentrated Flow Erosion with a Two-Dimensional Numerical Model ..... 90
Introduction ..... 90
Methods ..... 91
Erosion Equation ..... 91
Mathematical Model ..... 92
Baseline Scenario ..... 94
Results for the Baseline Scenario ..... 97
Results ..... 101
Study 1: Impact of Soil Type ..... 102

Study 2: Impact of Initial Saturation ..... 104
Study 3: Impact of Groundwater Depth ..... 106
Study 4: Impact of Soil Layers ..... 108
Discussion ..... 110
Influence of Subsurface Fluxes ..... 110
Soil Erosion and Management ..... 111
Possible Channel Shapes ..... 112
Summary ..... 114
Chapter 6 - Integrated Process-Based Modeling of Channelized Flow and Soil Erosion in Small Watersheds ..... 116
Introduction ..... 116
Mathematical Model ..... 119
Ephemeral Gully Representation ..... 120
Catchment Hydrograph ..... 121
Hydrograph and Routing ..... 121
Erosion ..... 124
Deposition ..... 129
Adjustment of the Soil Erodibility Parameters ..... 130
Model Validation ..... 132
Results ..... 133
Scenarios ..... 133
Detailed Example of the Selected Scenario ..... 134
Results for All Scenarios ..... 137
Discussion ..... 139
Conclusions ..... 141
Chapter 7 - Summary ..... 143
References ..... 149

# List of Figures

Figure 3.1 Maps of (a) the studied field and (b) ephemeral gully in Central Kansas, USA. ..... 31
Figure 3.2 Field equipment installed along the gully. ..... 33
Figure 3.3 (a) Pin-frame, (b) earth pins, and (c) base foundation platforms for measuring gully cross-sectional profile. ..... 35
Figure 3.4 Surface plots of elevation grid within the headcut area obtained by pin-frame measurements at the beginning and end of field campaigns in 2013 (a,b) and 2014 (c,d). Direction of surface runoff is from left to right. ..... 42
Figure 3.5 Gully elevation profiles at 10 cm cross-section in the headcut area ..... 44
Figure 3.6 Average daily soil moisture saturation ($m^3/m^3$), temperature (0C), and total precipitation (mm) in 2013 and 2014 campaigns. Twelve significant wet days are identified by purple bars. Survey periods of substantial gully erosion are shown above the chart. ..... 46
Figure 3.7 Hourly soil moisture saturation (%), precipitation and surface runoff (mm) for significant runoff event $E_{10}$ on 9-10 June 2014. Major event characteristics ($t_a$, $t_p$, $t_d$, $\theta_a$, $\theta_p$, $q_p$) are also shown. ..... 49
Figure 3.8 Acting shear stress in the headcut area versus the ratio of the differences in soil moisture saturation and time prior to a rainfall event (antecedent condition) and at the peak runoff rate for runoff events. $\tau c0 = 3.5$, $b = 1$, and $\beta = 0.4$. ..... 53
Figure 4.1 Critical shear stress as a function of seepage/drainage gradient: (a) representative linear form according to Equation 4.5, and (b) non-linear form shown in Equation 4.8 where $\tau cr$ 0= 0.455 and k=0.362. The experiment data from (S. Nouwakpo et al., 2010) are also shown in (b). ..... 64
Figure 4.2 Simulation domain and corresponding boundary conditions at each segment of the domain boundaries. ..... 67
Figure 4.3 Distribution of the acting shear stress at the channel bottom. ..... 68
Figure 4.4 Discretization of the domain. ..... 69
Figure 4.5 Simulation results of the experiment conducted by Huang et al. where $\varepsilon = 1.2$ and k = 0.07 ..... 76
Figure 4.6 Modeled vs. Experiment delivery rates for the experiment by Huang et al. ..... 77

Figure 4.7 Simulation results of the experiment performed by Wells et al. where ε = 1.2 and k = 0.07..... 80
Figure 4.8 Experiment vs. modeled final widths for the experiment performed by Wells et al... 80
Figure 4.9 Critical shear stress functions for various function parameters..... 82
Figure 4.10 Simulation results of the experiment conducted by Huang et al. with the gradient dependent soil erodibility..... 86
Figure 4.11 Experiment versus modeled delivery rates for the experiment conducted by Huang et al. with the gradient dependent soil erodibility..... 86
Figure 5.1 Synthetic rainfall and runoff for the numerical experiment. ..... 95
Figure 5.2 Critical shear stress and soil erodibility as functions of the hydraulic gradient. ..... 95
Figure 5.3 Soil pore pressure redistribution in time. ..... 97
Figure 5.4 Channel propagation in time: cross sections for the VEP model (a), cross sections for the CEP model (b), depth of the lowest point for VEP model (c), depth of the lowest point for the CEP model (d), width of the channel for the VEP model (e), width of the channel for the CEP model (f). ..... 99
Figure 5.5 Critical and acting shear stresses and the difference in the eroded volume in time for the VEP (a) and CEP (b) models. ..... 100
Figure 5.6 Soil erodibility and difference in the eroded volume in time for the VEP (a) and CEP (b) models. ..... 101
Figure 5.7 Six selected soils for numerical experiment. ..... 102
Figure 5.8 Cumulative erosion for six selected soils in time. ..... 104
Figure 5.9 Eroded area for three soils and variable initial saturation. ..... 105
Figure 5.10 Eroded area for three soils and variable groundwater depth. ..... 107
Figure 5.11 The eroded area for three soils and various layering conditions: Base is the baseline scenario, Ksat10 and Ksat100 is the scenarios with the 10 and 100 times lower saturated hydraulic conductivity consequentially, D15 is the scenario with the depth of top soil of 15 cm, and D15+Ksat10 and D15+Ksat100 are the combinations of the scenarios. ..... 109
Figure 5.12 W-shape channel cross sections in time. ..... 113
Figure 6.1 Flowchart of the proposed model. ..... 120
Figure 6.2 Geometrical representation of the ephemeral gully..... 121
Figure 6.3. Hydrograph discretization in time. ..... 122

Figure 6.4. Scheme of the sidewalls failure for higher equilibrium widths: red – failed material, green – deposited material. ..... 125
Figure 6.5 Modified scheme of widening and deepening of the channel. ..... 126
Figure 6.6 Temporary two-tier channel shape. ..... 126
Figure 6.7 Computed versus measured volumes of eroded soil. ..... 133
Figure 6.8 Channel flow in space and time. ..... 135
Figure 6.9 Channel depth in space and time. ..... 135
Figure 6.10 Channel width in space and time. ..... 136
Figure 6.11. Total soil loss for three practices and two antecedent conditions. ..... 137
Figure 6.12. Ephemeral gully erosion for three practices and two antecedent conditions. ..... 138
Figure 6.13. Performance of two practices with two antecedent conditions on the reduction of the total soil loss. ..... 139
Figure 6.14. Performance of two practices with two antecedent conditions on a reduction of ephemeral gully erosion. ..... 140

# List of Tables

Table 3.1 Summary for 14 survey periods. Rainfall (days, events, depth) and gully elevation changes were measured, and surface runoff and sheet and rill erosion were simulated. For erosion data, soil loss is positive, and sediment accumulation is negative. ..... 39
Table 3.2 Characteristics of twelve significant runoff events with potential to cause soil erosion within the ephemeral gully. ..... 48
Table 4.1 Mass conservation error in time. ..... 73
Table 4.2 Parameters of the experiment conducted by Huang et al. ..... 74
Table 4.3 Soil properties for the experiment conducted by Huang et al. ..... 75
Table 4.4 Parameters of the experiment performed by Wells et al. ..... 78
Table 4.5 Soil properties for the experiment performed by Wells et al. ..... 79
Table 5.1 Soil properties for numerical experiments. ..... 96
Table 6.1 Comparison of the physically based ephemeral gully erosion models ..... 118
Table 6.2. Input parameters to the WEPP model for three management practices. ..... 134

# Acknowledgements

I would like to express my sincere gratitude to my major advisor Dr. Aleksey Sheshukov for his guidance, support, and encouragement during my program. I would like to thank Dr. Gerard Kluitenberg for the knowledge and experience that I gained from his classes, and for advice and comments during the development of my model. Also, I would like to express my gratitude to Dr. Stacy Hutchinson for her advice in academic and professional development, and professional incentive, to Dr. Trisha Moore for her support, guidance, and comments about my work. I would like to thank my outside chair Prof. Lee Skabelund for his time and valuable knowledge and perspective of the environmental science.

I would like to thank following people who helped me in many ways during my program of study: Jonathan Zeller, Dr. Philip Barnes, Barb Moore, Lawrence Sekaluvu, Chinthaka Bandara, Gia Nguyen, Kari Bigham, Dr. Vahid Rahmani, Yang (Jeanne) Liu, and Kelsey McDonough.

I acknowledge the partial financial support by the USDA National Institute of Food and Agriculture (NIFA) under Agreement No. 2011-51130-31128 and Kansas NRCS-CIG grant No. 69-6215-13-0003.

Also, I would like to thank my family for their support and patience.

# Chapter 1 - Introduction

## Soil Erosion

Due to the growing population of the world, it is expected that there would be an increase in the global food demand. This surge in food demand would also be more intensified due to the constantly increasing standards of living which encourage people to seek quality food. For example, organic foods, which do not require the use of pesticides and sometimes requires tillage operations, is much more expensive than processed foods. Therefore, it is of paramount importance that food producers consider using new and innovative techniques to meet the demands of consumers. Additionally, these practices need to be sustainable in the long run to provide food security for future generations. One of the most significant problems that sustainable agricultural production is currently facing is soil erosion. Soil erosion is the gradual removal of the soil layer due to the runoff or wind. The topsoil is more susceptible to the erosion process; at the same time, it is the most valuable part of the soil that supports the biological activity needed for plants' growth. Another crucial requirement for a successful agricultural production is water. In geographical locations where there is sufficient water to grow crops, precipitation patterns can cause water runoff and soil erosion.

Soil erosion by water is caused by precipitation which exceeds the interception and infiltration capacity of the soil which is later transformed into surface runoff. Sometimes, surface runoff erosion occurs due to the snowmelt. In this case, melted water exceeds the infiltration capacity of the soil and runs off the field. Water runoff from arable land can cause land degradation as well as resulting in the sedimentation of the downstream ponds and reservoirs. What's more, nutrients washed off with soil can cause severe algae blooms in the reservoirs.

There are several types of soil erosion by water: sheet erosion, rill erosion, ephemeral gully erosion, classical gully erosion, and streambank erosion. The first type is sheet erosion. A physical process of sheet erosion occurs in the particle dislodgement due to the impacts of raindrops. Then, the dislodged particles are easily washed off by the sheet flow. The second type, rill erosion, occurs due to the concentration of the flow into small channels. In this case, the concentrated flow forces detached particles from the walls and at the bottom of the rill. Afterward, detached particles are washed downstream. Such rills can be identified easily in the field. However, they do not appear at the same location every year, and they can be removed easily with tillage operations. The third type is the ephemeral gully erosion. Similar to the rill erosion, ephemeral gullies are caused by concentrated flows, and they can be removed by tillage operations. However, unlike rills, they appear at the same location each year. Very often, ephemeral gullies reach the non-erodible layer of the soil caused either by the clay pans or by the compaction due to the excessive wheel traffic. The fourth type of erosion is the classical gully erosion; in this type of erosion, gullies cannot be removed by tillage operation. Classical gullies are referred to as the stage of channel development where land is taken out of the production. The last but not the least important type of erosion is the stream bank erosion, which is caused by a concentrated water flow whose source is from the undercutting of the streambank. The process then continues with the failure of the massive blocks of soil.

All the types of erosion described above can be reduced if sustainable agricultural practices are implemented. Many best management practices (BMPs) may work for all types of erosion because they increase infiltration capacity of the soil and decrease surface runoff. BMPs can also improve soil stability and soil health and reduce nutrient loss.

## Ephemeral Gully Erosion

On average, ephemeral gullies contribute to 30-40% of total soil loss, and it is reported in China and Europe that this erosion is responsible for up to 90% of total soil loss (Karimov, Sheshukov, & Barnes, 2014; J. Poesen, Nachtergaele, Verstraeten, & Valentin, 2003). As a result, there should be an urgent need to specifically address the issue of ephemeral gully erosion separately from evaluating total soil loss. It is recommended that ephemeral gully specific BMPs such as grassed waterway and double cropping be implemented in order to stop or at least reduce the erosion process.

To prevent soil loss and ephemeral gully erosion particularly, BMPs have to be modeled before the implementation so that their efficiency is optimized for a certain location, soil type, crop, and management practice. Ephemeral gully erosion is included in several erosion prediction models (S. M. Dabney et al., 2014; D. C. Flanagan, Gilley, & Franti, 2007; Fogle & Barfield, 1992; Foster & Lane, 1983; Merkel, Woodward, & Clarke, 1989; Morgan et al., 1998; Storm, Barfield, & Ormsbee, 1990) even though it has been ignored in such simple models as Universal Soil Loss Equation (USLE). Another reason to model ephemeral gully erosion is that there is a growing need to have more insights into the physical process of gully erosion. When the erosion modelling process accounts for multiple factors, new management practices can be discovered or be reconsidered due to findings of the research process. For example, grassed waterways can be used to prevent soil erosion from ephemeral gullies. Even though grassed waterway prevents land from being used for production, it prevents land degradation and reduces reservoir sedimentations. Another suitable BMP that can address ephemeral gullies is the double cropping in the area formed by ephemeral gullies. In this case, land is not taken out of the production, and the soil stability is improved at the same time. By modeling ephemeral gullies,

researchers can better estimate the efficiency of the existing BMPs and have more insights into the erosion process needed for inventing new BMPs. All other BMPs addressing soil erosion are also suitable for ephemeral gullies. These BMPs include, but are not limited to, cover crops, reduced tillage, and contour farming.

## Goals and Objectives

The focus of this research work is ephemeral gully erosion, including a model that has the potential to compare different management practices, soil types, and precipitation patterns while accounting for the physical processes and factors not yet considered in the ephemeral gully modeling. One of these factors is the soil moisture and its dynamics during runoff events. More specifically, this research aims to investigate the influence of the hydrological regime, soil pore pressure gradients and their interaction with the concentrated surface runoff causing the formation of ephemeral gullies.

To advance the approach of ephemeral gully modeling, a comprehensive literature review is needed in Chapter 2. The objective of this chapter is to explore the current state of the research area, ephemeral gully erosion. Current research interests from this literature review highlight the influence of the antecedent soil moisture condition. To investigate this influence, an experimental study is described in Chapter 3 where data would be collected in order to study the influence of soil moisture conditions before and during the rainfall event on an ephemeral gully erosion development. This experiment description and results were submitted for publication in a peer-reviewed journal and presented in Chapter 3 with minor changes in the description of methods. The influence of antecedent soil moisture conditions on the process of channel erosion, as shown in Chapter 3, gives additional insight into the modification of the excess shear stress

equation widely used in the modeling of channel erosion. A detailed explanation of this equation is given in Chapter 4 because it has a major objective in the development and testing of the two-dimensional model of the channel erosion due to the concentrated flow while accounting for the change in soil erodibility parameters due to subsurface fluxes. These subsurface fluxes are estimated via the hydraulic pressure gradient of the soil water pore pressure (also known as seepage/drainage gradient, pressure gradient, or hydraulic gradient). While Chapter 4 aims to develop and test the new model, the application of this model was considered in Chapter 5 with the aim of testing the impacts of various soil parameters on a channel erosion using the model described in Chapter 4. Equally important, parameters of interest include the soil type, antecedent soil moisture content, antecedent groundwater depth, and heterogeneity in soil layering.

The two-dimensional model developed in Chapter 4 can be used as a research tool. However, its application to the day-to-day estimation of soil erosion for various agencies is not suitable due to the complexity of data preparation and the relatively extended computation period. Thus, a separate model with the spatial and temporal distribution needs to be developed in order to apply new principles to larger scale projects. The aim of Chapter 6 is to develop such one-dimensional model. The other objective of this chapter is to test the new model performance with the data presented in Chapter 3. The investigations and developed models can be further applied to test influences of different parameters on ephemeral gully erosion. Also, a model from Chapter 6 can be used to estimate and compare ephemeral gully erosion at different conditions, including various BMPs. Hence, Chapter 6 aims to present an example of the comparison of the efficiency of different BMPs. Lastly, the purpose of Chapter 7 is to summarize all the research work as well as considering the limitation of developed models, their possible improvements,

and the potential integration into other soil erosion prediction models to estimate BMP efficiencies.

# Chapter 2 - Literature Review

## Introduction

Ephemeral gully erosion is a threatening problem acknowledged by producers, local authorities, state and national agencies, and the scientific community. Since 1980, there have been more than two hundred publications in scientific journals concerning ephemeral gully erosion from different perspectives, from the experimental studies to socio-economic impacts. This literature review considers three major groups of studies: (1) the qualitative description of the process and review papers, (2) computer modeling, and (3) field and experimental laboratory studies. Articles in each group are presented with the aim of showing the progress in understanding ephemeral gully erosion process and combining presented research ideas to have more insight into the current state of ephemeral gully modeling.

## Qualitative Description of the Ephemeral Gully Erosion Process and Reviews

Some research articles did not present results of conducting research or modeling efforts; rather, they provided expert opinions and insights into the problem. Findings of other research were also placed in this group.

The National Research Council (1986) provided a detailed overview of the problems of ephemeral gully erosion, including relevant techniques for erosion rate predictions. The presented methods contained the techniques driven by empirical equations, models with average annual outputs, and physically and process-based models. Stein & P Y Julien (1993) described the process of headcut migration and developed a theory with equations to distinguish two types of the process. One is a stepped headcut, and the other is rotating when headcut tends to flatten

during migration. Montgomery (1994) studied the impact of road construction on a natural stormwater system and emphasized on rill and gully initiation points. Theoretical equations were provided for the assessment of the erodibility, and they were compared for three study areas. Montgomery and Dietrich (1994) attempted to describe processes of channel initiation. By analyzing flow equations and their relationship with thresholds for the channel initiation, J. Poesen et al. (2003) discussed the importance of the problem of gully erosion in their review publication and summarized the research carried out in this area of study. The relationship between the channel width and the flow discharged was suggested in order to define ephemeral gullies. J. Poesen et al. (2003) pointed out that gully erosion was dependent on both spatial and temporal scale and that both of them could be major contributors to the total soil loss. Apart from providing a review of experimental studies in the area of ephemeral gully development, the researchers discussed the thresholds of critical shear stress for different soils and conditions, including conditions of ephemeral gully initiation. Valentin, Poesen, & Li (2005) studied how gullies were formed; these scholars also mentioned that the causes of gullies, such as farming without best management practices, increased precipitation intensity. Also explored were factors controlling gully formations such as topography, soil and lithology, land use and climate change. Similar conclusions about gully formation and its preventions were also found. A. Knapen, Poesen, Govers, Gyssels, & Nachtergaele (2007) reviewed a published research article, on the critical shear stress and soil erodibility, as parameters for the erosion process of concentrated flow erosion. They found that these parameters are not related: There was a wide variability in the measurements and ranges of these coefficients and their dependence on various parameters such as vegetation, soil type, soil and moisture. With aerial imagery analysis, Brooks, J G Shellberg, J Knight, & J Spencer (2009) conducted an analysis of alluvial gully formation

processes for northern Australia tropics. This group of researchers hypothesized that land-use change caused an increase in gullies formation. Kirkby & L J Bracken (2009) described the process of gully formation and the development of classical gullies by presenting two approaches to qualitative assessment of the gully development. In addition to that, G. Fox & Wilson (2010) summarized research attempts to model and understand the influence of subsurface flow processes on the channel erosion mainly by slope stability and pipe flow. A. Capra (2013) presented a review of studies carried out on some aspects of ephemeral gully and gully erosion, such as morphological characteristics, the contribution of gullies to overall erosion, and regression and mathematical models of ephemeral gully erosion.

Based on the review papers, it is observed that the number of scholars who understand the fundamentals and modeling of ephemeral gully erosion have increased considerably. This growth indicates that more people are interested in addressing the problems of ephemeral gully and that further research needs to be conducted on this research field.

## Modeling

In this section, academic articles related to modeling efforts were divided into topography based assessments, physically based models, and the application of the developed models. This division was done to estimate ephemeral gully erosion rates for particular locations on a field or watershed scales.

### Topography-Based Assessment

Moore & Burch (1986) studied gullies development by trying to create two and three-dimensional erosion/deposition model for idealized hillslope element. They used an equation for a sediment transport capacity which utilizes unit stream power, critical unit stream power when

the sediments motion occurs, functions of the median size, the kinematic viscosity of the water, and the terminal fall velocity of sediment particles in water. Moore, Burch, & Mackenzie (1988) applied their model of topographic analysis to define the soil saturation factor considering local upslope contributing area per unit width. They also utilized the slope and the measure of the erosive power of runoff to predict the location of ephemeral gullies. Several field tests and measurements were carried out to validate the model. Dietrich, Wilson, Montgomery, & McKean (1993) produced physically based model which uses digital terrain model. Researchers developed three simple theories to model the runoff, the threshold for slope stability, and the threshold of erosion by the saturation overland flow. To determine the thresholds, all three models used two parameters: the drainage area per unit contour length and the local ground slope. These data could be easily obtained from the digital elevation data. While the thresholds for runoff and erosion were determined by mass conservation, the threshold for slope stability was obtained by the infinite slope stability model. Desmet & Covers (1996) studied several routing algorithms for routing water on the available Digital Elevation Model. Researchers divided algorithms into three groups and the chose flux decomposition algorithm as the best algorithm for estimating zones with increased probability for ephemeral gully formation. Vandaele, Poesen, Govers, & Van Wesemael (1996) derived critical relations between the slope gradient and the upslope drainage area. They assembled results from previous researchers to conduct the survey. It was shown that critical slope gradient expression could be determined as a power function of a drainage area. Vandekerckhove, Poesen, Oostwoud Wijdenes, & De Figueiredo (1998) used the same approach to determine the thresholds through the slope and the catchment area. However, they paid attention to the field survey so that the data used for the assessment would be more accurate. Betts & DeRose (1999) implemented photogrammetric

technic to produce DEM for three cite areas and to study gully development. forestation and shadows were the problems encountered during this research. Besides, the average accuracy of the method was within 1 m. Acquired DEMs for different times were then used to estimate the gully growth. Meyer & Martínez-Casasnovas (1999) studied the probability of ephemeral gully development. The probability was calculated using the statistical model based on the GIS data of topography, soil, and management. Their model produced an 85% overall accuracy for their study area of Alt Penede-Anoia region (Catalonia, NE Spain). J. Nachtergaele & Poesen (1999) studied ephemeral gully erosion on on May 28, 1998, after the intensive rainfall event happened in Belgian Brussels and Leaven. They used high altitude aerial (stereo) photographs and field measurements of the gullies to compare the accuracy of each method. After comparing the results, it was shown that each method missed part of the gullies. A correction factor was proposed for the data acquired from aerial photographs. These data were used to estimate ephemeral gullies erosion rates. Furthermore, researchers suggested using this technic to collect inputted data of gullies geometry and the length for physically based models. Vandekerckhove et al. (2000) collected data from the literature and provided their data from the experimental study fields (in the Mediterranean region) to determine the critical relation of the local slope and catchment area for gully initiations. Researchers also mentioned the importance of the current vegetation, soil type and moisture condition of the field, stressing that they were among the factors affecting gully erosion. Daba, Rieger, & Strauss (2003) studied gully erosion in Ethiopia where they used topographic maps and photogrammetry to assess the volumes of nutrients lost during gully erosion. In that area, this group of scholars also tried to produce topographic indexes for the gullies. Souchère et al. (2003) produced the STREAM Ephemeral Gully Model to predict the erosion from the agricultural fields. Also developed to make calculations in the

ArcGIS software was the module GRID. Researchers calculated the sensitivity of gully erosion for a single rainfall event by multiplying parameters of the site such as slope factor, cohesion factor, and friction factor. Some similarities could be seen between the proposed and USLE equations. De Santisteban et al. (2005) studied two topographic index approaches used for modeling ephemeral gully erosion. These topographic indexes were area-weighted mean slope (AS1) and length-weighted average slope (AS2). Both models showed a good correlation with the observed data from actual fields in Spain. Some regression models could be estimated for certain areas. However, it was difficult to determine one effective regression model for any area. Also important was that climate data need to be considered. Cheng et al. (2007) used GPS measurements to study topographical characteristics of ephemeral gullies in the Loess Plateau of China. They investigated and determined several topographical indexes of the slope and the drainage area multiplication for the area of interest. Apart from measuring 49 ephemeral gullies were measured and the data of length, the critical slope gradient and upslope drainage area were determined for each gully. The relationship between the ephemeral gully length and the erosivity was determined for the area of interest. Kheir, John Wilson, & Yongxin Deng (2007) applied topographic analysis of DEM layer to identify classical gullies in Lebanon. TAPES-G software was used to estimate 11 different topographic attributes: the slope, contributing area, curvature, etc. DYNWET model was used with the soil properties to determine zones of saturation and topographic wetness indices. To assess ephemeral gully erosion on a watershed scale, Teasdale & Barber (2008) used aerial images. An erosion potential index was proposed to manage erosive soils more efficiently. From 1945 to 2006 , Gutiérrez, Schnabel, & Contador (2009) studied aerial photographs to determine the rates and causes of gully erosion. Findings show that land-use change contributed to the change in gully erosion rates significantly, while there was not

such a dependence for the precipitation. Gutiérrez et al. (2009) constructed a GID based model which predicts the location of the gully formation depending on numerous data such as topography, lithology, precipitation and soil data. It was found that the lithology and soil type had the most influence on the gully formation. Using topographic threshold approach, Svoray & Markovitch (2009) used high-resolution DEM to estimate gully initiation points. They also focused their attention on the tillage direction and locations of unpaved road as some of the major influencers. Orlandini, Paolo Tarolli, Giovanni Moretti, & Giancarlo Dalla Fontana (2011) applied the drainage area, area-slope, and Strahler order to determine gully location in Italian Alps. One of the major factors affecting results, according to the researchers, was grid size. These scholars also indicated the need for new methods to estimate and account for groundwater seepage. Lee & Kim (2010) used a comparative analysis of geomorphic characteristics to estimate drainage networks. Researchers found that the area threshold provides unreliable results, whereas the slope area threshold produces an acceptable drainage network. H. G. Momm, Bingner, Wells, Rigby, & Dabney (2013) investigated how the overall terrain slope, local relief variance, and DEM raster grid cell size affected the Compound Topographic Index (CTI) used for estimating the ephemeral gully development. Based on their findings, they suggested the use of normalized CTI.

Topography-based analysis of ephemeral gully process is the most rational method for large-scale projects. This approach covers larger areas and accounts for the soil properties and management practices at the same time. Most of the models use some a GIS software application to analyze data. Some models suggest the use of topographic indexes based on either the local or the average area, slope, and length. Data for model development and validation are usually based on DEM and aerial photographs when field surveys are inefficient.

## Physically Based Models

Foster & Lane (1983) presented a physically based model of channel development due to the concentrated flow. Their model computed the channel propagation with the excess shear stress equation. Propagation is assumed at a constant rate based on the equilibrium width of the channel for known flow rate, including the proposed acting shear stress distribution along the channel bottom. The model assumes that the maximum peak flow rate is applied during the event with the duration equal to that of rainfall. If the non-erodible layer is met, then the model allows the computation of the non-uniform rate of channel widening up to the final equilibrium width. Merkel et al. (1989) produce a physically based model to estimate ephemeral gully erosion. Researchers use an empirically based SCS curve number method for hydrology component and for calculating the peak runoff rate. However, the physically based approach was used to estimate the erosion caused by this runoff. The soil detachment rate is calculated using the channel erodibility factor, the average shear stress, and the critical shear stress of the soil. The Same equation is used in CREAMS model. Researchers used the assumption that gully erodes to the tillage depths. Storm et al. (1990) developed Erosion Model for Dynamic Rill Networks. Apart from utilizing the kinematic wave equation to compute water flow, it modified the two-tier channel Foster and Lane model to compute erosion rates. Fogle & Barfield (1992) continued the research work of Storm et al. (1990) and developed a CHANNEL, a process-based model that computes channel erosion by computing the distribution of the acting shear stress applied to the channel walls. K. M. Robinson & Hanson (1994) created a physically based model to estimate the gully headcut development due to the intensive overland flow. Their work was related more to the spillways than to rills and gullies; however, it described similar physical processes. Their

model had components that could predict the nappe profile, hydraulic stresses, and stresses in the headcut area. Those stresses were used to estimate the erosion with excess shear stress equation. Culmann method was used to calculate forces and the slope stability analysis in a two-dimensional problem. Hirschi & Barfield (1988) developed a process based KYERMO model to compute soil erosion on the hillslope, mainly for sheet and rill erosion. Rill erosion was computed with the track of change of the rill profile change. As for the unique assumption used in the rill deformation block, acting shear stresses were assumed to have a distribution along the profile and were calculated similarly as were in the CHANNEL model (Fogle & Barfield, 1992). Morgan et al. (1998) presented a European Soil Erosion Model (EUROSEM). EUROSEM is a physically-based, dynamic, spatially-distributed model that simulates sediment transport, rill and interrill erosion, and deposition processes for a single rainstorm event in a field or a catchment. Water and sediment routing were obtained from the KINEROS model. Sediment discharge was based on the numerical solution of the dynamic mass balance equation. The same approach was used for the surface runoff. The model had an adjustment parameter for rocky soils. The Manning's equation is used to calculate the runoff flow. Soil erosion is calculated as hillslope erosion and channel erosion considering sediment detachment by runoff and transport capacity of the concentrated flow. A. Sidorchuk & Sidorchuk (1998) described a three-dimensional model to predict initial gully development. This team of researchers used the equation of mass conservation and deformation to predict the rate of gully incision. The rate of particles detachment is determined by shear stress, flow velocity, and critical shear stress. Sidorchuk & Sidorchuk (1998) also investigated how temperature affects the erosion process. The model used topographic DEM to determine flow lines. The runoff from rainfall and snowmelt was calculated by the equation of kinematic wave with the Manning's equation. The model was verified on data

from Yamal Peninsula of 1986-1995. Developed a model of headcut migration, G. J. Hanson, Robinson, & Cook (2001) adopted more physical parameters of the soil and tried to produce a physically detailed model with the prediction of headcut migration with time. They also conducted series of experiments which showed that model could be used for headcut migration magnitude estimates. However, this model had not been calibrated and validated. Casalí, López, & Giráldez (2003) proposed a simple event-based erosion model, which was developed based on the river erosion model. Researchers used equations of mass conservation and conservation of momentum for water and sediments. They also assumed that erosion depended on the maximum bed shear stress as well as suggesting a formula for its calculation. This model was used to calculate the gully profile as a function of the calculated flow. Casalí et al. (2003) also made a simple model evaluation with variation of parameters and found that their model was very sensitive to soil parameters. Souchère et al. (2003) presented their STREAM model with the aim of estimating ephemeral gully erosion. They also estimated the overland flow with a set of parameters such as friction, which was defined by practices on the field. The shear strength was defined by parameter "cohesion," which was determined by the crust condition, plant cover and land use. The sensitivity to gully erosion was calculated with this formula: Sensitivity = Runoff x Slope x Friction x Cohesion. To apply the model, researchers calculated the set of streams for potential gully locations. The model was validated on four experimental catchments, and it showed the gully erosion was overestimated. Stolte, B Liu, C J Ritsema, H.G.M. van den Elsen, & R.Hessel (2003) created LISEM model, a physically based model that was built in the module to ArcGIS software. The detachment of soil was described by the stream power principle. Calibrated by the saturated conductivity, the model presented poor results on shallow slopes and worked better on steep slopes. Istanbulluoglu (2005) studied classical gullies with a geotechnical

approach. They considered the weights of the soil blocks and estimated slab failures along the critical planes. Istanbulluoglu (2005) also developed two models: one-dimensional model of slope stability and three-dimensional model of landscape development. These approaches were more suitable for large-scale gullies and could partially be applied to only agricultural ephemeral gullies estimations. Researchers also noted that there was a strong influence of soil cohesion on gully erosion, especially for unsaturated conditions due to the matric suction in the soil material. The shear stress threshold was also one of the major factors. As it had a lower value, it caused the gully to expand tremendously; when it had a higher value, the gully was likely to deepen. L. M. Gordon (2007) upgraded the AnnAGNPS model to account for the ephemeral gully erosion. The technique proposed by Alonso, Bennett, & Stein (2002) was introduced to adjust the headcut propagation. Also used to estimate the erosion from the gully was the EGEM approach. The model used SCS curve number methods to calculate the hydrograph peak discharge and the total runoff, and it was utilized to construct the triangular hydrograph for each cell representing the ephemeral gully. Based on the discharges for each cell and the time step gully widened, the sediment detachment and deposition were calculated. Yan, X X Yu, T W Lei, Q W Zhang, & L Q Qu (2008) developed a physically based 1-D Finite Element model of rill erosion. The dynamic wave equation was used for the hydrodynamics, and the sediment concentration continuity equation was used to simulate the erosion/deposition process. Researchers accounted for both the transport capacity and the erodibility as limiting factors of erosion. S. Dabney, Daniel Yoder, Dalmo A. N. Vieira, & Ronald Bingner (2011) further developed the RUSLE2 model and incorporated the estimation of the time-varying runoffs, including the estimates of the transport/deposition of the sediment on complex hillslopes. This modified approach was then applied to the CREAMS model so that ephemeral gully erosion was calculated for the

hypothetical catchment. D. C. Flanagan (2012) introduced a watershed version of the Water Erosion Prediction Project (WEPP) model, which had a component for estimates of the channel erosion. It was a spatially distributed one-dimensional model of the channel erosion. It utilized dynamic routing of the flow; however, it only used a peak rate value and the effective duration. Classical Foster and Lane approach was used to estimate the erosion rates and the channel shape. S. M. Dabney et al. (2014) produced physically based model of ephemeral gully erosion EphGEE (Ephemeral Gully Erosion Estimator) and used outputs from RUSLE2 program in the raster format to account for the runoff accumulation and infiltration. Also, calculations from the DEM channel network was used to simulate ephemeral gully. The development of the gully was considered as the deepening and widening of the rectangular cross-section on an event basis. The channel width was assumed based on the runoff flow amounts calculated in the RUSLER component.

There was a strong interest to model soil erosion due to the concentrated runoff. The most often used modeling process was the application of shear forces due to the concentrated flow when flow forces exceed the cohesion forces of the soil erosion. This principle was applied to models at a different extent depending on the scale of a project. However, in the development of models, there was a tendency to apply them to larger scale projects. For this reason, the accuracy sometimes was lost due to the simplification of the process.

Most of physically based models use an excess shear stress equation (G. Hanson, 1990; Partheniades, 1965):

$$E = K_e \cdot (\tau - \tau_{cr})^a \tag{2.1}$$

where $E$ is the erosion rate in (kg/s/m$^2$), $K_e$ is the soil erodibility (s/m), $a$ is the dimensionless parameter usually taken as 1, $\tau$ is the acting shear stress (Pa), and $\tau_{cr}$ is critical shear stress. Equation 2.1 defines the soil erosion rate $E$ as proportional to the difference of acting and critical

shear stresses. The soil erosion rate is the rate at which the soil is being detached from the bottom of the channel. If the acting shear stress is higher than the critical shear stress, then there is a particle detachment and so erosion. Thus, the critical shear stress defines the critical condition of the particles on the soil surface when they lose the ability to overcome the acting force from the moving water. While critical shear stress controls both the moment of the start of the erosion and the erosion rate, soil erodibility coefficient $K_e$ corresponds to the rate of the soil detachment or to the speed of how fast particles are being detached. Both parameters, critical shear stress and soil erodibility coefficient, are hard to define and they may have dependence on various parameters such as vegetation, soil moisture, management practices, etc. Studies on some of these parameters are presented further in this chapter in the section Field and experimental laboratory studies.

## Application of Models

Nachtergaele, J Poesen, L Vandekerckhove, D Oostwoud Wijdenes, & M Roxo (2001) applied EGEM to estimate the erosion from 86 actual ephemeral gullies. This team of researchers prepared EGEM input parameters from surveys of these ephemeral gullies. However, what were auto-generated by the model were parameters such as channel erodibility, critical shear stress, particle diameter, particle specific gravity and Manning's roughness coefficient. Their results showed that the most significant factor and input parameter to the model was the length of the ephemeral gully. Nachtergaele et al. (2001) continued their previous work and proved that EGEM could not predict ephemeral gully erosion for Belgian loess belt. They emphasized the urgent need for future research on the determination of ephemeral gully length. Alonso et al. (2002) studied the headcut development of ephemeral gullies, rills, and classical

gullies and used equations of mass conservation, conservation of the momentum and energy to achieve their objective. However, the developed model did not consider detailed processes of the sediment detachment from the headcut. Rather, the model simulated the propagation of the headcut, and all equations were written for the process of headcut propagation. Kirkby, L J Bull, J Poesen, J Nachtergaele, & L Vandekerckhove (2003) investigated the form of sediment transport laws of ephemeral gullies and channels. Scholars considered several forms of laws and compared them with theoretically derived formulas. They also compared results with experimental studies and concluded the difference in transport laws for event-based modeling versus continuous modeling. A. Capra, Mazzara, & Scicolone (2005) applied the EGEM model to predict ephemeral gully erosion in Sicily, Italy, where they modified the hydrology calculation method in order to adopt the model for the site. Ninety-two ephemeral gullies were measured to evaluate model performance, and results showed that the model produced higher values of soil erosion. However, improved hydrology calculations showed better results for their site. Duan & Pierre Julien (2005) simulated the inception of channel meandering with a two-dimensional bank erosion model. They used the effective element method to model the bank deformation during the erosion process and to refine the mesh for this purpose. The flow in the channel was calculated by solving the momentum and conservation equation. Channel bed erosion was proportional to critical shear stresses. Bank erosion was proportional to the difference between the entrainment and the deposition of bank material. Flores-Cervantes, Istanbulluoglu, & Bras (2006) studied regular gully propagation due to the plunging pool erosion, a continuation of the research work carried out by Alonso et al. (2002). Headcut retreat was calculated based on the assumption of proportionality between change in the depth of the plunge pool and the headcut movement. The change in depth was calculated through the excess shear stress equation. Shear

stress was calculated from the flow velocity, discharge, plunge pool geometry and water physical properties. Jet diffusion/non-diffusion and supercritical/subcritical flow states in the pool were also considered. Apart from studying the threshold conditions for the plunge pool erosion, the critical headcut height was determined. Three-dimensional simulations were performed in the CHILD model with the assumption of a constant headcut width. Infiltration and evapotranspiration were ignored; soil moisture content was not considered. The model was validated based on the data from the flume experiment. A. Sidorchuk (2006) applied a dynamic gully erosion model (A. Sidorchuk & Sidorchuk, 1998) to investigate the attributes of the state of self-organized criticality (SOC) for gullies. The researchers simulated gully formation and tracked the changes in gully volumes, which were analyzed for frequency magnitude relationships. Sidorchuk's aim was to identify the factors that contributed to the SOC. Researchers found the SOC changes for different conditions of the topography, texture, discharge, and base level. Licciardello (2007) applied the AnnAGNPS model to the area in Italy. The model produced satisfactory capability and proved that it could be applied in that region. L. M. Gordon, S J Bennett, C V Alonso, & R L Bingner (2008) used modified the EGEM model within AnnAGNPS to predict long-term soil losses. This model allowed them to compare conventional tillage with an annual filling of the eroded gully and no-till practice allowing the gully to develop. Also simulated were four regions: Belgium, Mississippi, Iowa and Georgia. Researchers reported that no-tillage practice could significantly reduce the soil loss. Eustace, M J Pringle, & R J Denham (2011) mapped the presence of the gullies in central Queensland, Australia. Based on the Lidar data, these scholars developed a model for some predictors (soil, topography, vegetation information), approbated it on the study area, and then applied it to create a map of gully locations. E. V. Taguas, Y Yuan, R L Bingner, & J A Gómez (2012) applied

AnnAGNPS model to estimate ephemeral gully erosion for different conservation practices on the olive orchard. Researchers also collected experimental data from the actual orchard with spontaneous grass cover with gully control to calibrate the model, which was used to predict the conservation practices estimation with economic cost/benefit analysis. P. Daggupati, Sheshukov, & Douglas-Mankin (2014b) used the processed based Overland Flow-Turbulent (OFT) model in ArcGIS environment to estimate ephemeral gully erosion. Researchers also compared results to the topographic index models and field observations. The OFT model with the precipitation excess, which was calculated in SWAT, resulted in the acceptable estimations of the ephemeral gullies with slight over-prediction of lengths compared to the observed data. Bingner, Wells, Momm, Rigby, & Theurer (2016) compared six equations in order to estimate ephemeral gully widening rates. Improved critical shear stress equation based on clay content and RUSLE practices parameter was suggested to be used in the AnnAGNPS model. Tekwa, Kundiri, & Chiroma (2016) tested the performance of the EGEM model on the field experiment data in Northeast Nigeria. The researchers concluded that the classical version of the EGEM model was not suitable for the area and that if some input parameters were adapted, then the model could produce acceptable results.

## Field and Experimental Laboratory Studies

flume experiments with various soils to investigate the influence of the soil texture, soil pore pressure and tail-water height as explicit parameters of the gully erosion rates. Their findings indicated that both soil texture and soil pore pressure affected erodibility parameters greatly. R. Wells, Carlos Alonso, & Sean Bennett (2009) used previously conducted experiment to assess the headcut propagation rates and compared them with the rates computed with the

model. The soil texture and pore pressure were considered and were found to influence propagation rates considerably. G. V. W. Wilson (2009) performed a flume test to estimate the possible mechanism of ephemeral gully erosion through the subsurface soil pipes. During his experiments, it was found that such pipes did not result in the sudden collapse and that they were not the possible cause of the ephemeral gullies. A. Knapen & J Poesen (2009) studied soil erosion resistance, including the relationship between the critical shear stress and the soil erodibility and the soil properties, such as (1) the initial gravimetric soil water content and soil erodibility, (2) the dry soil bulk density, (3) the saturated soil shear strength, and (4) the dry density of the organic material. They also investigated the conditions of the development of the ephemeral gullies and rills. Although A. Knapen & J Poesen (2009) assumed the same soil moisture conditions for all events which caused incision, they found that initiation points and dimensions were controlled by soil erosion resistivity, critical shear stress and erodibility. Hence, topographical thresholds were not the only major factors of ephemeral gully location and length. Tebebu et al. (2010) measured classical gully erosion rates in the Ethiopian Highlands and found that the development of the gullies was related to the high levels of groundwater tables. They also measured rill and interrill erosion rates, and results indicated that they were 20 times less than gully erosion rates. By investigating the geological processes with tracking of radionuclides and organic carbon isotopes, Carnicelli, Benvenuti, Ferrari, & Sagri (2009) studied gully formation processes, and their findings indicated that climate drivers were the most important factors for gully formations. Di Stefano & Vito Ferro (2011) conducted measurements of rill and ephemeral gullies in Sicily, Italy and used data from previously published article to check the power relationship of eroded volume as a function of length. What's more, they suggested a new relationship for the width, length, depth and volume to describe concentrated flow erosion

process (rill, EG and gully). Gao et al. (2011) studied soil moisture variability along gully transects in the Loess Plateau, China. They reported a strong difference in the soil moisture along transects and concluded that soil moisture differences were more likely due to the change in texture than due to the topographic features. Gong et al. (2011) conducted a flume experiment at different slopes and rainfall intensities to study ephemeral gully development and found that the development process could be classified into initial adjustment and intervals of stable development. Both supercritical and subcritical were possible for the ephemeral gully erosion process. Channel slopes were found to be major factors. And friction factors were found to be slope dependent. Hancock, Coulthard, & Willgoose (2011) applied landscape evolution model to study precipitation variability on the ephemeral streams development and reported that precipitation, due to the climate change and change in the land-use due to human activity, might significantly increase erosion rates. G. Wilson (2011) conducted soil pipe flow experiment in the laboratory environment with controlled pipe diameter and reported that critical shear stress values were essentially zero and that erodibility values were extremely high. Tunnel collapses were observed for 10 mm pipe with ephemeral gully formation at the top and rapid flow accumulation in the newly formed channel, proving that soil piping was one of the possible reasons for the ephemeral gully formation. R. Wells et al. (2013) conducted a flume experiment with the no erodible layer to study the widening rates of ephemeral channels. An empirical equation was also suggested based on the experiment data for various slopes and discharges. Q. Zhang, Dong, Li, Zhang, & Lei (2014) conducted flume experiments and tested WEPP formula to estimate rill and gully erosion rates. Researchers found that the equation was valid for steep slopes and high flow rates. H. G. Momm, Wells, & Bingner (2015) presented the photogrammetry technique adapted for the accurate and inexpensive measurement of ephemeral

gully erosion in the flume experiments. Tekwa et al. (2016) conducted a field experiment in Northeast Nigeria and tested empirical models based on the collected data from several watersheds. Models predicted that volume and mass of soil loss were better than area of soil loss. R. R. Wells, Momm, & Castillo (2017) tested several surveying techniques such as photogrammetry to measure ephemeral gully erosion and found that any of the techniques could be used with acceptable accuracy only if ground control points were used during the survey.

## Summary

Based on the literature review, it is evident that ephemeral gully erosion has been extensively studied for almost 40 years. Even though most studies have been conducted in several regions across the globe, some laboratory studies were carried out in a more controllable environment with the aim of investigating physical processes of channel erosion. The topographic analysis is very popular due to the relative simplicity of applying it on a large scale. What's more, ephemeral gully erosion is represented by a few models (see Chapter 6 to compare these models). Most models were conceptualized in 80's, and 90's probably due to an increased interests and funds availability from governments seeking environmentally sustainable solutions for the agricultural sector. Another contributing factor, which helped researchers to develop mathematical models, is that they had relatively easy access to desktop computers with tremendous computational power. Some models received scholarly attention and have been developed continuously up to this day. However, there is no complicated model that investigates the ephemeral gully erosion in detail and that accounts for the multiple factors and their interactions. For example, no model is yet to explore the influence of soil moisture conditions and soil erosion parameters such as critical shear stress and soil erodibility coefficient.

# Chapter 3 - Effects of Intra-Storm Soil Moisture and Runoff Characteristics on Ephemeral Gully Development: Evidence from a No-Till Field Study

Vladimir R. Karimov, Aleksey Y. Sheshukov, *Water* 2017, 9, 742/1-19



## Introduction

Increasing global population has raised demand for higher productivity from agriculture. One of the essential problems that limits agricultural productivity relates to soil degradation due to loss of topsoil and soil erosion processes. Soil erosion may be divided into three general types: sheet and rill erosion, ephemeral and classical gully erosion, and stream bank and bed erosion (National Research Council, 1986). Soil transported from upland areas through ephemeral and classical gullies contributes to stream and lake sedimentation and significantly intensifies nitrification in the reservoirs of the United States and globally (G. Fox et al., 2016; Hargrove, Johnson, Snethen, & Middendorf, 2010).

An ephemeral gully is a small channel with an average cross sectional area larger than 0.1 $m^2$ (or about 1 $ft^2$) that is formed due to concentrated surface runoff along the drainage pathways in the lower part of a cultivated field. Ephemeral gullies can normally be removed by tillage operation but tend to re-appear in the same location after intense rainfall events (National Research Council, 1986; Soil Science Society of America, 2008). Ephemeral gully can grow into classical gullies if left untreated for a prolonged time. The studies worldwide have shown that the impacts

of ephemeral gully erosion can vary from 30% to more than 90% with annual soil losses reaching up to 90 Mg/ha (P. Daggupati, Sheshukov, & Douglas-Mankin, 2014b; National Research Council, 1986; Osmond et al., 2012; E. Taguas, Guzmán, Guzmán, Vanwalleghem, & Gómez, 2015).

Ephemeral gully development is affected by a number of factors. In general, the factors are related to four categories: (i) rainfall characteristics, (ii) soil properties, (iii) topographic features, and (iv) land use and management (A. Capra et al., 2009; P. Daggupati, Sheshukov, & Douglas-Mankin, 2014b; G. Fox et al., 2016; Valentin et al., 2005; R. Wells et al., 2009; Y. Zhang et al., 2007). Higher rainfall intensities result in more erosive power in surface runoff, which increases the potential for gully erosion. Field hydrologic condition, crop type, root structure, vegetation density, and antecedent soil moisture content affect soil detachment and sediment transport. Topographic landscape features direct ways of flow accumulation and direction, controlling the amount of surface runoff and points of flow conversion. Ephemeral gully initiation points and trajectories have been explored by evaluating the attributes of slope, upstream drainage area, planar curvature, and defining topographic index thresholds (P. Daggupati, Douglas-Mankin, & Sheshukov, 2013; P. Daggupati, Sheshukov, & Douglas-Mankin, 2014a; Yi, Zhang, & Yan, 2017). Higher values of the threshold show areas of favorable conditions for concentrated flow pathways and gully trajectories.

Ephemeral gullies predominantly form on cultivated croplands where land cover and above- and below-ground vegetative biomass control their development (J. Poesen, Torri, & Vanwalleghem, 2010). Conventional tillage disrupts soil structure and reduces its resistance to soil erosion, promoting channelized flows and ephemeral gully development. In addition, continuous tillage creates a layer of compacted soil (often called a plow-pan) underneath a layer of tilled topsoil, which restricts or slows infiltration and contributes to faster soil saturation and higher

surface runoff. No-till, more sustainable management practice compared to conventional tillage, requires direct seed planting with minimum soil disturbance and leaves 30% to 100% of crop residue on the soil surface (Soane, Ball, Arvidsson, Basch, & Moreno, 2012). No-till has been widely used in the Great Plains due to improved soil health (organic matter, soil structure, carbon storage), increased infiltration, better conservation of subsurface water, and gradual removal of the residual plow-pan (Pollock & Reeder, 2010).

Soil texture and its resistance to soil erosion plays an important role in gully formation. The shearing force of the concentrated flow within the gully can initiate soil particle detachment if the critical threshold is exceeded. Soil critical shear stress $\tau_c$ depends on factors of texture, bulk density, particle size distribution, void space, soil cohesion, surface sealing, crusting, freezing and thawing, and may vary during a runoff event. For ephemeral gully formation, a range of $\tau_c$ can vary from 3 to 32 Pa for silt loam and from 17 to 74 Pa for sandy loams on agricultural fields in Europe (J. Nachtergaele et al., 2002; J. Poesen et al., 2003).

An effect of soil moisture content on gully initiation and channel deepening and widening was reported in literature after field and laboratory studies. A. Capra et al. (2009) indicated the impact by 3-day cumulative rainfall depth and the associated elevated soil moisture, while R. Wells et al. (2009) concluded the importance of soil texture, tailwater height, and pore water pressure on promoting gully erosion. Tebebu et al. (2010) also noticed the role of soil moisture and stated that gully development events only occurred when ground water table level was higher than the bottom of the gully. A. Knapen et al. (2007) reviewed factors that influence resistance to soil erosion and noted that gravimetric soil moisture content affected critical shear stress and soil erodibility.

Several techniques can be used to determine ephemeral gully erosion in field studies (Casalí, Rafael Giménez, & Sean Bennett, 2009; Castillo et al., 2012; Di Stefano & Vito Ferro,

2011; Gong et al., 2011; Karimov, Sheshukov, & Barnes, 2015; Thomas & Welch, 1988; R. Wells et al., 2013). The techniques vary from simple methods of approximating the gully cross-sectional area and length with a pole and a tape to complex approaches that utilize remote sensing and photogrammetry techniques. The 2-D based conventional techniques can be conducted at any time during the crop growing season, but yield a lower resolution reconstructed shape of the gully. Whereas 3-D based complex approaches can be very accurate, but the results can be affected by field condition, stems and canopy cover, as well as rely on equipment availability and cost (Castillo et al., 2012). One approach that combines the accuracy of complex methods while allowing to collect data with mature crop canopy is the use of micro-topographic profiler or a pin-frame as suggested by Casalí et al. (2009).

Ephemeral gully erosion models use process equations for surface flow, soil erosion, and channel development and incorporate model parameters that depend on topographic, land cover, soil and other properties of a field. Laboratory and field studies can be used to provide unique data needed to define functional forms and regression curves of significant physical parameters, and their values for model calibration and validation. However, such experiments on ephemeral gully erosion in controlled field environments with continuously monitoring setup are difficult to conduct for prolonged periods of time due to field availability, management practice, data collection load, climate variability, among other factors.

Therefore, the main goal of this research was to conduct a field study of ephemeral gully development on a cultivated crop field under active no-till management practice and analyze the factors responsible for soil loss within the gully. The specific objectives were (1) to develop a dataset of continuous changes in ephemeral gully profile and associated physical variables, such as soil moisture, precipitation, runoff, and sheet and rill erosion, (2) to evaluate the impacts of

individual runoff events on channel development, and (3) to evaluate channel erosion by analyzing different factors that affect soil detachment.

## Materials and Methods Study Area

A 32-hectare agricultural field in the Little Arkansas River watershed (8-digit Hydrologic Unit Code 11030012) near the city of McPherson in Central Kansas, U.S.A., was selected for this study (Figure 3.1). The field has been in cultivated crop production for more than 40 years. The soil was reported (KDASC, 2013) as Crete silt loam with a measured silt content of 55%, clay content of 37%, sand content of 8%, bulk density of 1570 $kg \cdot m^3$, and computed soil critical shear stress coefficient of 3.5 Pa (D. C. Flanagan & Nearing, 1995; Sheshukov, Daggupati, & Douglas-Mankin, 2011; USDA-NRCS, 2005). A slightly compacted layer of subsoil was detected at a depth of 0.4 m. The field received average annual precipitation of 830 mm from 1990 to 2010 (NOAA-NCEI, 2016). Majority of intensive rainfall events occurred in late spring and early summer when land was bare and poorly protected, and summer crops were in their early growing stages, which caused surface runoff and significant soil losses due to the sheet, rill, and ephemeral gully erosion (as measured and presented below).

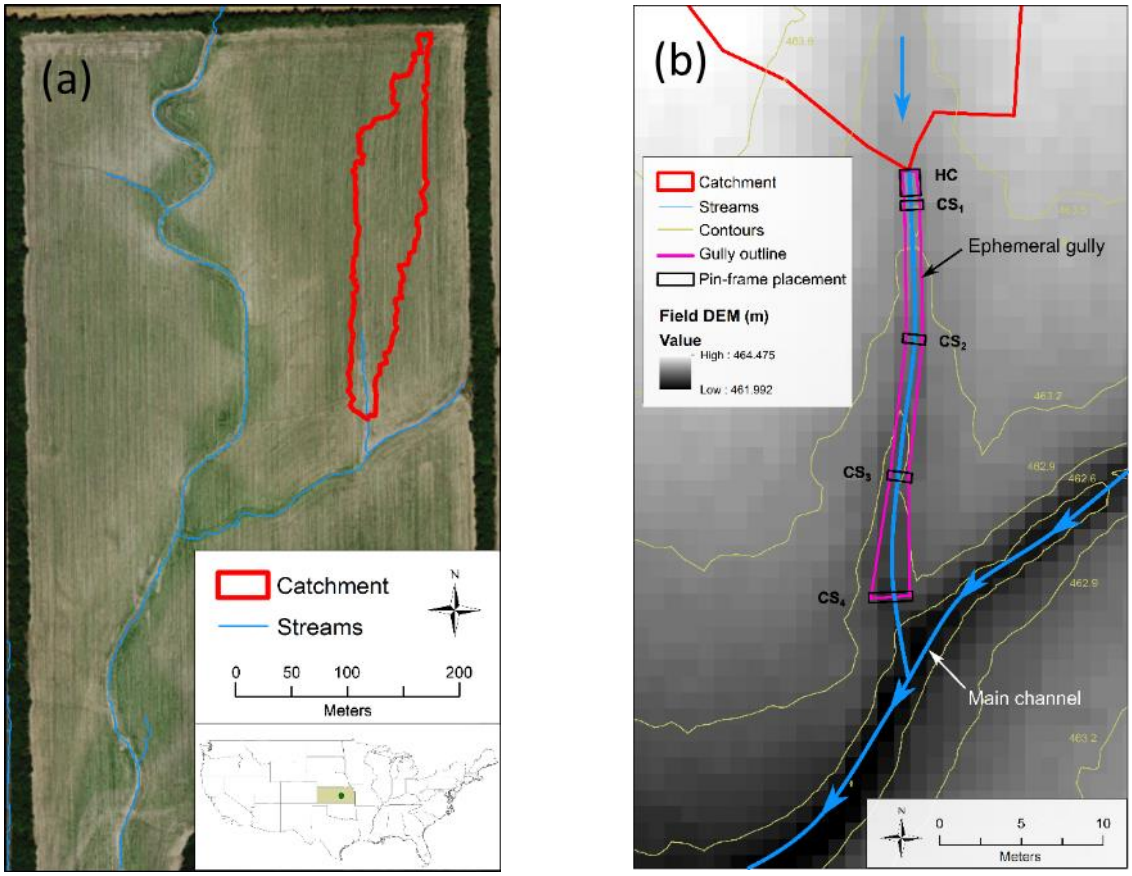


**Figure 3.1 Maps of (a) the studied field and (b) ephemeral gully in Central Kansas, USA.**

The contributing catchment is outlined by red line, while gully trajectory is shown as blue line. The map also shows the positions of pin-frame placement (black outlines) in headcut (HC) and along channelized part of the gully ($CS_1$ – $CS_4$), gully area (pink outline), and surface runoff direction from contributing catchment and within the downslope channel (blue lines and arrows).

From 2005 to 2014, the field was under continuous crop rotation schedule, mainly growing summer crops of corn, grain sorghum, and soybeans. During the studied period of 2013 and 2014, grain sorghum was planted in 2013 followed by soybeans in 2014. Corn was planted in 2012. Every year, residue was left uncollected after crop harvesting in the fall, and fertilizer was applied once a year in June. No-till was adopted for the past 10 years, although farming operations were

conducted up and down the slope without following the contours. This practice formed ridges of growing crops along the hillslope and caused the overland flow to concentrate between the rows and move toward the field outlet, thus accelerating rill and ephemeral gully erosion.

One catchment with a defined ephemeral gully in the northeast part of the field was selected for the detailed study of ephemeral gully development (Figure 3.1.a). The catchment was fully encapsulated within the field with no inflow from adjacent areas. The catchment drainage area was 1.2 ha with an average slope of 0.6% and the longest flow path of 321 m. Several years prior to 2013, the incised rill was formed on the north bank of the main channel and began progressing upslope with little disturbance from farming activities due to the adopted no-till. At the beginning of this study in the spring of 2013, the rill was enlarged into the size of the ephemeral gully and measured at 19 m from headcut to the junction with the main channel and had depth varied from 0.3 m to 0.5 m (Figure 3.1.b).

## Field Equipment

Field equipment was instrumented along the gully to measure hydrologic characteristics associated with ephemeral gully development: volumetric soil moisture content, soil temperature, precipitation depth, surface runoff, and channel morphology (Figure 3.2). A tipping bucket-type rain gauge (Onset RG3), solar panel, and data logger (Onset, 2013) were installed on the wooden post 1 m downslope of the headcut and 1 m east from the bank of the gully. Precipitation depth was recorded every 2.54 mm (0.01 in). Eight volumetric soil moisture probes EC-5 (Decagon, 2015) were carefully inserted with minimum disturbance into the soil 1.5 m downslope of the gully headcut and connected to the data logger. Factory calibration was accepted for the soil moisture sensors. Six probes were installed at depths of 5 cm, 20 cm, and 50 cm on both banks of the gully

channel and about 15 cm away from the edge. Two additional probes were placed in the middle of the gully at depths of 5 cm and 20 cm. To eliminate ambient temperature effect on soil moisture sensor reading, three temperature sensors were installed at the same depths and used for probe reading adjustment (Cobos & Campbell, 2007; Decagon, 2015). Soil moisture content and temperature were recorded continuously with a 2-min interval.

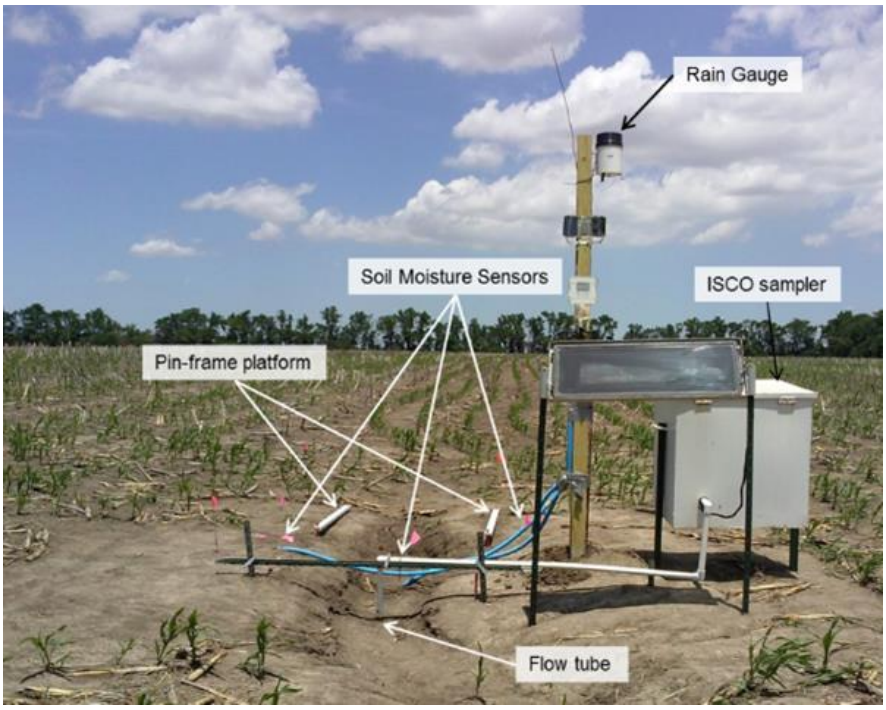


**Figure 3.2 Field equipment installed along the gully.**

A portable water sampler (Model 6700; ISCO Inc., Lincoln, Nebraska, USA) with automatic stage recorder module (Model 7300; ISCO Inc., Lincoln, Nebraska, USA) was installed 0.5 m downstream of soil moisture probes to continuously record channel inflow stage with time step of 2 minutes (ISCO, 2013). A bubbler tube was secured with PVC pipes in the center of the channel and connected to the stage recorder (Figure 3.2). Channel cross-section ($CS_1$; Figure 3.1. b) at the location of the bubbler tube was frequently surveyed during field visits. Local channel

slope at $CS_1$ was measured at 1.7%. Eight runoff events were recorded and event hydrographs were developed. These events were used for calibration of the soil erosion model.

## Measuring Channel Cross Sections

To measure an ephemeral gully cross-sectional profile, a custom pin-frame was designed and manufactured in the workshop of the Department of Biological and Agricultural Engineering at Kansas State University (Figure 3.3.a). The pin-frame device was made of a welded metal frame that contained 110 of 100-cm long fiberglass rods (or pins) equally spaced 1 cm apart from each other. The rods were mounted on the frame and allowed to freely fall when the pin-frame was placed above the ground. The fiberglass rods were made of lightweight material, which lowered an impact of the tip on the soil, thus decreasing potential soil deformation. A white cardboard with 0.5 cm horizontal marks was attached to the back of the frame as a reference board for depth measurements. When the rods touched the ground, their top ends formed a profile that was used to represent a gully cross-section. After that, the rods were photographed from 2 m distance with a high-resolution digital camera aimed perpendicular to the face of the frame. The digital image was digitized later in the lab during the post-processing steps. The accuracy of the depth measurement for each rod was evaluated to be within 0.5 cm.

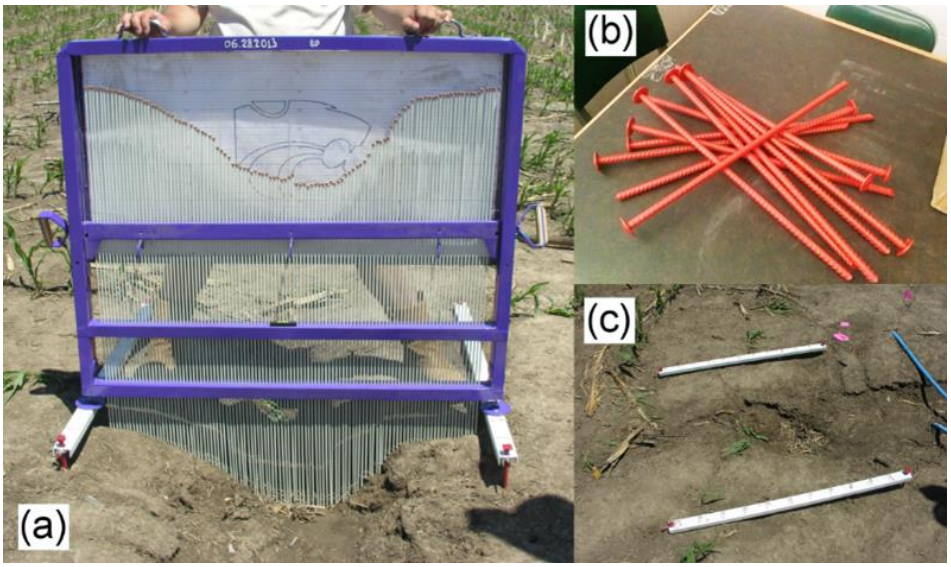


**Figure 3.3 (a) Pin-frame, (b) earth pins, and (c) base foundation platforms for measuring gully cross-sectional profile.**

To preserve the accuracy of repetitive measurements of the same cross-section, a leveled reference base for setting the pin-frame above ground was established by installing either individual earth pins (Figure 3.3.b) or base foundation platforms (Figure 3.3.c) on the banks of the gully. Earth pins were 60-cm long, made of a steel rebar with a 5 cm (2 in) washer welded to one end (Figure 3.3.b). The base foundation platform was 100-cm long, made out of a U-shape steel beam, with eleven locations marked every 10 cm for the placement of the pin-frame leg (Figure 3.3.c). The platform was held in place by two earth pins at both ends. The platform was designed to cover larger channel area within the headcut with cross-sections measured every 10 cm (shown HC in Figure 3.1.b), while earth pins were used for measurements of four individual cross-sections along the channelized part of the gully (identified as $CS_1$ to $CS_4$ in Figure 3.1.b). All pins and platforms were horizontally leveled and referenced to specific elevation on the wooden post with a laser level to ensure the same reference point. During field visits, they were frequently re-

referenced to ensure constant reference elevation for channel profile measurements with a pin-frame.

Taking pin-frame measurements at each 10-cm mark on the platform created a grid of 110 x 11 elevation points that completely covered the splash pool area at the beginning of 2013 campaign. The first location, $CS_1$, was at the ISCO bubbler tube place. The cross-section measurements at $CS_1$ were used to update the function of hydraulic radius in the Manning's equation to supplement the sampler readings for runoff hydrograph calculations. The second $CS_2$ and third $CS_3$ locations were 6 and 12 meters downstream of the first location, respectively. The fourth location $CS_4$ was 18 meters below the headcut and at the mouth of the gully confluence with the main channel (Figure 3.1.b). Gully width at $CS_1$, $CS_2$, and $CS_3$ was less than 100 cm, thus pin-frame covered the whole channel width. Between $CS_3$ and $CS_4$, the channel widened greater than the size of the pin-frame, reaching close to 200 cm in width at $CS_4$. Therefore, to measure the whole span of the channel profile, one 100-cm long earth pin was built and placed in the middle of the channel allowing the cross-section $CS_4$ to be measured as a combination of two pin-frame measurements.

## Estimating Ephemeral Gully Erosion

During the two-year data collection campaign of 2013-2014, fifteen elevation surveys were conducted. The change in channel depth was calculated based on measurements of cross-sections at HC, $CS_1$, $CS_2$, $CS_3$, and $CS_4$ (Figure 3.1.b). Eleven cross-sections in HC were referenced to the same level, which provided a 100 cm x 110 cm elevation grid. Four cross-sections $CS_1$-$CS_4$ were referenced to a different elevation, thus an assumption of linear interpolation along the channel slope was made, and the depth was calculated as a product of length and linear change in elevation

for each rod between the cross-sections. For the gully section between $CS_3$ and $CS_4$ where the gully widens from 100 cm to 200 cm, middle points in the profile were introduced at 0.5 cm interval in $CS_3$ and a planar interpolation was used to connect the points in $CS_3$ and $CS_4$. The outline of the simulated gully shape is shown by the pink line in Figure 3.1.b.

After gully elevation profiles were established, the changes in elevation depths and volumes of soil loss or accumulation between field visits were computed in Matlab software (Mathworks Inc, Natick, 2014).

## Estimating Sheet and Rill Erosion

The Water Erosion Prediction Project (WEPP) model (D. C. Flanagan & Nearing, 1995) was used to calculate rainfall excess and sheet and rill erosion rates from the contributing catchment. WEPP is a complex process-based soil erosion and hydrologic model uniquely designed for prediction of sheet and rill erosion on agricultural hillslopes. The model accommodates various components of the hydrologic budget and, as a result, simulates overland flow, soil moisture infiltration and redistribution, and evapotranspiration, among other water budget components. Soil hydraulic properties are determined by built-in empirical model based on the soil texture data. The event-based hillslope version of WEPP (D. C. Flanagan, Fu, Frankenberger, Livingston, & Meyer, 1998) uses field characteristics of the representative flow pathway, such as slope, soil properties, land management, growing plants, etc., and meteorological data as inputs into the model. The soil erosion rate along the flowpath, E ($kg \cdot m^{-3} \cdot s^{-1}$), is predicted based on the excess shear stress equation:

$$E = \begin{cases} K_e(\tau - \tau_C)^a, & \tau \geq \tau_C \\ 0, & 0 \leq \tau < \tau_C \end{cases} \quad (3.1)$$

where τ (Pa) is the acting shear stress in the rill, $\tau_c$ (Pa) is the critical shear stress, $K_e$ (s·m$^{-1}$) is the erodibility coefficient, and $a$ is constant (often assumed unity, $a$=1). If the acting shear stress $\tau$ is less than the critical value, $\tau_c$, there is no erosion and E = 0.

Input files for the WEPP model were prepared with the use of online datasets, field measurements, and according to personal communications with Kansas State University extension specialists. Digital Elevation Model (DEM), 1x1 m$^2$ LiDAR product from Kansas Data Access and Support Center (KDASC, 2013), was used in ArcGIS software (ESRI, 2015) to identify representative hillslope flowpath to the gully headcut. Based on major breaks in hillslope contours determined by the GIS analysis, the representative flowpath was divided into ten hillslope segments. Each segment had a constant slope and contained three soil layers. Each layer had unique properties of soil found from the soil database (Sheshukov, Daggupati, Douglas-Mankin, & Lee, 2011), land cover, management, and other operations. Grain sorghum was set as a crop in 2013, while soybeans were used for 2014. No-till option was selected for crop management and tillage operations. The precipitation and antecedent soil moisture content timeseries were built based on 2-minute raingauge and soil moisture sensor readings for each storm event.

The WEPP model outputs at the end of the representative flowpath are surface runoff hydrograph and event-total soil erosion rates. These outputs were collected for each rainfall event in 2013 and 2014. The runoff hydrograph was compared with flow data from ISCO sampler at eight events, and the WEPP model was calibrated by adjusting effective hydraulic conductivity and parameters related to field condition prior to each rainfall event, i.e. soil moisture content, surface roughness after last tillage, and depth of primary tillage layer. The calibrated model showed statistics of Nash-Sutcliffe Efficiency (NSE = 0.86) and percentage bias (pBIAS = -0.5) for total

runoff volume, and NSE = 0.65 and pBIAS = -67.5 for peak runoff rate that were qualified for good to very good performance (Moriasi et al., 2007).

# Results

## Soil Erosion and Accumulation between Soil Surveys

Changes in the ephemeral gully over the study period were obtained based on measured elevation profiles in the headcut (HC in Figure 3.1.b) and channelized parts of the gully ($CS_1$ to $CS_4$) from 15 field visits. In contrast, sheet and rill erosion from the contributing area was calculated by the WEPP model for each rainfall event and aggregated for each period between surveys. Summary of the measured and simulated data for fourteen periods $P_1$ to $P_{14}$ between 15 field surveys consists of a number of rain events, dry days, wet days, total rainfall and runoff, measured ephemeral gully erosion in headcut and channelized parts of the gully, and simulated sheet and rill erosion (Table 3.1).

**Table 3.1 Summary for 14 survey periods. Rainfall (days, events, depth) and gully elevation changes were measured, and surface runoff and sheet and rill erosion were simulated. For erosion data, soil loss is positive, and sediment accumulation is negative.**

| No | Survey period | All days | Wet days | Rain events | Rain-fall (mm) | Surface runoff (mm) | Sheet-rill erosion (kg) | Headcut erosion (kg) | Channel erosion (kg) |
|---|---|---|---|---|---|---|---|---|---|
| $P_1$ | 28 Jun 13 – 11 Jul 13 | 13 | 1 | 1 | 4 | 0 | 0 | 0 | 0 |
| $P_2$ | 11 Jul 13 – 6 Aug 13 | 26 | 11 | 17 | 270 | 131 | 831 | 124 | 645 |
| $P_3$ | 6 Aug 13 – 12 Aug 13 | 15 | 7 | 8 | 146 | 82 | 687 | -26 | 133 |
| $P_4$ | 21 Aug 13 – 19 Sep 13 | 29 | 2 | 3 | 79 | 0 | 0 | 0 | 0 |
| $P_5$ | 19 Sep 13 – 17 Oct 13 | 28 | 3 | 3 | 22 | 0 | 0 | 0 | -95 |
| $P_6$ | 17 Oct 13 – 7 Nov 13 | 21 | 4 | 4 | 53 | 7 | 24 | 0 | -571 |
| $P_7$ | 7 Nov 13 – 9 Apr 14 | 153 | 6 | 6 | 6 | 0 | 0 | 0 | 0 |
| $P_8$ | 9 Apr 14 – 9 May 14 | 30 | 4 | 5 | 56 | 36 | 542 | -50 | -1031 |
| $P_9$ | 9 May 14 – 31 May 14 | 22 | 4 | 5 | 40 | 14 | 84 | 0 | 0 |
| $P_{10}$ | 31 May 14 – 27 Jun 14 | 27 | 4 | 4 | 85 | 46 | 228 | 232 | 1937 |
| $P_{11}$ | 27 Jun 14 – 11 Jul 14 | 14 | 4 | 4 | 28 | 4 | 36 | 0 | 97 |
| $P_{12}$ | 11 Jul 14 – 5 Aug 14 | 25 | 2 | 2 | 16 | 1 | 12 | 0 | -43 |
| $P_{13}$ | 5 Aug 14 – 12 Aug 14 | 7 | 2 | 2 | 47 | 35 | 313 | 0 | -223 |

| | | | | | | | | | |
|---|---|---|---|---|---|---|---|---|---|
| $P_{14}$ | 12 Aug 14 – 14 Sep 14 | 34 | 3 | 3 | 131 | 89 | 687 | 28 | -834 |

Each period contained at least one wet day with at least one rainfall event. The largest total rainfall amount was detected in period $P_2$ (270 mm) followed by period $P_3$ (146 mm), both in 2013, while period $P_{14}$ (131 mm) was in 2014. Based on the number of wet days in each period, periods $P_4$ (2 wet days) and $P_{14}$ (3 wet days) had significantly higher daily average rainfall depth (40 mm/day and 44 mm/day, respectively) than other periods including 25 mm/day in $P_2$. However, while events in $P_2$ and $P_{14}$ caused soil loss, period $P_4$ did not produce any runoff and no soil loss was either calculated or measured. This shows that the factors other than rainfall depth and intensity can be important in gully progression.

Based on the model output, ten periods ($P_2$, $P_3$, $P_6$, $P_8 - P_{14}$) were found to generate runoff into the gully and have associated sheet and rill erosion, however, not all runoff events were able to cause soil loss in the gully. Measurements showed different fluctuations of soil profiles in headcut and channelized parts of the ephemeral gully. Of 14 periods, three periods ($P_2$, $P_{10}$, $P_{14}$) showed soil erosion in the headcut area, whereas the channelized part had soil loss in four periods ($P_2$, $P_3$, $P_{10}$, $P_{11}$). Sediment accumulation was detected between seven surveys ($P_5$, $P_6$, $P_8$, $P_{12} - P_{14}$) for the channelized part and in two periods ($P_3$, $P_8$) for the headcut. Only two periods ($P_2$, $P_{10}$) had erosion and one period ($P_8$) had a deposition in both, headcut and channelized, parts of the gully, while other periods with runoff ($P_3$, $P_5$, $P_6$, $P_{11} - P_{14}$) had opposite soil elevation changes in the gully.

Period $P_2$ had the largest total rainfall and runoff (Table 3.1) and caused soil erosion in all parts of the gully. However, in comparison to $P_2$, $P_{10}$ had had a 65% smaller runoff, an 87% higher headcut erosion, and a 200% higher channel erosion, whereas sheet and rill erosion was 73% lower. Periods $P_3$ and $P_{14}$ with higher rainfall and runoff than in period $P_{10}$ showed opposite soil losses in

headcut and channel while generating similar sheet and rill erosion rates. This link between surface runoff and ephemeral gully erosion signifies the fact that erosion within the gully does not follow main lumped characteristics of rainfall and runoff but rather depends on other factors related to intra-storm characteristics of overland flow and dynamic soil properties.

## Seasonal Changes in the Headcut Area

Headcut elevation maps in Figure 3.4 show seasonal progression of the gully at the beginning and end of 2013 and 2014 campaigns. At the beginning of the study in 2013, the nick point of the gully was well defined with the headcut at about 50 cm and a splash pool at 75 cm marks on the base platform (Figure 3.4.a). The elevation drop at the nick point was about 20 cm and the splash pool area was around 20 x 20 $cm^2$.

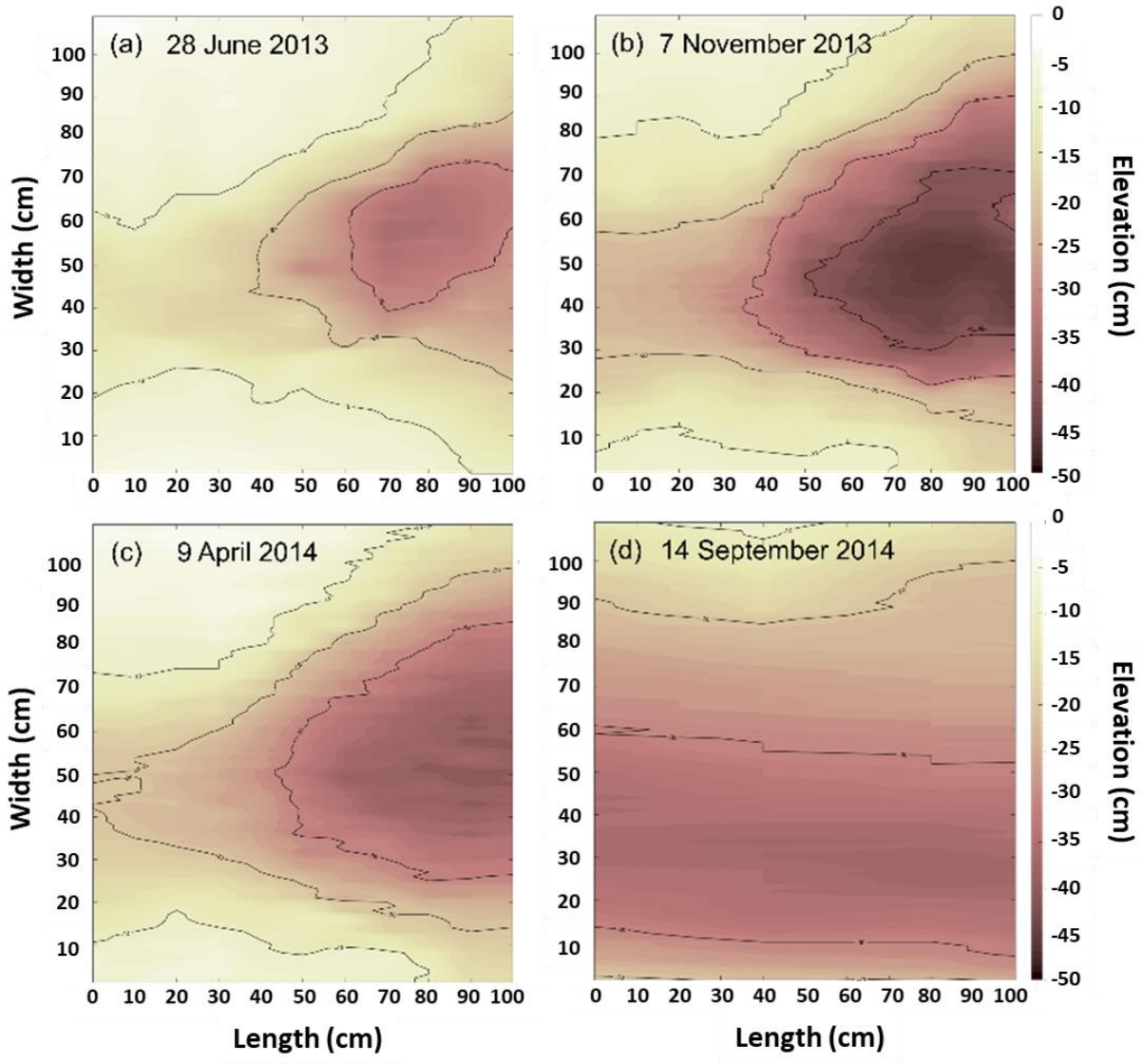


**Figure 3.4 Surface plots of elevation grid within the headcut area obtained by pin-frame measurements at the beginning and end of field campaigns in 2013 (a,b) and 2014 (c,d). Direction of surface runoff is from left to right.**

After one growing season, the headcut area became deeper by 12 cm and wider by 15 cm, whereas the uphill rill started to cut deeper into the soil connecting with the drop point into the splash pool (Figure 3.4.b). The months of cold weather between November 2013 and April 2014 slightly extended the splash pool area and had about 5 cm of sediment deposited in it, however, the nick point stayed at the same place (Figure 3.4.c). Rainfall events during the summer of 2014

generated sufficient runoff into the gully, which eroded the area immediately uphill and connected the incoming rill with the splash pool. As a result, the headcut nick point moved upstream and away from the base platform coverage (Figure 3.4.d), converting the headcut area into a channelized part.

## Elevation Changes along Ephemeral Gully

Elevation profiles at the 10-cm mark on the base platform are shown in Figure 3.5 for seven representative survey periods. Surveys for the periods $P_3$-$P_7$ between 6 Aug 2013 and 9 Apr 2014 were combined into a single thick blue curve due to small changes of surface elevations. In 2013, only a single significant change was observed between field visits on 11 July and 6 August. During the 26-day period ($P_2$ in Table 3.1), there were 11 wet days with 17 rainfall events. Total precipitation of 270 mm generated 131 mm of runoff, mainly in late July, which caused erosion of 1 cm on the sides and almost 15 cm in the center of the gully. The drop was consistent for all cross-sections throughout the base platform in the headcut. Total mass of lost soil from the headcut alone during that period was estimated at 124 kg with the sediment load of 0.10 tn/ha. In August of 2013, 146 mm of rainfall in $P_3$ did not cause erosion, although generated 82 mm of runoff into the gully. The events during periods $P_4$, $P_5$ and $P_6$ had no effect on the headcut while forced a deposition of 666 kg of sediment at the lower part of the channel. Freezing and melting processes during winter of 2014 ($P_7$) smoothed soil surface in the headcut but did not force the gully to advance (Figure 3.4.b,c). Small rainfall events combined with low temperatures in periods $P_7$, $P_8$ and $P_9$ slightly eroded the east bank by 5 cm and shifted the thalweg to the east by 10 cm, but did not deepen the gully (Figure 3.5). Significant sediment deposition during periods $P_6$ and $P_8$ was partially caused by the impact of farming equipment

driving across parts of the gully channel during harvesting and fertilizer application operations resulting in 571 kg and 1031 kg of soil accumulation, respectively.

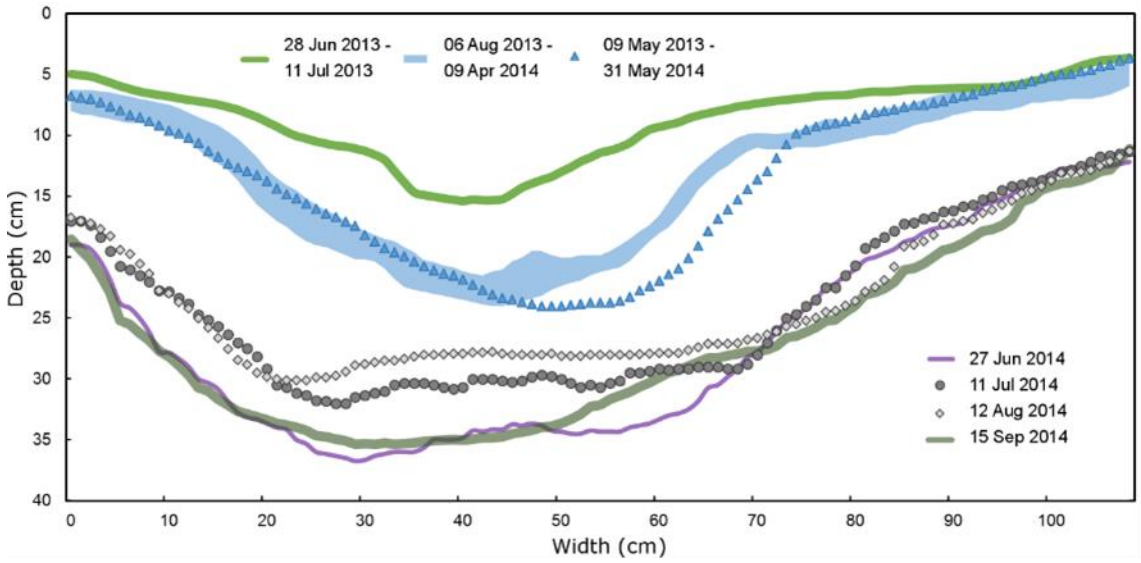


**Figure 3.5 Gully elevation profiles at 10 cm cross-section in the headcut area (see Figure 3.4) for 15 field surveys in 2013 and 2014.**

A substantial change in elevation occurred during a sequence of rainfall events in the first half of June in period $P_{10}$. The depth increased by 10 cm on the sides and close to 15 cm in the thalweg area in $CS_1$. The total soil loss from the headcut area was estimated at 232 kg with the load of 0.19 tn/ha. In addition, most of the sediment deposited in periods $P_5$, $P_6$, and $P_8$ was moved downstream from the channel (erosion of 1937 kg) and banks were undercut forcing their sloping, and gully deepening and widening.

While the headcut was contained within the pin-frame coverage for the duration of the whole year in 2013, runoff events in June 2014 ($P_{10}$) forced the headcut to move uphill from the pin-frame coverage (curves for 31 May and 27 June 2014 in Figure 3.5). After June 2014, the splash pool below the headcut was converted into a channelized part of the gully and started to exhibit the behavior similar to cross-sections $CS_1$ to $CS_4$. The following runoff events caused gully

depth fluctuations due to deposition of incoming sediment from the sheet and rill erosion as result of the insufficient power of runoff to fully transport it through the whole length of the gully. The runoff events at the beginning of September 2014 ($P_{11}$) moved the accumulated in July sediment further downstream.

## Daily Climate Dataseries

Changes in an ephemeral gully depend on the characteristics of rainfall events and specific field conditions. Daily timeseries of precipitation, air temperature, and soil moisture saturation are presented in Figure 3.6. The survey dates are identified by vertical dashed lines. Data collection was interrupted during two periods in 2013 (19-24 August; 18-23 September) due to farming operations affecting the data logger; however, no rainfall and changes to ephemeral gully were detected. Data for winter period $P_7$ are not presented in Figure 3.6 . Readings from eight soil moisture sensors at the depths of 5 cm, 20 cm and 50 cm showed a range of soil moisture condition around the gully.

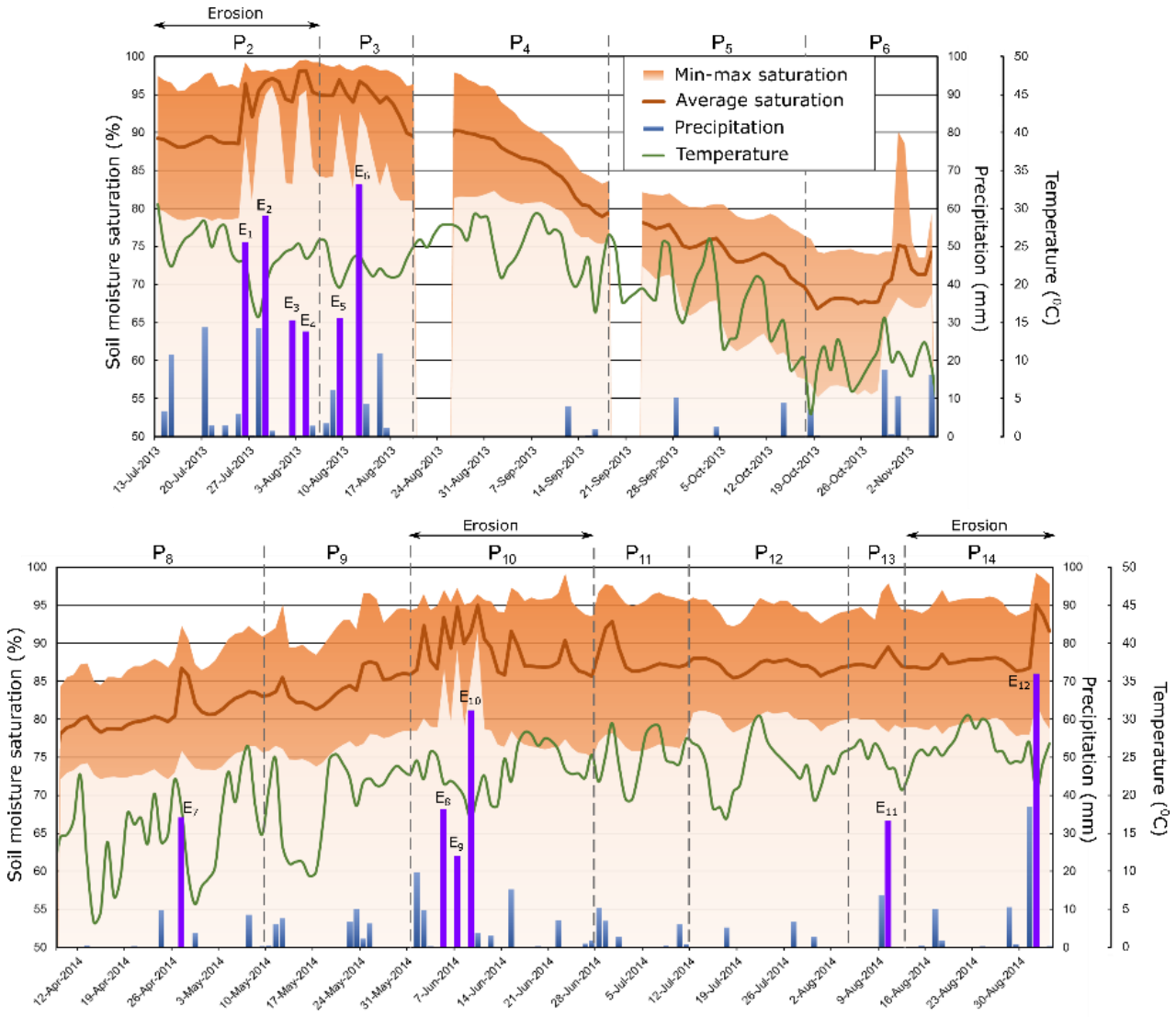


**Figure 3.6 Average daily soil moisture saturation ($m^3/m^3$), temperature (0C), and total precipitation (mm) in 2013 and 2014 campaigns. Twelve significant wet days are identified by purple bars. Survey periods of substantial gully erosion are shown above the chart.**

Of the 291 monitored days in 2013 and 2014 field campaigns (excluding winter period $P_7$), there were recorded 51 wet days and 61 rainfall events with 977 mm of total rainfall. In 2013, the majority of rainfall (416 mm) occurred in periods $P_2$ and $P_3$ in July and August when crop had established canopy cover, whereas in 2014 a series of high intensity rainfall events occurred in early June ($P_{10}$, 85 mm) when the crop was in its early growing stage, and soil was poorly protected

by vegetation. Strong events in early September 2014 ($P_{14}$, 131 mm) also had an impact on soil erosion.

For all periods except $P_5$ and $P_6$, the measured daily average soil moisture saturation was above 75%. The range of soil moisture content was within 15% to 20% for most days excluding eight multi-day periods in 2013 and 2014, in which the lower end of the soil moisture range increased to above 87%. During these days, soil around ephemeral gully profile was considered fully saturated. Six of these eight periods occurred during periods $P_2$ and $P_{10}$ of positive gully erosion.

Seventeen days had daily rainfall higher than 20 mm (Figure 3.6) with 21 identified individual rainfall events. Based on the results from the WEPP model, it was found that only 12 events from 12 days had generated surface runoff. Rainfall on these 12 days is highlighted by purple bars in Figure 3.6, and the selected 12 events presented in Table 3.2. Six significant events $E_1$ to $E_6$ in 2013 occurred in periods $P_2$ and $P_3$ of July and August, while six events $E_7$ to $E_{12}$ of 2014 were distributed over four periods $P_8$, $P_{10}$, $P_{13}$ and $P_{14}$ from April to September.

According to field surveys (Table 3.1), gully erosion occurred during periods $P_2$, $P_{10}$, and $P_{14}$, which makes surface runoff generated during events $E_1$-$E_4$, $E_8$-$E_{10}$ and $E_{12}$ responsible for soil detachment and sediment transport within the gully. Events $E_5$, $E_6$, $E_7$ and $E_{11}$ were not able to cause erosion although soil was highly saturated (saturation higher than 85%). Interestingly, event $E_6$ had one of the highest daily rainfall (67 mm) and produced high surface runoff (11 mm), but was not able to cause changes in the ephemeral gully. Events $E_1$-$E_6$ and $E_8$-$E_{10}$ exhibited a significant reduction in the range of soil moisture content and an increase in its average value, which contrasted with events $E_7$, $E_{11}$, $E_{12}$ that had only a minor increase.

**Table 3.2 Characteristics of twelve significant runoff events with potential to cause soil erosion within the ephemeral gully.**

| Event Number | Survey period | Date | $t_{pa}$ (hr) | $t_d$ (hr) | $\theta_a$ (%) | $q_p$ ($10^{-2}$ $m^3s^{-1}$) | $h_p$ (cm) | $\tau$ (Pa) |
|---|---|---|---|---|---|---|---|---|
| $E_1$ | $P_2$ | 25-Jul-13 | 4 | 6.7 | 84 | 3.8 | 11 | 10.9 |
| $E_2$ | $P_2$ | 29-Jul-13 | 10 | 5.5 | 96 | 1.4 | 7 | 6.7 |
| $E_3$ | $P_2$ | 2-Aug-13 | 2 | 4 | 89 | 1.7 | 8 | 7.4 |
| $E_4$ | $P_2$ | 4-Aug-13 | 4 | 8.3 | 83 | 1 | 6 | 5.9 |
| $E_5$ | $P_3$ | 9-Aug-13 | 3 | 8.8 | 91 | 1.3 | 7 | 6.2 |
| $E_6$ | $P_3$ | 12-Aug-13 | 2 | 5.3 | 80 | 6.2 | 14 | 13.6 |
| $E_7$ | $P_8$ | 27-Apr-14 | 3 | 4 | 75 | 1.9 | 8 | 6.2 |
| $E_8$ | $P_{10}$ | 5-Jun-14 | 5 | 8 | 85 | 1.1 | 7 | 5.2 |
| $E_9$ | $P_{10}$ | 7-Jun-14 | 6 | 6 | 83 | 0.5 | 5 | 3.8 |
| $E_{10}$ | $P_{10}$ | 9-Jun-14 | 7 | 17.8 | 81 | 1.8 | 9 | 6.1 |
| $E_{11}$ | $P_{13}$ | 10-Aug-14 | 3 | 5 | 76 | 1.8 | 8 | 5.9 |
| $E_{12}$ | $P_{14}$ | 1-Sep-14 | 4 | 6.2 | 75 | 12.1 | 16 | 16 |

## Significant Runoff Events

Twelve significant runoff events, selected on the criteria of at least 20 mm daily precipitation and non-zero surface runoff, were analyzed at the hourly time-step using measured rainfall and soil moisture content and WEPP-simulated runoff hydrograph. Seven characteristics were extracted for each significant event (Table 3.2): time at peak runoff hydrograph, $t_p$ (hr); time 1-hour prior to rainfall event, $t_a$ (hr); duration of runoff event, $t_d$ (hr); antecedent soil moisture saturation $\theta_a$ (%) at $t=t_a$; 60-minute peak runoff rate $q_p$ ($m^3 \cdot s^{-1}$) and channel flow depth $h_p$ (cm) at $t=t_p$. The characteristics of peak runoff were selected due to the highest runoff erosion potential and the highest acting shear stress at the peak discharge in a gully during the event. The time from 1-hr prior to rainfall beginning to runoff peak discharge $t_{pa} = t_p - t_a$ identifies runoff intensity and ability to saturate the soil. The duration of runoff td provides the information on the impact of flow in the gully and potential to deposit sediment produced by sheet and rill erosion.

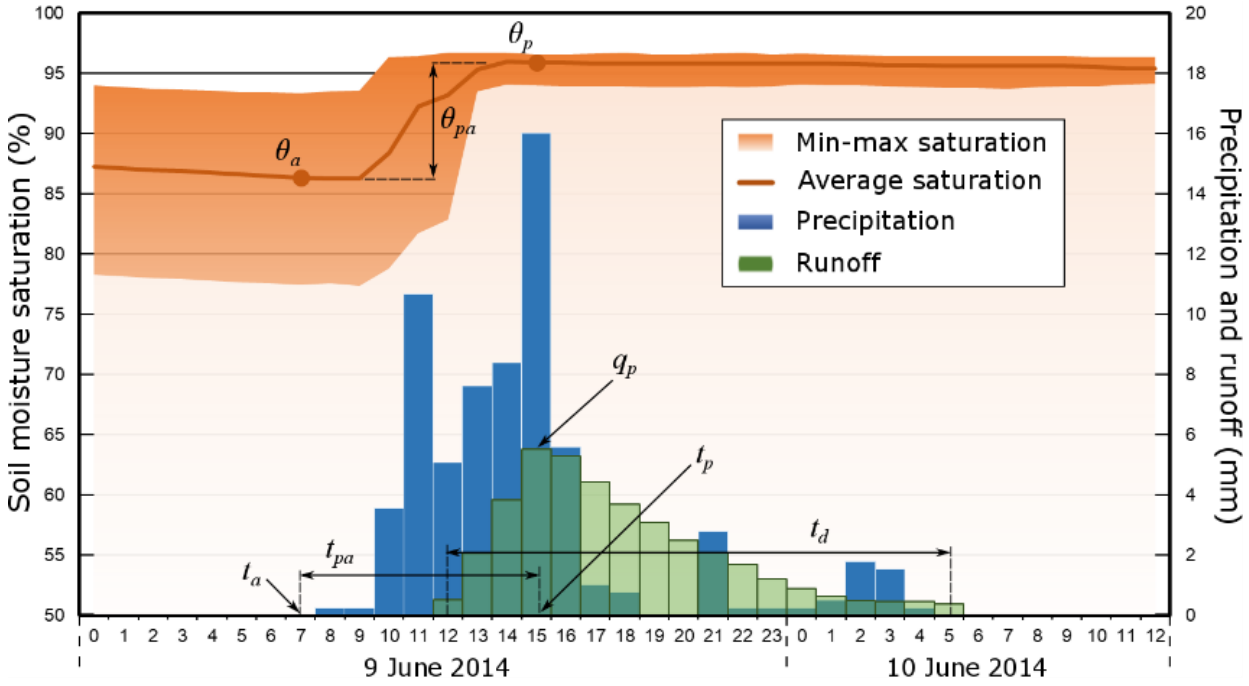


**Figure 3.7 Hourly soil moisture saturation (%), precipitation and surface runoff (mm) for significant runoff event $E_{10}$ on 9-10 June 2014. Major event characteristics ($t_a$, $t_p$, $t_d$, $\theta_a$, $\theta_p$, $q_p$) are also shown.**

Each significant event had unique hydrologic and erosion characteristics of runoff hydrographs. An example of hourly rainfall, runoff and soil moisture distributions for significant runoff event $E_{10}$ is shown in Figure 3.7. The duration of runoff ($t_d$) across all events ranged from 4 to 17.8 hours with an average time of 7.1 hours, whereas the time from rainfall to peak runoff ($t_{pa}$) ranged from 2 to 10 hours on average of 4.4 hours. The event $E_2$ had significantly longer time $t_{pa}$ to peak runoff (10 hours) than the other events while having below average duration of runoff $t_d$. In addition, high antecedent soil saturation (96%) and low rainfall rates prior to peak runoff time $t_p$ during event $E_2$ were able to fully saturate the soil and create favorable conditions for surface runoff while making soil less cohesive and susceptible to soil detachment. In contrast, event E10 was unique by having very long runoff duration (17.8 hours) continuously supported by rainfall that lasted 20 hours (see Figure 3.7). Except for the event $E_2$ with its unique rainfall pattern prior to $t_p$, all other events

yielded longer runoff duration $t_d$ than time to peak $t_{pa}$ while having lower antecedent soil moisture saturation.

Events $E_1$, $E_6$ and $E_{12}$ generated peak discharges $q_p$ into the gully significantly higher than other events, which translated into high depths of peak channel flow $h_p$ within the gully. While events $E_1$ and $E_{12}$ occurred during periods $P_2$ and $P_{14}$ with visible gully erosion, event $E_6$ occurred during the period $P_3$ when no erosion was detected. Therefore, while peak surface flow discharge is important for generating maximum shear stresses on the soil surface during an event, the actual soil erosion may depend on other factors including soil moisture content that change during the event. This will require developing a holistic approach to consider the interactions between channel flow and dynamic soil characteristics.

# Discussion

## Characteristics of the Critical Shear Stress

The analysis of field measurements and surface modeling results revealed twelve runoff events that created favorable conditions for soil erosion within the ephemeral gully. The events produced peak surface runoff that was sufficient to generate hydraulic shear stresses higher than the base critical shear stress of 3.5 Pa for silty clay soil. According to the excess shear stress Equation 3.1 with the base critical shear stress value, all of these twelve events should be able to cause soil erosion within the gully. However, field measurements showed that only events during periods $P_2$, $P_{10}$ and $P_{14}$ made substantial changes in gully profiles, while the other events either did not produce erosion in any part of the gully or showed soil accumulation. This points to the fact that modifications to the critical shear stress definition are required.

The hydraulic shear stress of flow in the gully depends on flow discharge, density of flowing water, channel wetted perimeter, average slope of the gully, and gully bed roughness, according to the Manning's equation. One widely used formula for $\tau$ is the following D. C. Flanagan & Nearing, 1995:

$$\tau=\gamma RS \tag{3.2}$$

where $\gamma$ (kg·m$^{-2}$·s$^{-2}$) is the specific weight of water, $R$ (m) is the hydraulic radius, and $S$ is the average channel slope. Since shear stress $\tau$ depends on the geometry of the channel, the same runoff hydrograph pattern can yield different peak shear stresses calculated at different stages of gully development, i.e. $\tau$ is higher for gullies with the higher hydraulic radius $R$.

The soil critical shear stress coefficient $\tau_c$ defines the critical threshold for τ, at which it allows flow to detach soil particles and cause soil erosion. According to (D. C. Flanagan & Nearing, 1995), the base $\tau_c$ (specified here as $\tau_c^0$) can be defined based on the fractions of very fine sand ($m_{vfs}$) and clay ($m_{clay}$) in the surface soil and is assumed to be constant during the runoff event:

$$\tau_C^0 = \begin{cases} 2.67 + 6.5 \cdot m_{clay} - 5.8 \cdot m_{vfs}, & m_{vfs} \geq 0.3 \\ 3.5, & m_{vfs} < 0.3 \end{cases} \tag{3.3}$$

The laboratory experiments on soil erosion (C. Huang & Laften, 1996; S. Nouwakpo & Chi-hua Huang, 2012; S. K. Nouwakpo, Huang, Bowling, & Owens, 2010) and tests on soil erodibility parameters (A. Al-Madhhachi, Fox, Hanson, Tyagi, & Bulut, 2014; Regazzoni, Marot, & Nguyen, 2010) among other evidence in the literature showed the dependency of erodibility parameters, including $\tau_c$, on soil properties other than the texture in (3), such as soil moisture content, pore pressure, seepage forces, soil cohesion, etc. In addition, (Tebebu et al., 2010) showed that soil detachment can depend on (antecedent) soil moisture content prior to the beginning of the rainfall event. Following these considerations, one can express the critical shear stress as a product of two terms, $\tau_c^0$ and $\tau_c^1$:

$$\tau_c = \tau_c^0 \cdot \tau_c^1\left(\theta_a, \theta_p, t_p, t_d, \ldots\right) \tag{3.4}$$

where $\tau_c^0$ was defined by Equation 3.3, and $\tau_c^1$ is a function of event specific soil and peak flowrate characteristics.

Taking into account that acting shear stress is higher than nominal critical shear stress ($\tau_c^0$) for all twelve significant runoff events (see Table 3.2), the following functional form of $\tau_c^1$ was proposed depending on the change of soil moisture saturation from the antecedent condition at $t_a$ to that at the peak runoff time $t_p$:

$$\tau_c^1 = 1 + \beta\left(\frac{\theta_p - \theta_a}{t_p - t_a}\right)^b = 1 + \beta \cdot i^b, \tag{3.5}$$

where $i=(\theta_p - \theta_a)/(t_p - t_a)$ is the rate of soil moisture change from before the event to peak flowrate, and coefficients $\beta > 0$ and $b > 0$ are constants.

According to Equation 3.5, the critical shear stress remains close to the base value $\tau_c^0$ if there was a very small change in soil moisture content from antecedent to peak time. This may occur for two conditions: (i) if soil was already pre-wet prior to the rainfall event (antecedent saturation is high), and most rainfall was converted to runoff, or (ii) if the raising limb of runoff hydrograph took long time, hence runoff reached its peak value very slow, and the denominator $t_{pa}$ in Equation 3.5 had high value. In both cases, soil becomes very saturated before the peak runoff is reached, which reduces soil cohesion and promotes soil particle detachment. This situation is consistent with the findings by S. K. Nouwakpo & Huang (2012), which postulated that under saturated condition channel bottom appeared to behave as a fluidized bed with rates of soil erosion much higher than defined with standard or base critical shear stress. For other situations when $i > 0$ in Equation 3.5, $\tau_c$ is larger than the base value $\tau_c^0$, which requires higher runoff rates and larger values of $\tau$ to case soil erosion.

## Applicability of the Critical Shear Stress Function to Field Experiment

The proposed functional dependency of $\tau_c$ on soil moisture change $i$ in Equation 3.5 was tested on the collected data for 12 significant runoff events (Figure 3.8). The values of shear stress τ acting on the bottom of the gully were determined based on the Equation 3.2 using peak runoff rates, shape and slope of the channel, and flow depth specific to each significant event (Table 3.2). The rate of soil moisture change $i$ was calculated using the recorded soil moisture data and $t_{pa}$.

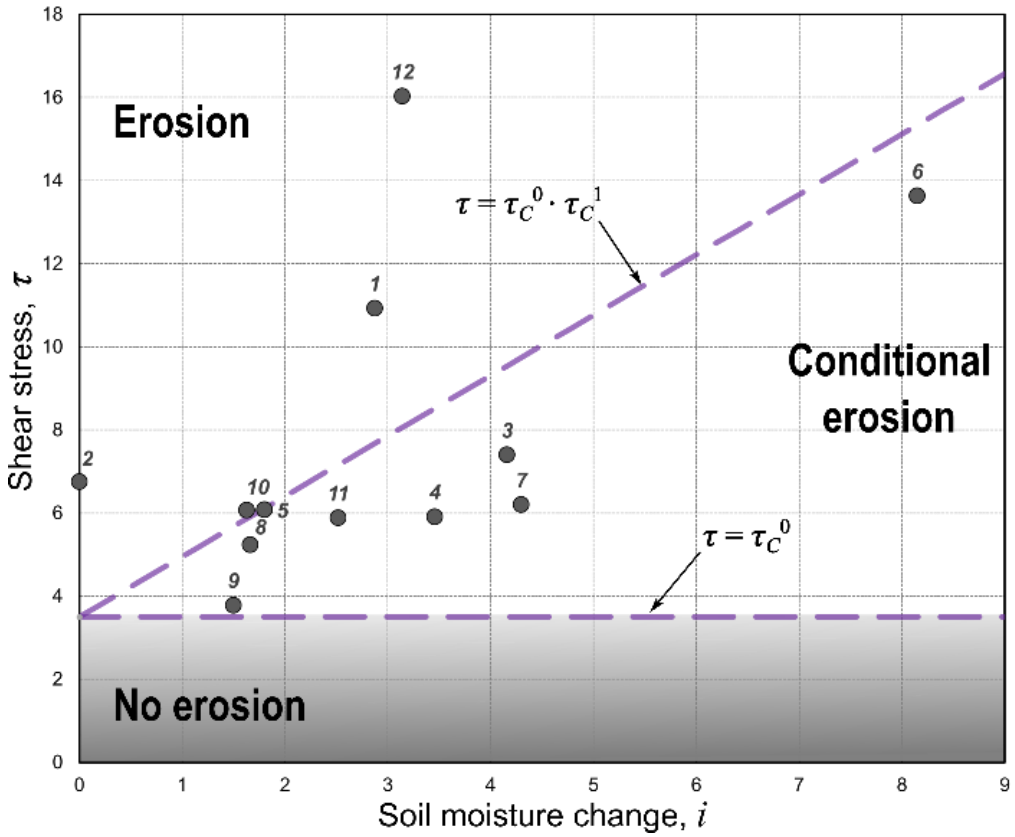


**Figure 3.8 Acting shear stress in the headcut area versus the ratio of the differences in soil moisture saturation and time prior to a rainfall event (antecedent condition) and at the peak runoff rate for runoff events. τc0 = 3.5, b = 1, and β = 0.4.**

For all events, $\tau$ was found greater than $\tau_c^0$ = 3.5, while $i$ varied from 0 to 8.1. Ten events had a value of $i$ between 1.5 and 4.5 with the exclusion of events $E_2$ and $E_6$. Event $E_2$ had high antecedent soil moisture saturation that forced $i$ to be close to zero with $\tau$=6.7. Event $E_6$ had low

$t_{pa}$, low $\theta_a$, which caused $i$ to be greater than 8 and had a high $\tau$ of 13.6. In addition, event $E_{12}$ had extremely high $q_p$ and $\tau$=16, but low $\theta_a$ and $t_{pa}$.

Based on the characteristics of eight events during three survey periods $P_2$, $P_{10}$, $P_{14}$ when gully erosion was detected, four events were found to cause soil erosion more likely than the other events: $E_1$ and $E_2$ in $P_2$, $E_{10}$ in $P_{10}$, and $E_{12}$ in $P_{14}$. Event $E_{12}$ was the only runoff event in $P_{14}$; $E_{10}$ had the highest $\tau$ comparing to other runoff events in $P_{10}$; $E_1$ had the highest $\tau$ in $P_2$, while $E_2$ exhibited the fully saturated condition prior to the rainfall. These events are presented in the upper left half of the chart in Figure 3.8, where the excess shear stress Equation 3.1 would show soil erosion if the critical shear stress coefficient were to depend on soil moisture change $i$ in Equation 3.4.

To follow the framework and functional equations defined above, the whole domain in Figure 8 can be divided into three zones:

1) a zone of definite erosion ($\tau > \tau_c^0 \tau_c^1,\ \tau_c^1 > 1$);
2) a zone of no erosion ($\tau < \tau_c^0$); and
3) a zone of conditional erosion ($\tau_c^0 < \tau < \tau_c^0 \tau_c^1,\ \tau_c^1 > 1$).

The four events that caused soil erosion ($E_1$, $E_2$, $E_{10}$, $E_{12}$) fall into the zone of definite soil erosion if $b$ = 1 and $\beta$ = 0.4 in Equation 3.5. This yields the general form of critical shear stress as $\tau_c$ = 3.5 (1 + 0.4 $i$). The other significant events form Table 3.2 were placed into the zone of conditional erosion. Other events from 2013 and 2014, not presented in Table 3.2, had either no runoff ($\tau = 0$) or low $q_p$ and fell into the zone of no erosion.

## Factors Affecting Ephemeral Gully Erosion

Many intra-storm factors can contribute to soil loss within an ephemeral gully. The most considered are peak runoff depth and peak runoff intensity due to their effect on submerged shear forces that act on soil particles in a headcut zone from the inflowing overland water. High antecedent soil saturation decreases infiltration, reduces time of concentration, and promotes surface runoff from a contributing catchment to reach a higher peak rate faster. Specifically for silty clay loams, higher soil moisture saturation generally decrease cohesion between soil particles, which may affect soil erodibility properties.

This study evaluated the change in soil moisture content during a rainfall event and showed that factors related to soil moisture condition can affect soil detachment as much as the hydraulic shear forces. The change in soil moisture can be viewed as an indicator of how rapid soil becomes fully saturated and loses its cohesion, which forces a channel bed to behave similarly as a fluidized bed with much higher potential for particle detachment (S. K. Nouwakpo & Huang, 2012). Similar findings on a link between antecedent moisture content and erosion rates were reported by Tebebu et al. (2010).

The mechanism of the impact of soil saturation on soil erosion has yet to be fully understood, but studies reported influence of subsurface seepage forces on soil stability and decrease of the critical shear stress (A. Al-Madhhachi et al., 2014; G. Fox & Wilson, 2010; S. K. Nouwakpo & Huang, 2012). These forces can cause side walls to slide and channel to meander. Two other factors that are specific to the studied gully, high water table and compacted layer below the soil surface (or a plow pan), could also be contributed to gully erosion by decreasing the time to reach full saturation around the gully. Planted soybeans in 2014, compared to grain sorghum in 2013, may have higher rainfall interception due to increased canopy cover and so may cause lower

runoff thus decreasing hydraulic forces of flow in the gully. These factors in addition to concentrated flow and soil moisture condition must be considered in future field, laboratory and modeling studies on ephemeral gully erosion.

## Conclusions

This study examined intra-storm characteristics and impacts of surface runoff and soil saturation on the development of an ephemeral gully on a cultivated crop field under no-till management in Central Kansas. Data collection included continuous sub-hourly precipitation, soil moisture content, soil temperature, and 15 field surveys of ephemeral gully cross-sectional profiles in headcut and channelized parts. Soil losses and sediment accumulation within the gully were calculated based on cross-sectional profiles for each period between the surveys. Rainfall excess from the contributing catchment was calculated with the WEPP model for all runoff events and validated on channel flow measurements. Analysis of hourly and daily results were conducted for all precipitation events during crop growing seasons in 2013 and 2014 and ephemeral gully conditions were documented. Factors affecting soil erosion within the ephemeral gully were discussed.

The results of the study can be summarized as the following:

- Of fourteen survey periods, soil erosion was observed during three periods in headcut and four periods in the channelized part of the ephemeral gully, whereas sediment accumulation was detected during two periods in headcut and six periods in channelized part. Fluctuations of soil loss and accumulation in headcut area were mainly caused by physical interactions between hydraulic shear forces at soil surface, soil condition, and sediment load. In addition to physical factors similar to the ones in

headcut, the channelized part of the gully experienced elevation changes due to side wall collapsing, channel meandering, farming operations, and soil crusting.

- Twelve significant runoff events from six survey periods were identified to create hydraulic shear stresses at the peak flow rate higher than the base critical value. Under standard considerations all of these events must cause soil erosion, however, it is contradictory to observed erosion in three out of the six periods.
- Intra-storm flow and soil characteristics were found to provide additional insight on channel development. Hydraulic shear stress and soil moisture content at peak flow rate, antecedent soil moisture content, and channel geometry were examined at twelve significant runoff events. The analysis provided the basis to extend the definition of the critical shear stress and explain the reasons for soil erosion in four significant events.
- One functional form of the critical shear stress function was suggested by incorporating the changes in soil moisture content from its antecedent condition to the time of highest runoff intensity and tested with collected data. This form allowed the excess shear stress equation to define the specific $\tau$ versus $i$ function and determine the zones of definite erosion, conditional erosion, and no erosion for the studied ephemeral gully.

Future studies in other agricultural dominated areas are needed to develop a better understanding of physical mechanisms associated with gully progression. In addition to the established factors of antecedent soil moisture content and peak runoff rate, other physical factors (such as temperature, pressure differences, etc.) that vary during the event must be considered and analyzed experimentally and by modeling. This will provide additional insight into the gully erosion process and improve mitigation strategies for soil loss reduction from agricultural fields.

# Chapter 4 - Evaluating the Effects of Subsurface Seepage and Drainage on Channel Development with Two-Dimensional Numerical Modeling

## Introduction

Today, the world is much more concerned about the impacts of soil erosion and how it can be controlled to sustain agriculture. Soil erosion can be considered one of the major environmental problems caused by the current use of conventional practices on agricultural fields. There are five types of soil erosion: raindrop erosion, sheet erosion, rill erosion, gully erosion, and stream bank erosion. Erosion associated with overland concentrated flow includes erosion from rills, ephemeral gullies, and classical gullies. Also important are the processes of soil stability for the gullies and streams.

Associated with concentrated flows are two major factors that affect erosion processes: (i) the amount and intensity of the concentrated flow, and (ii) the mechanical properties of the soil. Other factors can also impact flow characteristics and soil properties. The concentrated flow characteristics differ from every gully due to different catchment size, shape, and slope, including the amounts of runoff controlled by soil properties, vegetation, and management. For similar flow conditions and the same field, soil erosion rates can also be different because of the differences in soil mechanical properties to withstand erosion at any particular time. A. Knapen & J Poesen, (2009) investigated the influence of soil erodibility parameters on the initiation points of rills and gullies. They found a significant relationship between soil properties and soil erosion. This relationship that has proven that topographic parameters such as slope and

catchment area are not the only major parameters. The antecedent soil moisture content, vegetation, management practices and hydrologic regime can also be different from soil mechanical properties, and they can increase or decrease soil erodibility.

Both experimental and modeling studies have been carried out to investigate the influence of many of these parameters such as the rainfall amount and runoff, soil type and texture, topography, and land management (A. Capra et al., 2009; Valentin et al., 2005; R. Wells et al., 2009; Y. Zhang et al., 2007). Special attention was also given to the influence of the soil hydrologic regimes (such as seepage/drainage) on the erosion processes. Investigating the process of particle detachment by lift forces, B. N. Wilson & Barfield (1986) applied the Einstein's bed load transport concept (Einstein, 1950) and calculated the probability of lift force exceeding particle weight. B. Wilson, (1993a) further continued his approach of fundamental analysis of forces involved in the detachment process and determined the critical shear stress by equilibrating moments acting on the particle. What's more, the cohesive moment was related to the weight of the particle; then, detachment rates were associated with the probability of evidence of turbulent forces. This approach was validated with experimental data (B. Wilson, 1993b). Further exploring the problem and developing a relationship with the parameters of B. Wilson (1993b) model as a function of seepage forces, A. Al-Madhhachi, Fox, Hanson, Tyagi, & Bulut (2013) conducted jet and flume tests to prove such relationship. Their results showed the strong nonlinear dependence of model parameters (proportional to the critical shear force and the erodibility) on the seepage forces.

Furthermore, series of other experiments showed the dependence of the erosion process on the soil moisture and seepage conditions. Vanapalli, Fredlund, Pufahl, & Clifton (1996) measured the soil shear strength for soils with different levels of saturation and the bulk density

to distinguish the relationship between the critical shear stress, measured shear stress and characteristics of the water retention curve. However, seepage forces were not considered in this study. Bryan, Hawke, & Rockwell (1998) conducted an experiment to assess the influence of subsurface soil moisture conditions on the erosion process and found that saturation significantly increases soil erodibility and critical shear stresses. Gabbard, Huang, Norton, & Steinhardt (1998) carried out an experimental study with flume and controlled seepage/drainage conditions. They found that the seepage condition resulted in significantly higher erosion rates. It was assumed that this increase can be possibly explained by the reduction of the critical shear stress due to seepage. Evaluating the influence of matric suction on bank stability, Simon, Curini, Darby, & Langendoen (2000) found that matric suction had a major influence on the critical shear stress of the bank slope. However, they did not discuss the critical shear stress of particle detachment from hydraulic forces. A flume experiment, which was conducted by Owoputi & Stolte (2001) with controlled seepage, showed a strong dependence of the erosion rates on the seepage condition. They suggested that that runoff from rainfall and seepage cannot be used as a major predictor and that soil erodibility should account for the seepage condition. Apart from finding a significant influence of seepage forces on the erosion process of the hillslope, C. Huang et al. (2002) noted that the detachment process depended on the seepage condition, which significantly increases soil erodibility. Rockwell (2002) noticed the influence of soil saturation on the erosion process and particularly the groundwater level prior to the rainfall event. They found that the more the soil shear strength decreases, the more the soil water pore pressure increases. In another research, Lobkovsky, Jensen, Kudrolli, & Rothman (2004) studied the effects seepage erosion of non-cohesive materials on the designed hillslope model. The change in shear stress was accounted, as an additional term from the seepage, as one of the forces acting on

the particle. S. K. Nouwakpo et al. (2010) found a significant influence of the hydraulic gradient on the critical shear stress. By conducting the flume experiment, researchers determined that a positive hydraulic gradient decreases critical shear stress. Studying the effect of seepage forces on cohesionless sediment detachment rate, X. Liu & Chiew, 2014; X. Liu & Chiew (2012) found that while downward seepage increases critical shear stress, upward seepage decreases it.

Results of the several experiments have shown that currently used modeling approaches with constant critical shear stress cannot account for the hydraulic conditions. The goal of this study is to develop a modeling approach of the channel erosion by calculating cross-sectional changes while considering the hydraulic regime of the subsurface flows.

## Physical Model

A well-recognized and widely accepted approach for estimating soil erosion rates, due to concentrated water flow, is based on the excess critical shear stress equation shown below (G. Hanson, 1990; Partheniades, 1965):

$$E = K_e \cdot (\tau - \tau_{cr})^a \tag{4.1}$$

where $E$ is the erosion rate in (kg/s/m$^2$), $K_e$ is the soil erodibility (s/m), $a$ is the dimensionless parameter usually taken as 1, $\tau$ is the acting shear stress (Pa), and $\tau_{cr}$ is critical shear stress. Equation (4.1) that the soil erosion rate $E$ is proportional to the difference in shear stresses if the acting shear stress is higher than the critical shear stress. The soil erosion rate refers to the rate at which the soil is being detached from the bottom of the channel. The definition of this rate is of a particulate interest in the area of soil erosion. The acting shear stress depends on hydraulic properties of surface flow, while the critical shear stress can be determined as a property of the soil and may be estimated from regression equations (Clark & Wynn, 2007; D. C. Flanagan, 2012; Julian & Torres, 2006; A. Knapen et al., 2007). It is usually assumed that the critical shear

stress in Equation 4.1 depends on soil properties that are held constant during the runoff event. Such definition of the constant critical shear stress is called CCSS. Even though this assumption is generally valid, some mechanistic models and experiments showed that seepage and near seepage conditions could significantly decrease the critical shear stress value (A. Al-Madhhachi et al., 2014; A. Al-Madhhachi et al., 2013; C. Huang & Laften, 1996; B. N. Wilson & Barfield, 1986).

Proposed by B. Wilson (1993a) and further modified by A. Al-Madhhachi et al. (2014) to account for seepage forces, the mechanistic model of soil detachment assumes that a soil particle can be detached when the momentum of the drag force applied to some points on the particle exceeds the momentum of all other forces holding the particle in place. This model may represent the critical shear stress as a function of the seepage gradient *I* (A. Al-Madhhachi et al., 2014):

$$\tau_{cr} = \frac{k_r}{K_0} g(\rho_s - \rho_w) d(K_{ls} - K_s + f_c) \tag{4.2}$$

$$K_s = I \frac{\rho_w}{(\rho_s - \rho_w)} \frac{\cos(\alpha_s)(l_2 - l_5 S_w)}{l_3 + l_4 \frac{K_L}{K_f}} \tag{4.3}$$

where $I$ is the seepage gradient, $g$ is the acceleration of gravity, $\rho_s$ is the particle density, $\rho_w$ is the density of water, $\alpha_s$ is the angle of the slope of the channel bed, $l_2, l_3, l_4$ and $l_5$ are the lengths of the momentum forces acting on the particle, $d$ is the particle diameter, and $k_r$, $K_0$, $K_{ls}$, $f_c$, $S_w$, $K_L$, $K_f$ are auxiliary parameters of the model defined by particle geometry and flow conditions. The details of the Equation 4.2 derivation and parameter definition can be found at A. Al-Madhhachi et al. (2014).

Substituting Equation 4.3 into Equation 4.2 gives the following equation:

$$\tau_{cr} = \frac{k_r}{K_0} g(\rho_s - \rho_w) d(K_{ls} - I \frac{\rho_w}{(\rho_s - \rho_w)} \frac{\cos(\alpha_s)(l_2 - l_5 S_w)}{l_3 + l_4 \frac{K_L}{K_f}} + f_c) \tag{4.4}$$

Rearranging the terms in Equation 4.4 yields the critical shear stress equation for a single particle in a linear function form of the seepage/drainage gradient *I* following the Wilson's model (B. N. Wilson & Barfield, 1986):

$$\tau_{cr} = A - BI \tag{4.5}$$

$$A = \frac{k_r}{K_0} g(\rho_s - \rho_w) d(K_{ls} + f_c), \tag{4.6}$$

$$B = \frac{k_r}{K_0} g(\rho_s - \rho_w) d \frac{\rho_w}{(\rho_s - \rho_w)} \frac{\cos(\alpha_s)(l_2 - l_5 S_w)}{l_3 + l_4 \frac{K_L}{K_f}} \tag{4.7}$$

If *I* is positive, the form of $\tau_{cr}$ in Equations 4.5-4.7 accounts only for the seepage force acting on the particle when water seeps from the soil. However, it is proposed to include the force *I* that can be positive and negative and to account for both seepage and drainage. This proposition does not change the equation even though it would affect only the sign of the seepage/drainage gradient *I*. The linear form of Equation 4.5 forces $\tau_{cr}$ to cross the zero value at some positive value of *I* (Figure 4.1.a) and assumed to be equal to zero for higher values of *I*. In that case, once $\tau_{cr}$ is zero, any applied hydraulic force would cause a particle to detach. This finding is identical to the assumption reported by S. Nouwakpo, Chi-hua Huang, Laura Bowling, & Phillip Owens (2010) who noted that when a certain soil saturation or seepage force is reached, the soil starts to behave as a fluidized bed with very low resistance to soil detachment.

The relationship of the critical shear stress as a function of seepage/drainage gradient, which is presented in Figure 4.1.a, may be considered as a critical shear stress function which describes the detachment process of some imaginary particles sitting at the bottom or at the side of a channel. Unarguably, many particles have different sizes and compounds, and the geometry and flow conditions are constantly changing, thus suggesting that the critical shear stress function would look like a set of lines for various particles at a different state of erosion with a

different state of seepage/drainage. However, the common tendency towards the proposed shape should be seen in the averaged process of particle detachment.

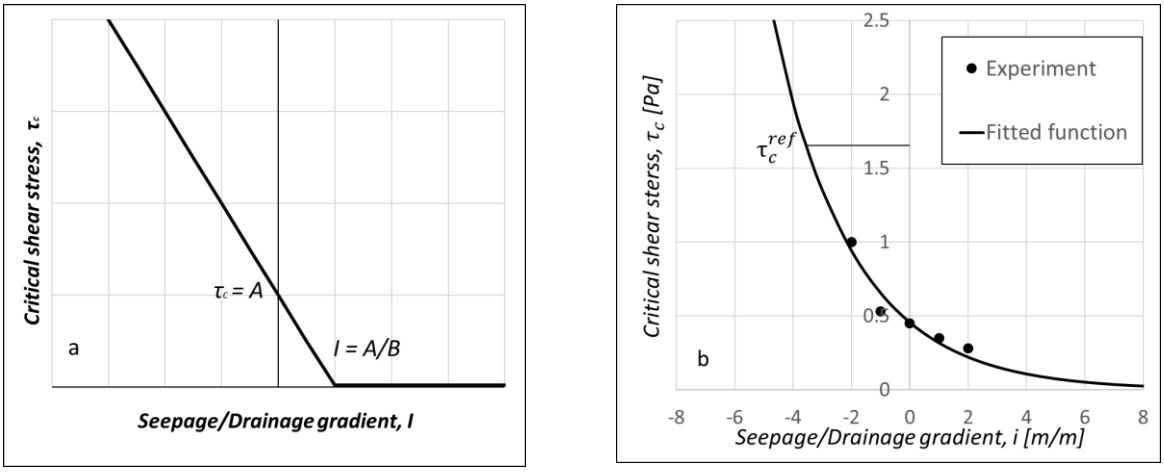


**Figure 4.1 Critical shear stress as a function of seepage/drainage gradient: (a) representative linear form according to Equation 4.5, and (b) non-linear form shown in Equation 4.8 where $\tau_{cr\,0}$= 0.455 and *k*=0.362. The experiment data from (S. Nouwakpo et al., 2010) are also shown in (b).**

The experiment of S. K. Nouwakpo & Huang (2012) showed that the rate of change of the critical shear stress varied with the change in the seepage gradient *I* (Figure 4.1). The experiment of A. Al-Madhhachi et al. (2013) indicated that the proxy to the critical shear stress of Wilson's model (parameter $b_0$) also had a nonlinear behavior for positive values of seepage gradients. These experiments suggest that a nonlinear model may be developed in order to represent the critical shear stress function for the soil. Considering the shape of the critical shear stress function derived from the mechanistic model, the exponential function can be proposed as a first approximation:

$$\tau_{cr}(I) = \tau_{cr\,0} \cdot e^{-kI} \tag{4.8}$$

where $\tau_{cr}(I)$ is the critical shear stress as a function of the seepage/drainage gradient ($I$), $k$ is the model parameter related to the rate of change of the critical shear stress with the change of $I$, and $\tau_{cr\,0}$ is the value of critical shear stress at the point where the system is in equilibrium and no

seepage or drainage into the soil ($I = 0$). Additionally, $\tau_{cr\,0}$ may further be approximated as $\tau_{cr\,0} = \varepsilon\, \tau_c^{ref}$ which when substituted to Equation 4.8 gives the following equation:

$$\tau_{cr}(I) = \varepsilon\, \tau_c^{ref} \cdot e^{-kI} \tag{4.9}$$

where $\tau_c^{ref}$ is the reference critical shear stress (in Pa) determined from regression curves or standard forms for various soils, and $\varepsilon$ is the coefficient that can be found based on the experimental data. The reference critical shear stress can also be described as a value of the critical shear stress at a certain seepage/drainage gradient *I* used in testing regression formulas.

## Mathematical Model

To determine a seepage/drainage gradient at the channel bed surface in Equation 4.5, the soil pore pressure gradients must be calculated by solving the problem of soil moisture and pressure redistribution. The Richards's equation (Equation 4.10) was used to calculate the water redistribution and infiltration into the soil profile:

$$\frac{\partial \theta}{\partial t} = \frac{\partial}{\partial z}\left[K(h)\frac{dh}{dz}\right] - \frac{\partial K(h)}{\partial z} + \frac{\partial}{\partial x}\left[K(h)\frac{dh}{dx}\right] \tag{4.10}$$

where $\theta$ is the volumetric water content, $h$ is the matric potential, $K$ is the hydraulic conductivity as a function of matric potential, z is the vertical coordinate, *x* is the horizontal coordinate, and t is the time. The porous medium was assumed rigid and homogeneous within each layer.

The functions of the soil water content and hydraulic conductivity, which depends on soil matric potential, are expressed according to the Van Genuchten (1980) form:

$$\theta(h) = \frac{(\theta_s - \theta_r)}{(1+|\alpha h|^n)^m} + \theta_r \tag{4.11}$$

$$K(h) = K_s \frac{[1-|\alpha h|^{n-1}(1+|\alpha h|^n)^{-m}]^2}{(1+|\alpha h|^n)^{m/2}} \tag{4.12}$$

where α [1/cm], *n*, and *m* are empirical constants.

Three soil layers, which were introduced to specify the heterogeneity of the domain, were placed horizontally slightly sloped toward the channel area (Figure 4.2). The top layer represents the topsoil on the agricultural field with relatively higher values of the hydraulic conductivity, while the two other layers underneath the top layer represent natural vertical heterogeneity. Also, the middle layer can be set with low hydraulic conductivity to mimic the effect of a plow pan prevalent on agricultural fields under the conventional tillage practice. It was assumed that each soil within the domain has homogeneous properties so that the symmetry of the channel erosion process can be assumed, including only half of the soil domain used for the calculations of the water pore pressures.

An initial condition for the whole domain was a uniform ambient pressure head distribution:

$$t = 0\text{: } h = h_a$$

According to the sides of the domain specified with letters A-E (Figure 4.2), boundary conditions were specified:

- Boundary AE zero horizontal and zero vertical fluxes,

$$AE\text{: } q_x = 0, q_z = 0$$

- Boundary AB zero horizontal flux, vertical flux defined by the precipitation (ignoring evaporation due to relatively short duration of the modeled event),

$$AB\text{: } q_x = 0, q_z = q_{top}(t)$$

- Boundary BC head based boundary condition according to the depth of the flow,

$$BC\text{: } h = z - z_w(t)$$

- Boundary CD zero horizontal and zero vertical fluxes,

$$CD\text{: } q_x = 0, q_z = 0$$

- Boundary DE is a zero-horizontal flux, while the vertical flux can be either unit gradient or impervious,

$$DE:\ q_x = 0, \frac{\partial h}{\partial z} = 0\ \ or\ \ q_z = 0$$

where $q_x$ and $q_z$ are fluxes in the horizontal and vertical directions, respectively. The initial channel shape was assumed as a trapezoidal channel. However, during the computation, the process channel assumes the "U" shape (see Figure 4.2).

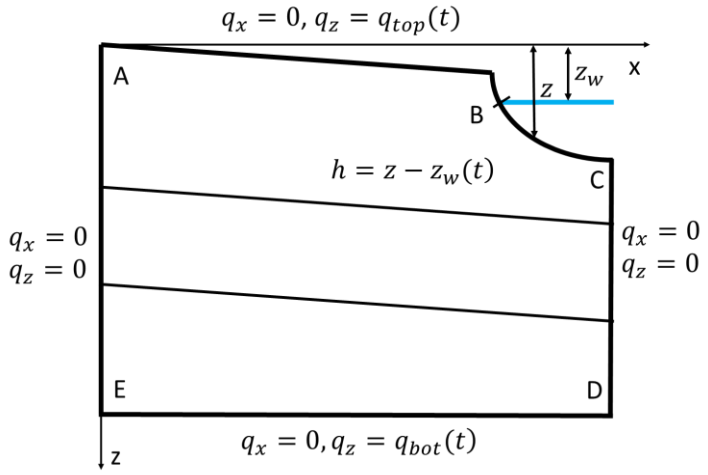


**Figure 4.2 Simulation domain and corresponding boundary conditions at each segment of the domain boundaries.**

The rate of boundary BC retreat can be described by the soil eroding at the channel bed due to water flowing into the channel. The excess erosion rate equation (Equation 4.1) can be applied to calculate the retreat rate (propagation in time of the line representing the channel boundary) in the normal direction at any point of the wetted perimeter:

$$\left.\frac{dl}{dt}\right|_{normal} = E = K_e \cdot (\tau - \tau_{cr})^a \qquad (4.13)$$

where $\tau$ is the acting shear stress variable along the wetted part of the channel wall. For natural channels, $\tau$ may be described by a symmetrical function of distance along the wetted perimeter

from the water surface (Foster & Lane, 1983; Graf, 1984) with the maximum value at the center and zero at the water surface (see Figure 4.3).

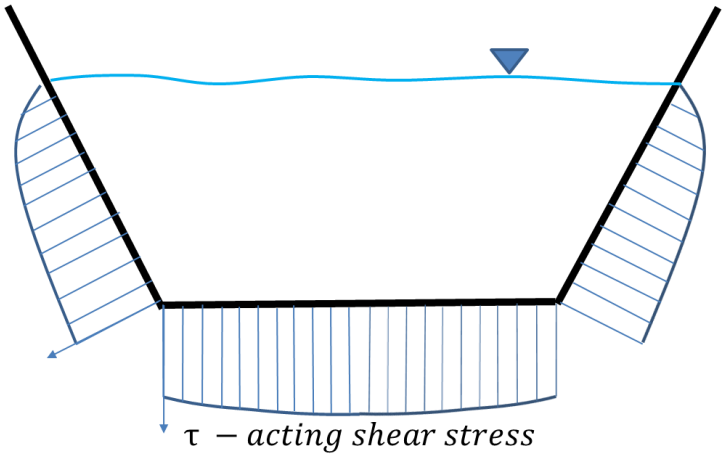


**Figure 4.3 Distribution of the acting shear stress at the channel bottom.**

There are also experimentally determined distributions for rectangular and trapezoidal channels (Kabiri-Samani, Farshi, & Chamani, 2012; Khatua & Patra, 2007; Khodashenas, Abderrezzak, & Paquier, 2008; Knight, Demetriou, & Hamed, 1984). Trapezoidal and some natural channels may have a distribution with a W-shape, thus resulting in the maximum acting shear stresses in the corners of the channel. Given that the distribution has a non-uniform shape with the distribution rapidly reaching an average value and then gradually increasing, uniform distributions are often assumed across the cross section (D. C. Flanagan, 2012). In that case, the average acting shear stress can be calculated with the equation shown below:

$$\tau = \gamma RS \tag{4.14}$$

where $\gamma$ is specific gravity of water, R is the hydraulic radius of the channel, and S is the channel bed slope.

The hydraulic radius *R* can be implicitly determined with Manning's equation:

$$q = \frac{A_{cs} R^{2/3} S^{1/2}}{n_m} \tag{4.15}$$

where $q$ is the flux known for each time step channel flow ($m^3/s$), $A_{cs}$ is the cross-sectional area ($m^2$), $R$ is the hydraulic radius (m), $n_m$ is Manning's n ($m^{1/6}$). Critical shear stress $\tau_{cr}$ is defined as a function of the hydraulic gradient, based on Equation 4.9.

The presented mathematical formulation of the channel erosion problem is nonlinear; it requires solving the partial differential equation for the flow in a porous domain with the moving boundary. Thus, the numerical solution is based on the iterative procedure with the use of the finite difference method for the Richards equation as well as resizing the domain during each time step.

## Numerical Scheme

Three soil layers compose a soil domain with layer centered node allocation. The backward-implicit approximation scheme (Figure 4.4) was used to discretize Equation 4.10. The soil node grid consisted of the nodes with the vertical and horizontal spacing at 1 cm for the area around gully defined by the 50 cm region from the center of the gully. Nodes beyond this region were spaced at 10 cm in order to save computation time.

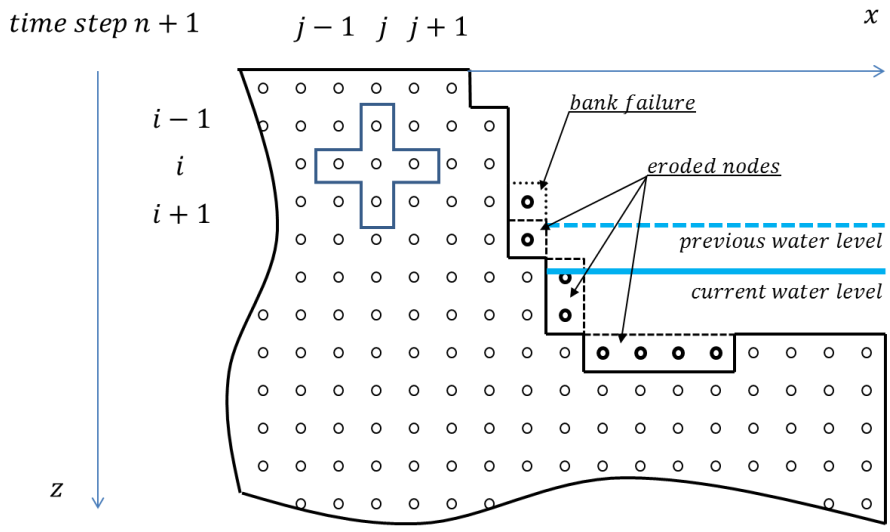


**Figure 4.4 Discretization of the domain.**

The discretized form of Equation 4.10 is below:

$$\frac{\theta_{i,j}^{n+1,l+1}-\theta_{i,j}^{n}}{\Delta t}=\frac{K_{i+\frac{1}{2},j}^{n+1,l}}{\Delta z}\left[\frac{h_{i+1,j}^{n+1}-h_{k,j}^{n+1}}{\Delta z}-1\right]-\frac{K_{i-\frac{1}{2},j}^{n+1,l}}{\Delta z}\left[\frac{h_{i,j}^{n+1}-h_{i-1,j}^{n+1}}{\Delta z}-1\right]+\frac{K_{i,j+\frac{1}{2}}^{n+1,l}}{\Delta x}\left[\frac{h_{i,j+1}^{n+1}-h_{i,j}^{n+1}}{\Delta x}\right]-\frac{K_{i,j-\frac{1}{2}}^{n+1,l}}{\Delta x}\left[\frac{h_{i,j}^{n+1}-h_{i,j-1}^{n+1}}{\Delta x}\right] \quad (4.16)$$

where $K_{i+\frac{1}{2},j}^{n+1,l}=\frac{K_{i+1,j}^{n+1,l}+K_{i,j}^{n+1,l}}{2}$, $K_{i-\frac{1}{2},j}^{n+1,l}=\frac{K_{i-1,j}^{n+1,l}+K_{i,j}^{n+1,l}}{2}$, $K_{i,j+\frac{1}{2}}^{n+1,l}=\frac{K_{i,j+1}^{n+1,l}+K_{i,j}^{n+1,l}}{2}$, $K_{i,j-\frac{1}{2}}^{n+1,l}=\frac{K_{i,j-1}^{n+1,l}+K_{i,j}^{n+1,l}}{2}$,

where $l$ is the index for a Picard iteration within one time-step as part of the mass conservative scheme. The use of the Picard iteration (superscript $l$ in the Equation 4.16) within each time step allows one to solve the nonlinear equation by improving the estimate of the hydraulic conductivity $K$ and specific water capacity $C$ within each time step.

The left-hand side of the discretized equation can be further discretized with a mass conservative scheme (Celia & Bouloutas, 1990):

$$\frac{\theta_{i,j}^{n+1,l+1}-\theta_{i,j}^{n}}{\Delta t}=\frac{\left[\theta_{i,j}^{n+1,l}+C_{i,j}^{n+1}\left(h_{i,j}^{n+1,l+1}-h_{i,j}^{n+1,l}\right)\right]-\theta_{i,j}^{n}}{\Delta t}=\frac{\theta_{i,j}^{n+1,l}-\theta_{i,j}^{n}}{\Delta t}+\frac{C_{i,j}^{n+1}}{\Delta t}\left(h_{i,j}^{n+1,l+1}-h_{i,j}^{n+1,l}\right) \quad (4.17)$$

where

$$C(h)=\frac{nm\alpha(\theta_s-\theta_r)}{(1+|\alpha h|^n)^{m+1}}|\alpha h|^{n-1} \quad (4.18)$$

The scheme, which results in Equation 4.17, is used for the discretization of the Richards equation, and it produces a penta-diagonal matrix for a rectangular domain. However, when the number of elements in the rows of the discretized domain is not equal to the previous row (Figure 4.4), two additional diagonals are added to the matrix of coefficients of the system (see Equation 4.17). A solution of the linearized system of equations is done with the Matlab software function *mldivide*, which simultaneously utilizes a number of solver algorithms to minimize the computation time for the given system (Mathworks Inc, Natick, 2014).

Since the discretized Equations 4.16 and 4.17 are written with unknown pressure head, these equations can be used for both saturated and unsaturated conditions. Under saturated

conditions, the pressure head is positive and the hydraulic conductivity is constant and equal to the saturated hydraulic conductivity.

The seepage/drainage gradients at the channel bed (boundary BC in Figure 4.2) were calculated for each of the three possible options of the nodes of soil in contact with water: (1) a node that has contact with water only through the horizontal boundary and thus defines the vertical gradient, (2) a node that has contact with water only through the vertical boundary and thus defines the horizontal gradient, and 3) a node that is in contact with water through both horizontal and vertical boundary (see Figure 4.4):

$$I_{i,j}^{vertical} = \frac{h_{i+1,j} - h_{i,j}}{\Delta z} - 1 \tag{4.19}$$

$$I_{i,j}^{horizontal} = \frac{h_{i,j-1} - h_{i,j}}{\Delta x} \tag{4.20}$$

$$I_{i,j}^{corner} = \cos\left(arctan\left(\frac{\Delta x}{\Delta z}\right)\right) I_{i,j}^{horizontal} + \sin\left(arctan\left(\frac{\Delta x}{\Delta z}\right)\right) I_{i,j}^{vertical} \tag{4.21}$$

## Channel Erosion

Channel erosion is calculated based on the boundary retreat rates (Equation 4.1) for each boundary cell of the soil with the same grid as for the solution of soil hydraulic gradients. Retreat rates define how fast each cell erodes on its boundary. This rate is defined by the possible propagation of the edge of the soil node cell, defined by the Equation 4.13. The erosion rate is calculated for each grid-cell that is in contact with water in the channel (Figure 4.4). At any given time step, the volume of eroded soil within each grid-cell can be less and not more than the volume of the cell. The percentage of the eroded volume is calculated, and its value is stored in each cell of the non-eroded soil node cells. Once the eroded volume exceeds the volume of the grid cell, the grid node is considered to be fully eroded and removed from the domain in the next time-step computation.

Figure 4.4 shows an instance where the movement of the boundary is not uniform due to the differences in critical shear stresses for different nodes. Some nodes from those in contact with water were fully eroded away, whereas the other nodes were not due to lower erosion rates. If fully eroded grid-cells had non-eroded grid-cells immediately above them, the non-eroded grid-cells were removed from the domain. This prevents having grid cells with undercut soil below them. This finding can be considered consistent with bank sloping during runoff events when the channel flow undercuts side walls at the level below the bankfull.

In this case of undercut grid-cells, the cross-sectional profile, water level and hydraulic radius were adjusted to a new state. The water level is also subject to changes due to the change in the channel flow. A new form of the domain with the adjusted boundary conditions is then used to compute the distribution of soil water pressure. Furthermore, the computational scheme allows soil erosion for any node on the channel bottom so that both “U”(see Figure 4.2 and Figure 4.3) and “W”(the shape of the channel when center of the channel is not the lowest point, as shown in Figure 4.4) channel shapes can be accounted for if hydraulic conditions cause such distribution of erosion because of the early erosion of the nodes in the corners of the channel.

## Model Testing

The validity of the developed numerical model was investigated by: (i) testing the soil water mass balance, (ii) comparing the sediment delivery rate for seepage and drainage conditions for the flume experiment carried out by C. Huang & Laften (1996), and (iii) evaluating channel widening rates for soils with an impermeable layer.

## Mass Conservation Test

The numerical model for the redistribution of soil moisture was set with boundary conditions of no flow in the channel (zero depth of the channel flow for the boundary BC in Figure 4.2) and a constant precipitation flux; it was run for a prescribed period. The top boundary flux was set to 0.3 cm/h, and the initial condition of the domain was set to negative 50 cm with the flat distribution across the domain. Apart from using spatial discretization as described above, soil hydraulic properties were used for the Crete silt loam soil (for more detail see Chapter 5).The total mass of water in the system was calculated at each time step, and the difference from the initial condition at $t$=0 was computed. Results for 10-minute intervals of a 2-hour test are presented in Table 4.1. Also known as the residual, the mass conservation error is below 5% after 10 minutes. It decreases with time, thus showing the stability of the process.

**Table 4.1 Mass conservation error in time.**

| Time, min | 10 | 20 | 30 | 40 | 50 | 60 | 70 | 80 | 90 | 100 | 110 | 120 |
|---|---|---|---|---|---|---|---|---|---|---|---|---|
| Error, % | 5.5 | 4.6 | 4.2 | 4.0 | 3.8 | 3.8 | 3.7 | 3.7 | 3.7 | 3.6 | 3.6 | 3.6 |

## Evaluating the Model with the Experiment Conducted by Huang et. al.

To test the model performance and its ability to differentiate the seepage and drainage, it was evaluated and tested on experimental data with channel erosion considering seepage/drainage conditions. Because of the lack of such experimental data, no formal validation was conducted, and the best fit of the model parameters was utilized to test the model performance.

C. Huang & Laften (1996) conducted a concentrated flow flume experiment with controlled seepage/drainage conditions. The soil was packed within the flume, which was divided into six sections. Three sections were instrumented in applying the seepage condition,

while the other three sections were used for drainage. Seepage was controlled by the additional channel parallel to the main flume, which was supplied with water flow 2 cm higher than the soil surface in the main channel. The drainage condition was controlled by the opening of the drain hole at the bottom of the main flume. Consequently, five levels of the flow rate were applied to the channel, and sediment delivery rates and water fluxes were measured at the bottom end of the flume. Reported as a function of water flow for seepage and drainage conditions were the average sediment delivery rates.

The parameters related to the flume experiment conditions and flume geometry were applied to numerical model (Table 4.2). The boundary condition at the upper boundary was calculated according to the depth of water in the channel. The boundary condition at the lower boundary was assumed as a constant pressure head of 27 cm for seepage and 0 cm for drainage. The initial distribution of the soil pore pressure was computed according to the reported sample preparation procedure, and it included the simulation of the full saturation and draining for 1 hour of the soil profile. This simulation led to the linear distribution of positive pore pressures. Channel flows used in the model were set like the ones in the flume experiment.

**Table 4.2 Parameters of the experiment conducted by Huang et al.**

| Parameters | Values |
|---|---|
| Channel width, cm | 20 |
| Channel depth, cm | 4 |
| Topsoil layer depth, cm | 25 |
| Total Soil Profile depth, cm | 25 |
| Flume width, cm | 120 |
| Bottom Boundary Condition | h=27 cm, h=0 cm |
| Top Boundary Condition | h=flow depth |
| Flume slope, m/m | 0.1 |
| Channel flow, l/min | 3.5, 8.2, 15.7, 31.9 |

The Glynwood clay loam from the no-till field was used to determine soil hydrological parameters (Table 4.3) from soil texture information using the ROSETTA model (Schaap, Leij,

& Van Genuchten, 2001). The bulk density was assumed to be 1.1 g/cm$^3$ because the soil was reported non-compacted. For the earthen channels, the Manning's n was assumed to be 0.35 (Huffman, 2013). Both the intrinsic soil critical shear stress and the soil erodibility coefficient (Table 4.3) were computed with the formulas obtained from the WEPP model documentation (D. C. Flanagan, 2012):

$$\tau_{cr\,0} = \begin{cases} 2.67 + 6.5 \cdot clay - 5.8 \cdot vfs, with\ vfs = 0.4\ if\ vfs < 40\% \\ 3.5, \qquad\qquad for\ sand\ content < 30\% \end{cases} \tag{4.22}$$

$$K_e = \begin{cases} 0.00197 + 0.030 \cdot vfs + 0.03863 \cdot e^{-184\,orgmat}, with\ vfs = 0.4\ if\ vfs < 40\% \\ 0.0069 + 0.134 \cdot e^{-20\,clay} \qquad\qquad for\ sand\ content < 30\% \end{cases} \tag{4.23}$$

During simulations, the critical shear stress function parameters $\varepsilon$ and $k$ were adjusted to ensure the best fit of modeled sediment delivery rates to the experimental data for both seepage and drainage conditions. After numerous simulations, these parameters were found to be 1.2 (unitless) and 0.07 (unitless) for $\varepsilon$ and $k$, respectively. Apart from conducting two model runs for each condition seepage and drainage, sediment delivery rates for all scenarios were estimated from the change in channel depths divided by the area of the flume used in the experiment. The model was also run for the constant CSS function. Figure 4.5 depicts the results for seepage and drainage modeling runs with variable and constant CSS along with experiment data.

**Table 4.3 Soil properties for the experiment conducted by Huang et al.**

| Soil | Sand | Silt | Clay | $\rho$ | $\theta_s$ | $\theta_r$ | $\alpha$ | $n$ | $m$ | $K_s$ | $\tau_{cr\,0}$ | $K_d$ | $n_m$ |
|---|---|---|---|---|---|---|---|---|---|---|---|---|---|
| | % | % | % | g/cm$^3$ | cm$^3$/cm$^3$ | cm$^3$/cm$^3$ | 1/cm | - | - | cm/h | Pa | s/m | m^1/6 |
| Glynwood clay loam | 22 | 49 | 29 | 1.1 | 0.4575 | 0.0824 | 0.008 | 1.547 | 0.354 | 0.741 | 3.5 | 0.0028 | 0.35 |

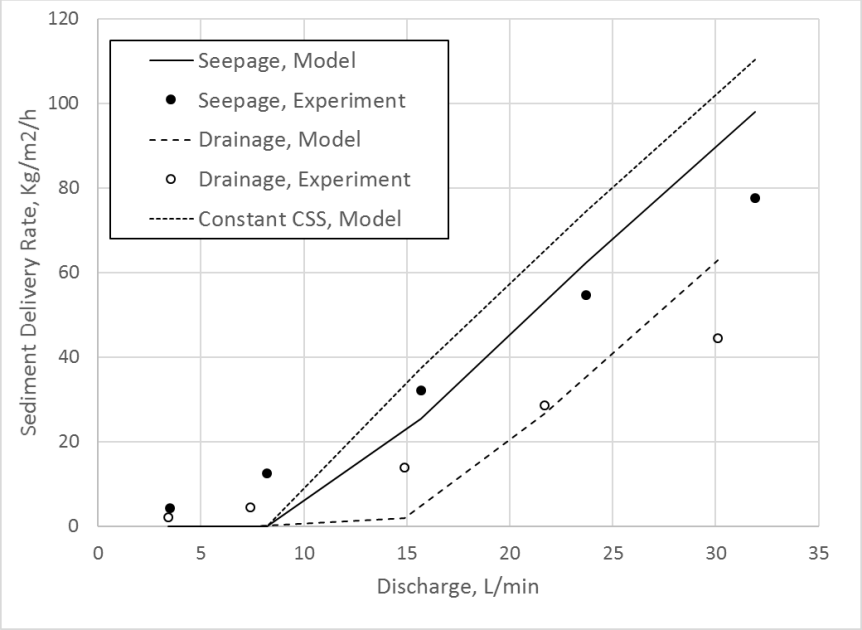


**Figure 4.5 Simulation results of the experiment conducted by Huang et al. where $\varepsilon$ = 1.2 and $k$ = 0.07.**

In sum, a comparison of simulated sediment delivery rates with the experiment performed by Huang et al. showed a good model performance (Moriasi et al., 2007) with the statistics of Nash-Sutcliff Efficiency Coefficient of 0.79 and the adjusted $R^2$ = 0.76 (Figure 4.6).

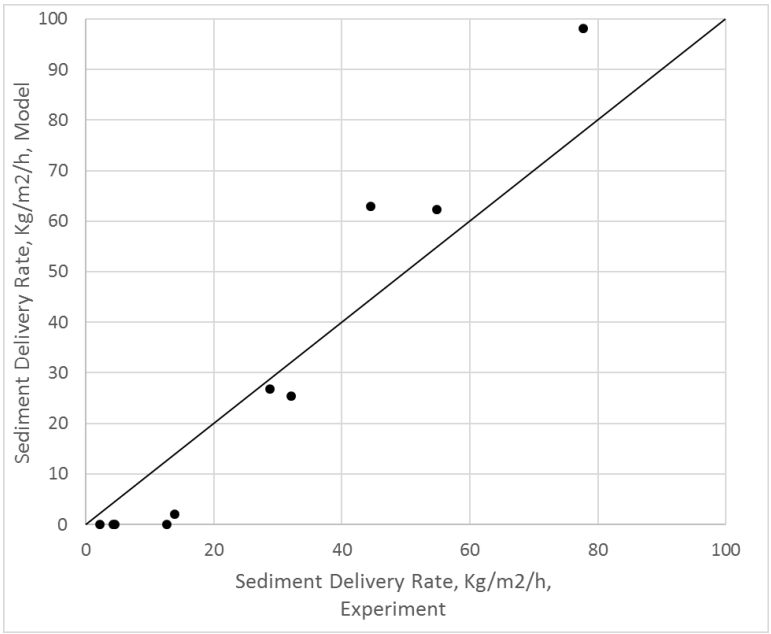


**Figure 4.6 Modeled vs. Experiment delivery rates for the experiment by Huang et al.**

Sediment delivery rates for the seepage and drainage scenarios vary for both the experiment and the modeling study. The differences in sediment delivery rates for seepage and drainage conditions is 2-33 $Kg/m^2/h$ for the experiment and 0-33 $Kg/m^2/h$ for the simulation. For both the experiment and the simulation, the differences between seepage and drainage sediment delivery rates is directly proportional to the discharge. These differences can be explained by the differences in the critical shear stresses, assuming that the process is described by the same erosion equation and that the same discharges and acting shear stresses were applied to the channel bottom. Erosion rates increase for both seepage and drainage curves exponentially for both the experiment and the modeling. However, the modeling shows that sediment delivery rates become a direct proportion for high values of discharge for the simulation.

As for constant critical shears stress function, the seepage and drainage conditions do not introduce any change in the value of critical shear stress and the simulation results. Thus, only one curve is presented in Figure 4.5 for the CCSS model. This model with constant critical shear stress also produced sediment delivery rates compared to the ones in the experiment. However, it could not separate seepage and drainage conditions and produce an overall prediction of erosion rates for higher value of the discharge.

## Evaluating the Model with the Experiment Performed by Wells et al.

R. R. Wells et al. (2013) conducted a flume experiment under controlled flow and slope. In that study, three flow discharges and three flume slopes were tested. The impermeable layer below the layer of packed soil was built into the flume. In other words, the study focused only on the channel widening. The final width of the channel was measured and reported for each of nine test runs.

Furthermore, parameters for the numerical model were developed according to the features of the experiment and are presented in Table 4.4. It was assumed that upper and lower boundaries have no flux boundary condition. More so, the initial soil moisture content was distributed, 20 minutes after the application of rainfall simulator, according to the reported information from the sample preparation process. The model used constant channel flows during runs, according to the experiment. The model was run with a time step of 2 or 4 seconds depending on soil erosion rates. Nine scenarios were simulated in the experiment, thus combining three flume slopes and three flow discharge rates.

**Table 4.4 Parameters of the experiment performed by Wells et al.**

| Parameter | Value |
|---|---|
| Channel width, cm | 10 |
| Channel depth, cm | 4 |
| Top soil layer depth, cm | 4 |
| Total Soil Profile depth, cm | 22 |
| Flume width, cm | 60 |
| Bottom Boundary Condition | q=0 |
| Top Boundary Condition | q=0 |
| Flume slope, m/m | 0.01, 0.05, 0.11 |
| Channel flow, $m^3/s$ | 0.00025, 0.00067, 0.00108 |

Atwood sandy clay loam was used as soil in the experiment. In addition, the soil texture and bulk density were extracted to determine soil hydrological parameters (Table 4.5) using the ROSETTA model (Schaap et al., 2001). The soil organic matter content and Manning's n for earthen channels were assumed to be 0.5% and 0.35 respectively (Huffman, 2013). Equations 4.22 and 4.23 were also used to compute the intrinsic soil critical shear stress and soil erodibility coefficient (Table 4.5).

The non-erodible layer with a depth of 4 cm was introduced into the model. It was assumed that the saturated hydraulic conductivity of this layer was 100 times lower than that for the original soil. The intrinsic critical shear stress was also assumed to be 100 times larger than

that of the original soil. Critical shear stress function parameters were taken from the best fit of the function in Equation 4.9 to the one in the experiment carried out by S. K. Nouwakpo et al. (2010), where nominal critical shear stress was computed with Equation 4.22.

**Table 4.5 Soil properties for the experiment performed by Wells et al.**

| Soil | Sand | Silt | Clay | $\rho$ | $\theta_s$ | $\theta_r$ | $\alpha$ | $n$ | $m$ | $K_s$ | $\tau_{cr\,0}$ | $K_d$ | $n_m$ |
|---|---|---|---|---|---|---|---|---|---|---|---|---|---|
| | % | % | % | g/cm³ | cm³/cm³ | cm³/cm³ | 1/cm | - | - | cm/h | Pa | s/m | m^1/6 |
| Atwood sandy clay loam | 59 | 17 | 24 | 1.56 | 0.3891 | 0.0628 | 0.023 | 1.333 | 0.25 | 0.616 | 0.808 | 0.035 | 0.35 |
| Impervious layer | - | - | - | - | 0.3891 | 0.0628 | 0.023 | 1.333 | 0.25 | 0.006 | 80.8 | 0.0035 | 0.35 |

The width of the channel was computed for all scenarios with a proposed model (Equation 4.9) based on the channel flow, slopes and time of duration. The model was also run based on the assumption of constant critical shear stress for the same conditions. The results for nine scenarios were presented in the same format as it was done in the study performed by R. Wells et al. (2013). Figure 4.7 presents the final channel width and the product of channel flow and slope.

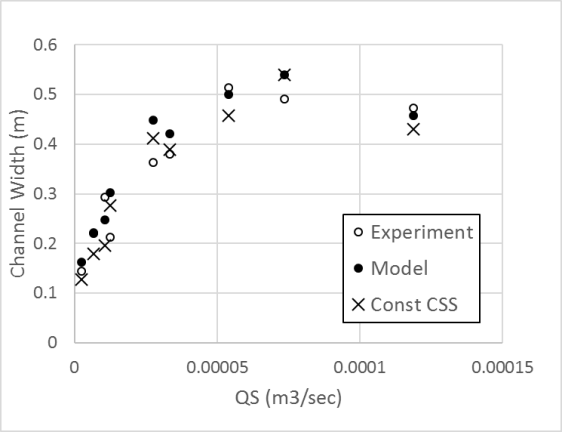


**Figure 4.7 Simulation results of the experiment performed by Wells et al. where $\varepsilon$ = 1.2 and $k$ = 0.07.**

The simulation showed good model performance (Moriasi et al., 2007) with Nash-Sutcliff Efficiency of 0.85 (Figure 4.8).

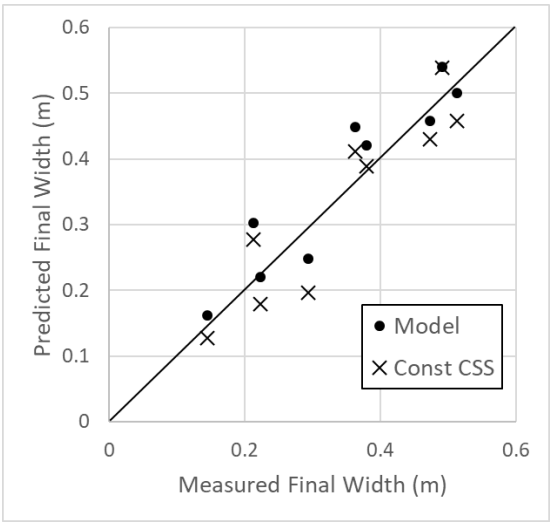


**Figure 4.8 Experiment vs. modeled final widths for the experiment performed by Wells et al.**

There are no clear trends in the differences in the behavior of models (CCSS model and proposed model with variable critical shear stress) from this test. Moreover, if the proposed model is over predicting erosion compared to the experiment then CCSS model would also over predict the erosion rate. The trend is identical for the underprediction of the erosion rates.

The application of the CCSS model produced slightly lower NSE value of 0.82. Interestingly, channel widths for CCSS were always lower than those computed with the reduced critical shear stress model. This observation suggests that actual hydraulic gradients decrease the value of the critical shear stress.

## Discussion

The use of the proposed model with the critical shear stress, which is defined as a function of hydraulic gradient, shows overall acceptable results. It allows one to simulate and account for dynamic hydraulic processes of soil erosion due to the concentrated flow. However,

it is challenging to parameterize the functional form the proposed critical shear stress coefficient because of the lack of experimental data on seepage/drainage conditions.

## Effect from the Change of Model Parameters

The influence of parameters of the critical shear stress function may be examined by the analysis of Figure 4.9 which represents various scenarios of different soils and different critical shear stress functions (functions 1 to 3), different hydrological regimes (drainage with $I$ = - 4 and seepage with $I$ = 2) and different flows (two levels of acting shear stress 4Pa and 1 Pa which can be defined using Equation 4.14). Figure 4.9 shows the function (1, 2 or 3) of critical shear stress ($y$-axis) as a dependent variable from the hydraulic gradient I ($x$-axis). There are also two levels of acting shear stress, (also on the $y$-axis).

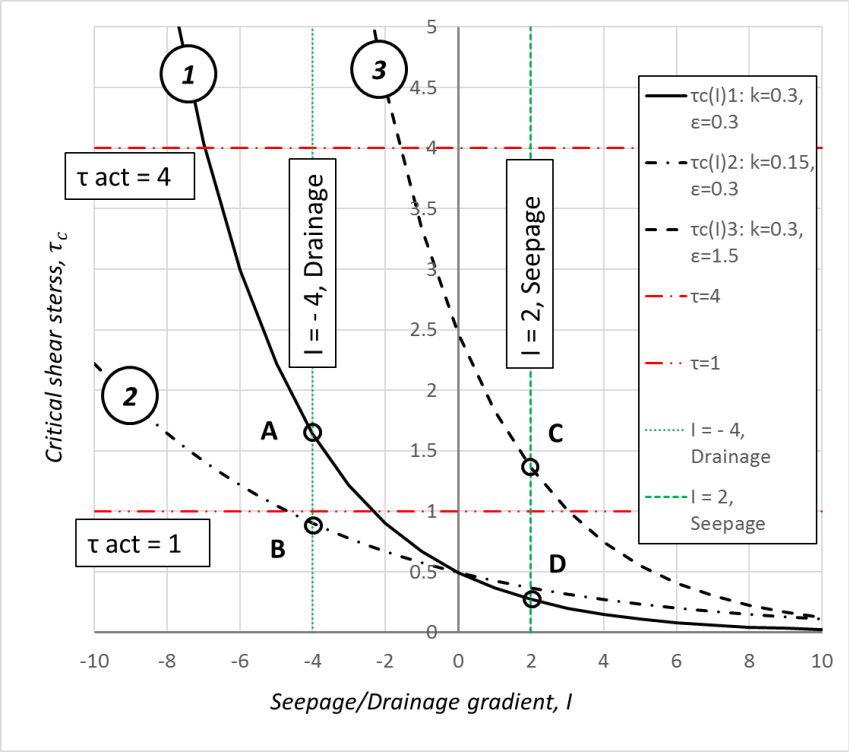


**Figure 4.9 Critical shear stress functions for various function parameters.**

Four possible scenarios represent some events which are characterized by two parameters:

1) The hydraulic gradient and the corresponding critical shear stress for this event; and
2) The acting shear stress representing the conditions of the flow.

Each letter corresponds to some hydraulic gradients and some critical shear stress functions:

- A is a drainage condition for the function 1,
- B is a drainage condition for function 2,
- C is a seepage condition for function 3, and
- D is a seepage condition for function 1.

If the critical shear stress corresponding to the soil and hydrological regime is less than the acting shear stress, then there will be a soil detachment. This means that for all scenarios A-D, there will be erosion for the higher case of acting shear stress of 4 Pa.

However, when the lower acting shears stress is considered, the condition of the start of erosion can be changed due to different behaviors of the critical shears stress for various hydraulic gradients. The comparison of scenarios A and D represents two different hydrologic states (drainage vs. seepage) for one soil (critical shear stress function 1). It appears that for the scenario D, there is erosion; on the other hand, for the scenario A, there no erosion because of the critical shear stress is more than the acting shear stress.

Scenarios A and B show the influence of the parameter *k*, which changes the inclination of the critical shear stress function, including the difference between the acting shear stress and the critical shear stress for the pressure gradient. As for the case of A and B, it was sufficient to allow erosion for the scenario B because it is lower than the level of the acting shear stress.

Similarly, scenarios C and D represent the influence of the parameter $\varepsilon$. If $\varepsilon$ is increased/decreased, the critical shear stress function will move to the right/left and so too will the difference in stresses decrease/increase accordingly (compare function 1 and 3). If $\varepsilon$ parameter increases, then the critical shear stress function shifts to the right, thus resulting in the lower difference between acting and critical shear stresses and a decrease in erosion rate. In the case of C and D, scenario C had an increased critical shear stress. Hence, there is no erosion.

For all scenarios, high negative values of hydraulic gradient cause the infinite increase of the critical shear stress, thus resulting in the elimination of the erosion. It has to be noted that the hydraulic gradient during the actual rainfall and runoff events usually have a drainage nature. Even without the expected extreme values of drainage and seepage, there are possibilities of drainage conditions resulting in the significant increase in the critical shear stress. This finding may explain the tendency in overprediction of the erosion when the constant critical shear stress is used.

## Shear Stress and Soil Erodibility

The results presented in previous sections showed that the change in parameters $\varepsilon$ and $k$ can significantly impact channel erosion rates for seepage and drainage conditions. The modeling results of the Huang's experiment (C. Huang & Laften, 1996) showed that the difference in predicted erosion rates for seepage and drainage is directly proportional to the channel flow (Figure 4.5). The difference in the critical shear stress should only cause a shift in the rates. However, the seepage condition causes more rapid increase in the erosion rates with the increase in flow rates compared to the drainage condition. To say it another way, the seepage

condition has a steeper curve than the drainage condition. This observation may suggest that the soil erodibility may also be a function of the hydraulic gradient.

A study conducted by A. Al-Madhhachi et al. (2014) showed from the pore scale analysis that the physical process of soil erosion and particle detachment could depend on a function of hydraulic gradient. They derived the following form of the excess shear stress equation based on Wilson's soil detachment model (B. Wilson, 1993a):

$$E_r = b_0(I) \cdot \sqrt{\tau} \cdot \left\{1 - \exp\left[-\exp\left(3 - \frac{b_1(I)}{\tau}\right)\right]\right\} \tag{4.24}$$

$$b_0(I) = \rho_s \frac{k_r}{K_{ew}} \sqrt{\frac{K_n + \mu_{st} g I d \rho_w}{k_{dd}(\rho_s - \rho_w)}} \tag{4.25}$$

$$b_1(I) = \frac{\pi}{e_v \sqrt{6}} \frac{k_r(K_{ls} - K_s(I) + f_c)}{K_0} g(\rho_s - \rho_w) d \tag{4.26}$$

where $K_{ew}$, $k_{dd}$, $\mu_{st}$ and $e_v$ are parameters of the Wilson's model, which depended on soil properties and characteristics of channel flow. A detailed derivation of Equation 4.24 can be found in (A. Al-Madhhachi et al., 2014).

The form of the erosion rate E in Equation 4.24 does not directly depend on the critical shear stress and the erodibility coefficient; it contains coefficients b0 and b1. However, based on the discussion of A. Al-Madhhachi et al. (2014), the parameter $b_0$ can be considered an equivalent of the soil erodibility coefficient $K_e$. The experiment performed by A. Al-Madhhachi et al. (2014) showed an almost linear relationship between $b_0$ and the hydraulic gradient *I*. Considering the theoretical and experimental relationships, the soil erodibility coefficient $K_e$ is proposed to be linearly dependent on the hydraulic gradient *I*:

$$K_e(I) = \eta K_e^{ref}(1 + k_K I) \tag{4.27}$$

where $K_e^{ref}$ is the reference soil erodibility value in [m/s] determined from specific experiments on different soils, and $\eta$ and $k_K$ are two model parameters.

An introduction of this relationship modifies the excess shear stress (see Equation 4.9) as follows:

$$E(I) = \eta K_e^{ref}(1 + k_K I) \cdot (\tau - \varepsilon\, \tau_c^{ref} \cdot e^{-kI})^a \quad (4.28)$$

In Equation 4.28, parameters $\varepsilon$, $k$, $\eta$ and $k_K$ can be found experimentally. For example, when the search for the parameters is done based on the data of Huang's experiment which ensures the best fit of the model to the experimental data (Figure 4.10), it produced NSE of 0.99 and adjusted $R^2$ of 0.98 (Figure 4.11) with the following set of parameters: $\varepsilon = 0.75$, $k = 0.1$, $\eta = 0.55$ and $k_K = 0.1$.

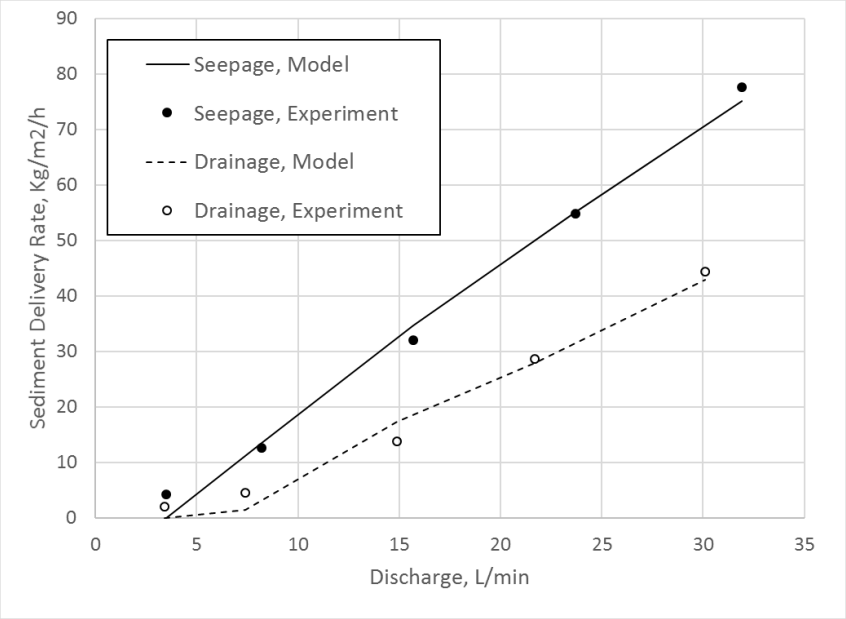


**Figure 4.10 Simulation results of the experiment conducted by Huang et al. with the gradient dependent soil erodibility.**


**Figure 4.11 Experiment versus modeled delivery rates for the experiment conducted by Huang et al. with the gradient dependent soil erodibility.**

The values of four parameters obtained in Equation 4.28 can be used as a first approximation for soil erosion modeling, which accounts for the hydraulic gradient in clay loam soils. Further research is nevertheless needed to find parameters for the other soil types and to investigate the effects of soil texture and structure on the proposed relationship of erosion process from the hydrologic regime of subsurface flows.

The presented results show that dependence of critical shears stress function and soil erodibility coefficient on the pre-hydraulic gradient can play a significant role in soil erosion due to the concentrated channel flow. The proposed approach, which aims to account for the hydraulic gradients with the application of excess shear stress model and proposed parameters, appears to be simpler than the use and definition of numerous parameters utilized by A. Al-Madhhachi et al. (2014). It is recommended that further simplifications be applied to the existing

prediction models to increase the robustness of the approach and improve its applications in larger scale projects.

## Summary

In this section, a physical channel erosion model was developed to account for pore pressure effects on soil particle detachment, specifically the pore pressure gradient in the critical shear stress function and soil erodibility coefficient. Apart from providing mathematical formulations of the erosion problem in order to adjust the erosion rates due to the hydrologic regime such as seepage/drainage, the numerical solution of the problem was suggested by computing Richards equation in the two-dimensional soil profile for half of the channel cross-section. Results showed a significant difference in erosion rates for seepage and drainage conditions. Moreover, the overall acceptable model performance with NSE values is 0.88 and 0.85 for two experiments. The sensitivity of proposed model parameters was made, and their influence on the erosion process was discussed. In this section, results also showed that CCSS might be applied to the events with strong negative pore pressure gradients, while events with near zero and positive pressure gradients should account for the reduction of the critical shear stress and the possible increase in the erosion rates.

This chapter also revealed that there is a lack of experimental data on the dependence of soil erosion rates on the pressure gradients for various soils. It was suggested that in the future, known and used critical shear stress measurement techniques should take into account various hydrologic conditions. Other directions of the further research could include the improvement of the prediction of the acting shear stress for channel flow with the possible determination of the profile stress distribution. Since A. Knapen et al. (2008) showed that soil erodibility depends on the antecedent soil moisture content, soil erodibility may also depend on the hydrologic regime.

Regarding the research of G. V. Wilson et al. (2008), G. V. W. Wilson (2009), and G. Wilson (2011) that subsurface processes affect the formation of ephemeral gullies, it is expected that the pressure-dependent critical shear stress model may be helpful in predicting the headcut propagation of channels like rills and gullies.

What's more, certain improvements can be made to the numerical model scheme; for example, the use of irregular instead of discrete boundary and node placements can improve the computational scheme and provide smoother transitions when the nodes are removed from the domain due to erosion. Another potential improvement can include the bank stability module which will not just fail nodes on top of the eroded one but will also fail the wall of the channel according to some stability criteria.

This section has shown that the presented model requires a large set of parameters to prepare the model run. Thus, it has limitations to be applied to the larger scale projects. However, it can be used as a research tool to meticulously study the processes of channel erosion, especially in terms of soil hydrological regime.

# Chapter 5 - Impacts of Subsurface Fluxes on Concentrated Flow Erosion with a Two-Dimensional Numerical Model

## Introduction

Soil erosion by water on agricultural hillslopes is a complex but dynamic process. Among all types of soil erosion, channel erosion due to concentrated water flow has been given maximum attention because several types of erosion can be explained by the physics of the concentrated flow. These types of erosion range from the small rills and ephemeral gullies on the arable land to the permanent streams and classical gullies.

Besides, numerous parameters control the soil detachment and erosion rates. Obvious influencing parameters – such as the runoff amount, runoff duration and basic soil erosion properties (critical shear stress and soil erodibility) –were intensively studied and used in models. However, often overlooked and not considered in the modeling research are the influence of other parameters such as the soil moisture content, the groundwater presence, or the presence of the impervious layers. The mechanism of the influence of these parameters on the erosion is of the same complexity as the erosion process itself. For example, the antecedent soil moisture affects the infiltration rate as does the amount and intensity of the runoff. At the same time, the antecedent soil moisture may influence the detachment parameters of the soil. Another example is the rise of the groundwater table. The depth of the groundwater table near the surface significantly increases the soil erosion rates, even though modeling would not show any difference for such case. More simply, the influence of many of these parameters can be felt if the process of the dynamic water redistribution in the channel itself is accounted for.

The aim of this study was to investigate the influence of the subsurface water fluxes on the erosion processes due to the concentrated flow for various soils, assuming that the critical shear stress and soil erodibility depend on the underground seepage/drainage. Several studies have been carried out on different soils, various antecedents soil moisture contents, groundwater depths and the presence of the impervious layer.

# Methods

## Erosion Equation

The excess shear stress equation is widely used in most process-based models that estimate soil erosion rates from the concentrated flow. The equation below assumes that erosion can occur only when the acting shear stress from the channel flow exceeds the critical shear stress of the soil while the erosion rate is proportional to their difference by the factor of soil erodibility coefficient:

$$\left.\frac{dl}{dt}\right|_{normal} = E(I) = K_e^{ref} \cdot (\tau_{act} - \tau_c^{ref})^a \quad (5.1)$$

$$\tau_{act} = \gamma RS \quad (5.2)$$

where $K_e^{ref}$ is the reference soil erodibility, $\tau_c^{ref}$ is the reference critical shear stress, $a$ is the power parameter usually equal to 1, $\tau_{act}$ is the acting shear stress calculated as the product of $\gamma$ (the specific gravity of water), $R$ is the hydraulic radius, and $S$ is the local channel slope. The constant parameters in Equation 5.1 is assumed in the standard formulation of the excess shear stress equation, and such formulation is called the Constant Erosion Parameter (CEP) model.

In Chapter 4, an extension to the CEP model was suggested by utilizing a variability in $K_e$ and $\tau_c$ with the change in subsurface fluxes at the soil boundary. The modified critical shear

stress equation or the Variable Erosion Parameter (VEP) model accounts for the seepage/drainage forces in the form of hydraulic pressure gradient ($I$):

$$\left.\frac{dl}{dt}\right|_{normal} = E(I) = \eta K_e^{ref}(1 + k_K I) \cdot (\tau_{act} - \varepsilon\, \tau_c^{ref} \cdot e^{-kI})^a \quad (5.3)$$

where $\varepsilon$, $k$, $\eta$ and $k_K$ are model parameters, which are assumed to be constant. Regarded as the properties of the soil, these four model parameters depend on various conditions such as the soil type, soil texture, and particle size distribution, and they need to be calibrated on individual soil. In Chapter 4, these parameters were tested for clay loam soil and were selected as: $\varepsilon = 0.75$, $k = 0.1$, $\eta = 0.55$, and $k_K = 0.1$. This selection was based on fitting the results of the numerical model to experimental data for two reported experiments.

## Mathematical Model

To simulate soil erosion process in conjunction with the water redistribution around the channel, a 2-D numerical experiment was conducted. Also selected for modeling was a 2-D vertical porous medium domain perpendicular to the uniform soil channel (Figure 4.2). The porous medium was assumed to be homogeneous within each soil layer. Excluding the upper boundary and the flow in the channel, no other external sources of water were considered in the model, such as zero subsurface fluxes upstream and downstream of the domain. As the channel shape was assumed to be symmetrical, only half of the channel was considered for computations.

Furthemore, the soil domain was discretized with the grid node density of one node per 1 cm² for the area around the gully and one node per 100 cm² for the rest of the area. The same network of nodes was used to compute the channel boundary retreat due to soil erosion and soil pressure redistribution. To make the computation process much easier, time steps for pressure redistribution and channel boundary retreat were also selected.

The erosion rates were calculated only for each soil node that was in contact with water in the channel, and it was assumed that the acting shear stress has a constant distribution on the wetted perimeter. If nodes are undercut from underneath by the eroded grid cells below, they are assumed to be unsupported and are taken out of the domain.

The Richards equation was solved for pressure distribution *h* in the soil domain:

$$\frac{\partial \theta}{\partial t} = \frac{\partial}{\partial z}\left[K(h)\frac{dh}{dz}\right] - \frac{\partial K(h)}{\partial z} + \frac{\partial}{\partial x}\left[K(h)\frac{dh}{dx}\right] \tag{5.4}$$

where $\theta$ is the volumetric water content, $h$ is the matric potential, $K$ is the hydraulic conductivity as a function of matric potential, z is the vertical coordinate, *x* is the horizontal coordinate, and t is time. An assumption of rigid porous medium with three layers was made, and the soil was assumed to be homogeneous within each layer.

A set of (Van Genuchten, 1980) functions were used to determine the relationship between pressure, hydraulic conductivity, and water content within the soil:

$$\theta(h) = \frac{(\theta_s - \theta_r)}{(1+|\alpha h|^n)^m} + \theta_r \tag{5.5}$$

$$K(h) = K_s \frac{[1-|\alpha h|^{n-1}(1+|\alpha h|^n)^{-m}]^2}{(1+|\alpha h|^n)^{m/2}} \tag{5.6}$$

where α, *n* and *m* are empirical constants.

Also, the initial and boundary conditions were selected as a known pressure head for the initial condition and flux-based boundary condition, if the area in contact with water where head based boundary condition was not applied. With the scheme proposed by Celia and Bouloutas (1990), the numerical solution of the Richards equation was used. The calculated pore pressures were also used to compute seepage/drainage gradients on the boundary of the channel. The numerical scheme allowed the computation of pressures and soil erosion for both U-shaped and W-shaped channels (see Chapter 4 for more details and mathematical formulation of the problem).

## Baseline Scenario

The baseline scenario was investigated in detail to describe the impact of the dynamics of the soil pressure redistribution during the runoff event on channel erosion processes. An initial channel of a symmetrical trapezoidal shape was selected for the study. As for its dimensions, the depth of the small rill was 7 cm and the width at the bottom of the channel was 16 cm. While the channel sides had a slope of 5/3, the slope of the soil around the channel was 1/20 and that of the channel itself was 1.5%.

Also used in the study was a synthetic channel flow of 3-hour duration with a peak flux of 0.003 m3/sec during the middle hour. The channel flow hydrograph is presented in Figure 5.1, and precipitation was applied with the constant rate of 0.3 cm/h. Such channel flow and precipitation rates may relate to an NRCS type 2 rainfall with a return period of 1 year on a 1 ha catchment with an average slope of 1% located in Central Kansas. As it was assumed that the contribution of the lateral surface flow was negligible, it was not taken into account.

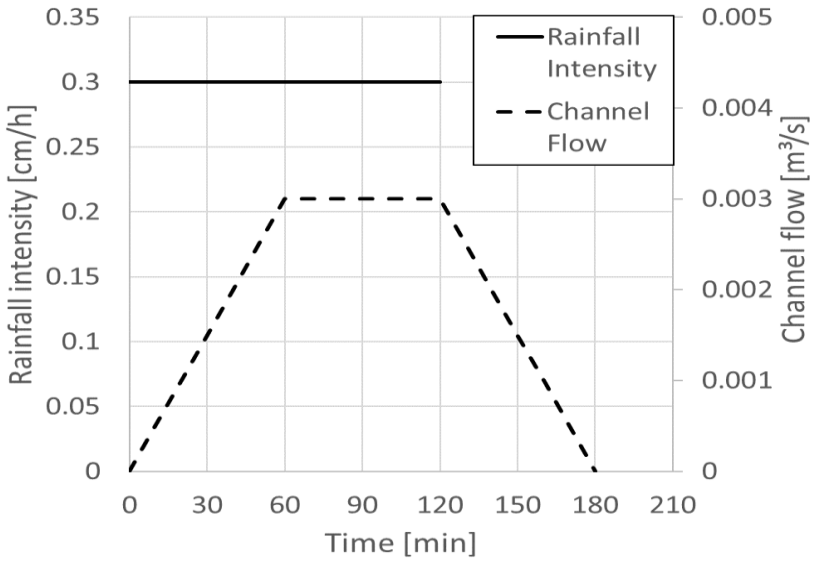


**Figure 5.1 Synthetic rainfall and runoff for the numerical experiment.**

The Clark-Ost soil was selected for the baseline scenario as there is experimental data for the similar type of soil (Chapter 4). Four parameters of the VEP erosion equation (Equation 5.3) were determined in the Chapter 4 and are suggested for use here. These parameters define the critical shear stress and soil erodibility as functions of the hydraulic gradient (Figure 5.2).

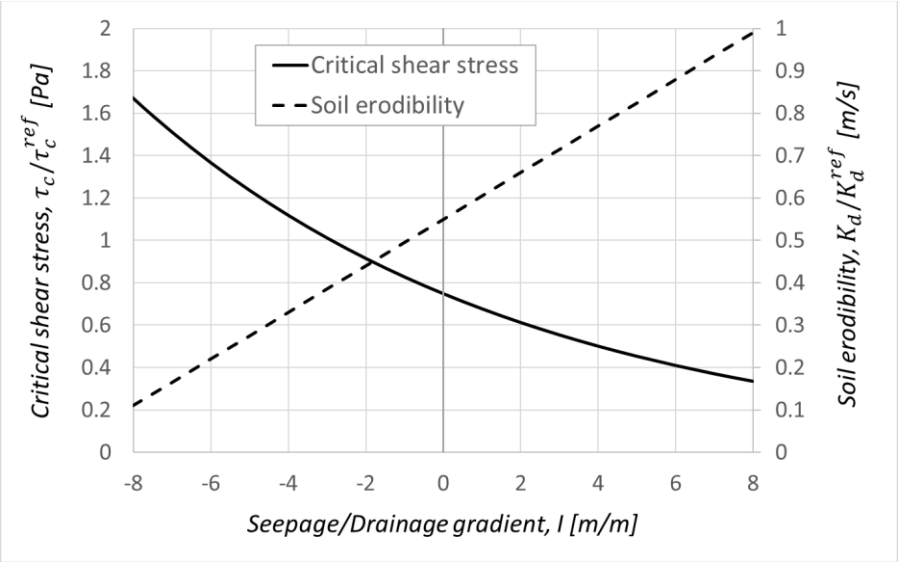


**Figure 5.2 Critical shear stress and soil erodibility as functions of the hydraulic gradient.**

Van Genuchten (1980) parameters in Equations 5.5 and 5.6 were calculated with the ROSETTA model (Schaap et al., 2001) based on the texture and bulk density data acquired from the SSURGO database (KDASC, 2013) for two soil layers (see Table 5.1).

**Table 5.1 Soil properties for numerical experiments.**

| | Sand | Silt | Clay | Org.mat. | $\rho$ | $K_s$ | $\alpha$ | $\theta_s$ | $\theta_r$ | $n$ | $\tau_{cr\,0}$ | $K_d$ |
|---|---|---|---|---|---|---|---|---|---|---|---|---|
| | % | % | % | % | g/ cm³ | cm/h | 1/cm | cm³/cm³ | cm³/cm³ | - | Pa | s/m |
| Crete Silt loam | | | | | | | | | | | | |
| 0-30 cm | 7 | 69 | 24 | 3 | 1.37 | 0.632 | 0.006 | 0.4525 | 0.0796 | 1.611 | 3.5 | 0.0080 |
| 30-100 cm | 4 | 50 | 46 | 2 | 1.35 | 0.409 | 0.0127 | 0.4943 | 0.0988 | 1.372 | 3.5 | 0.0069 |
| 30-40 cm - PP | 4 | 50 | 46 | - | 1.485 | 0.189 | 0.0121 | 0.4556 | 0.0947 | 1.366 | - | - |
| Farnum Loam | | | | | | | | | | | | |
| 0-30 cm | 42 | 38 | 20 | 2 | 1.4 | 0.595 | 0.0102 | 0.4042 | 0.0618 | 1.515 | 1.65 | 0.0041 |
| 30-100 cm | 56 | 15 | 29 | 1.1 | 1.45 | 0.870 | 0.0206 | 0.4265 | 0.0739 | 1.35 | 2.235 | 0.0083 |
| 30-40 cm - PP | 56 | 15 | 29 | - | 1.595 | 0.432 | 0.0234 | 0.3856 | 0.067 | 1.272 | - | - |
| Goessel Silty clay | | | | | | | | | | | | |

| | | | | | | | | | | | | |
|---|---|---|---|---|---|---|---|---|---|---|---|---|
| 0-30 cm | 6 | 53 | 41 | 3 | 1.35 | 0.439 | 0.0111 | 0.4861 | 0.0959 | 1.424 | 3.5 | 0.0069 |
| 30-100 cm | 6 | 48 | 46 | 2 | 1.4 | 0.323 | 0.0126 | 0.4774 | 0.097 | 1.374 | 3.5 | 0.0069 |
| 30-40 cm - PP | 6 | 48 | 46 | - | 1.54 | 0.147 | 0.0122 | 0.4373 | 0.0922 | 1.352 | - | - |
| Clark-Ost Clay loam | | | | | | | | | | | | |
| 0-30 cm | 34 | 37 | 29 | 1.5 | 1.4 | 0.422 | 0.0106 | 0.4293 | 0.0774 | 1.475 | 2.235 | 0.0056 |
| 30-100 cm | 35 | 38 | 27 | 0.5 | 1.55 | 0.210 | 0.0114 | 0.3872 | 0.0691 | 1.43 | 2.105 | 0.0186 |
| Ninnescah Fine sandy loam | | | | | | | | | | | | |
| 0-30 cm | 57 | 27 | 16 | 2 | 1.4 | 1.378 | 0.0184 | 0.4081 | 0.0539 | 1.452 | 1.39 | 0.0041 |
| 30-100 cm | 66 | 19 | 15 | 2 | 1.5 | 1.443 | 0.0269 | 0.3924 | 0.0516 | 1.439 | 1.325 | 0.0041 |
| Ladysmith Silty clay loam | | | | | | | | | | | | |
| 0-30 cm | 7 | 60 | 33 | 3 | 1.3 | 0.650 | 0.0082 | 0.4844 | 0.0901 | 1.512 | 3.5 | 0.0071 |
| 30-100 cm | 6 | 47 | 47 | 2 | 1.4 | 0.323 | 0.0129 | 0.4783 | 0.0974 | 1.365 | 3.5 | 0.0069 |

The reference critical shear stress and soil erodibility coefficient values were calculated based on the Equations 4.22 and 4.23 (see Table 5.1). In addition to specifying the boundary conditions, the Manning's n coefficient was assumed to be 0.35 for the earthen channel (Huffman, 2013). The initial condition was assumed to be a constant pressure along the soil profile for a saturation of 85% (as an average soil saturation for the rainy season in Central Kansas) calculated with the Equation 5.5. More so, the CEP model was used to perform the similar computation of channel erosion for the same channel flow; the results for both VEP and CEP models were compared and presented in the next section.

## Results for the Baseline Scenario

The pressure redistribution in time was presented as a sequence of the pressure plots of the half of the soil profile for every 20 minutes of the simulations (Figure 5.3).

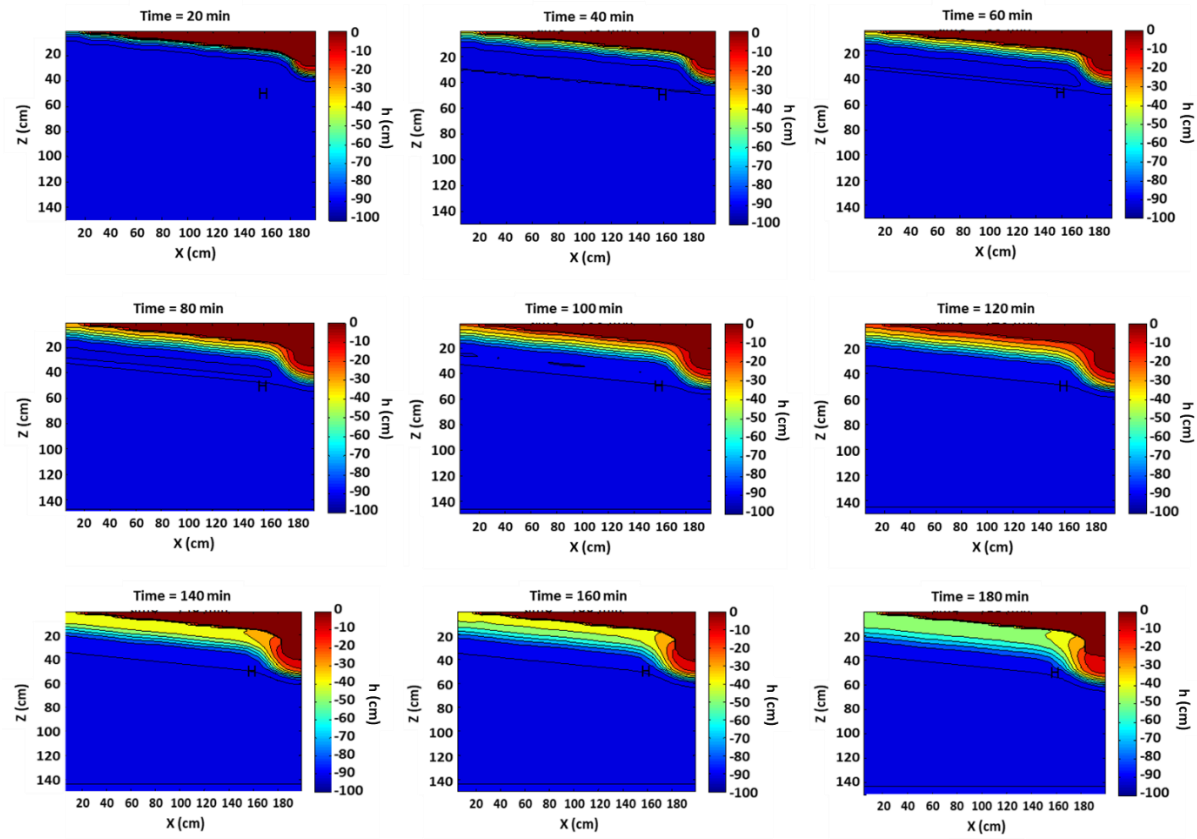


**Figure 5.3 Soil pore pressure redistribution in time.**

It is very evident that the soil profile receives most of the water from the infiltration from the channel. Area around the channel is wetter and close to saturation compared to other areas of the profile. Moreover, propagating water from the channel into soil profile causes negative (drainage) pressure gradients, thus resulting in an increase in the critical shear stress and a decrease in soil erodibility at the channel boundary. Equation 5.3 indicates that it will be harder for soil particles to detach from the channel bottom and that the rate of erosion will be smaller for the seepage condition. However, if the CEP model is used, the erosion rates do not depend on the soil pressure gradient at the channel boundary and may fluctuate regardless of the processes within the soil. Thus, a separate comparison is needed.

To compare the erosion rates developed with CEP and VEP models, the same conditions were applied to the baseline scenario. The results for channel propagation in time for VEP and CEP models are presented in Figure 5.4.a,b.

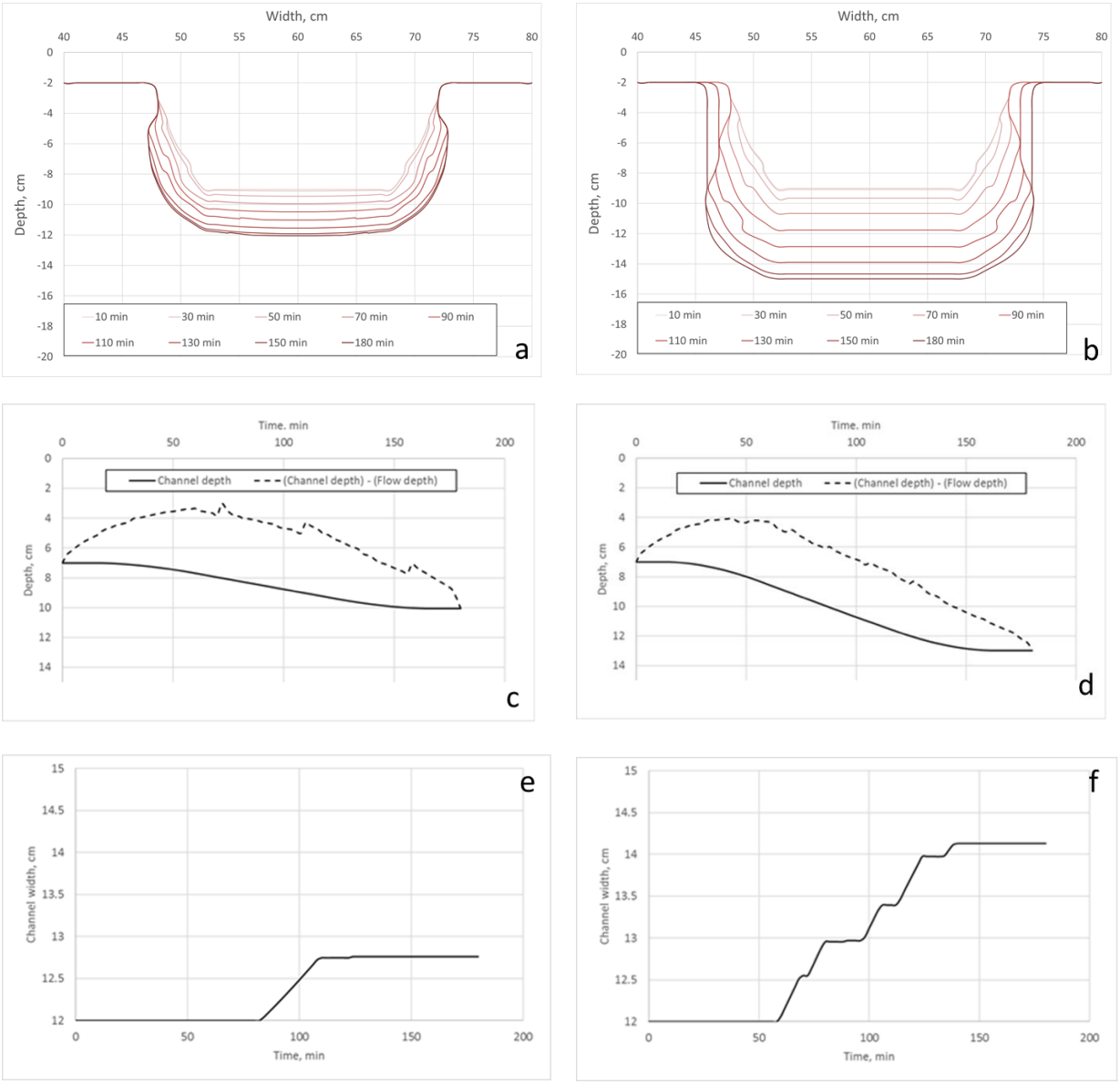


**Figure 5.4 Channel propagation in time: cross sections for the VEP model (a), cross sections for the CEP model (b), depth of the lowest point for VEP model (c), depth of the lowest point for the CEP model (d), width of the channel for the VEP model (e), width of the channel for the CEP model (f).**

An increase in density of the channel profile lines in Figure 5.4.a,b clearly shows that the development of the channel is slower at the beginning and at the end of the simulation for both VEP and CEP models. However, the application of the CEP model caused a deeper and wider channel. In addition, the CEP model caused two vertiual bank failures due to the undercutting of the banks. While there was none for the VEP, undercutting was noticed Figure 5.4.c,d shows the channel depth development in time and the difference between the channel depth and the channel flow depth. Both graphs start at the same point as they have the same initial conditions and the same channel flow. However, due to the different erosion computation approaches between VEP and CEP models, the development of the channel is different in time. The channel depth, in this case, was determined for the deepest point of the channel cross-sectional profile. Overall, the propagation of the channel downward is very similar for VEP and CEP models with the maximum propagation rate determined by the maximum flow rate in the middle of the hydrograph. Similarly, the channel width (Figure 5.4.e, f) was considered the largest width of the half of the channel. The channel width is assumed to advance only after a whole grid-cell has been eroded. Interestingly, the VEP model showed widening of the channel only for a short period. This time interval starts with the moment of the channel profile width reaching the initial width, and it ends with a decrease in the channel flux accompanied by deepening of both the channel depth and the water flow depth.

A minimum channel propagation at the beginning and at the end of the simulation experiment can be explained by the fact that the critical shear stress exceeds the acting shear stress at those periods (Figure 5.5). In addition, both models (VEP and CEP) respond with zero erosion rate for these low flux conditions. However, the change of the critical shear stress

function for the VEP model caused a slight shift in the erosion process as the critical shear stress is higher at the beginning of the process due to the observed large pressure gradients.

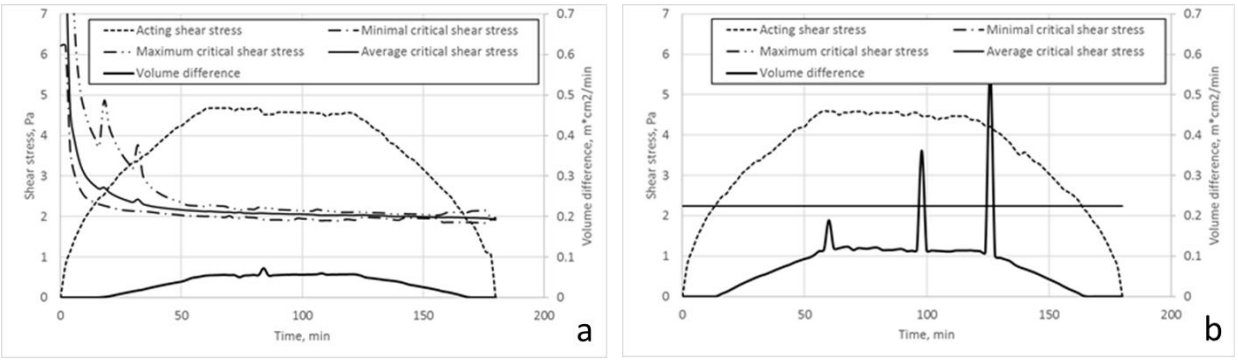


**Figure 5.5 Critical and acting shear stresses and the difference in the eroded volume in time for the VEP (a) and CEP (b) models.**

For both VEP and CEP models, erosion is present only when the acting shear stress exceeds the critical shear stress (Figure 5.5). The main difference between VEP and CEP models is that in the former, the critical shear stress and soil erodibility vary with time. Higher critical shear stresses for the VEP model can be explained by the lower hydraulic pressure gradients at the channel boundary due to a relatively dryer soil profile compared to the positive water pressure of the channel.

The peaks in the erosion rate graphs (Figure 5.5 and Figure 5.6) can be explained by the bank failure due to soil grid cell undercutting. An increase of the channel depth with time (Figure 5.4) can explain high jumps in eroded volume graphs in Figure 5.5.b and Figure 5.6.b. Overall higher erosion rates for the constant erosion parameters (CEP) model are explained by the significant decrease (by 45% of reference value alone) of the soil erodibility for the VEP model.

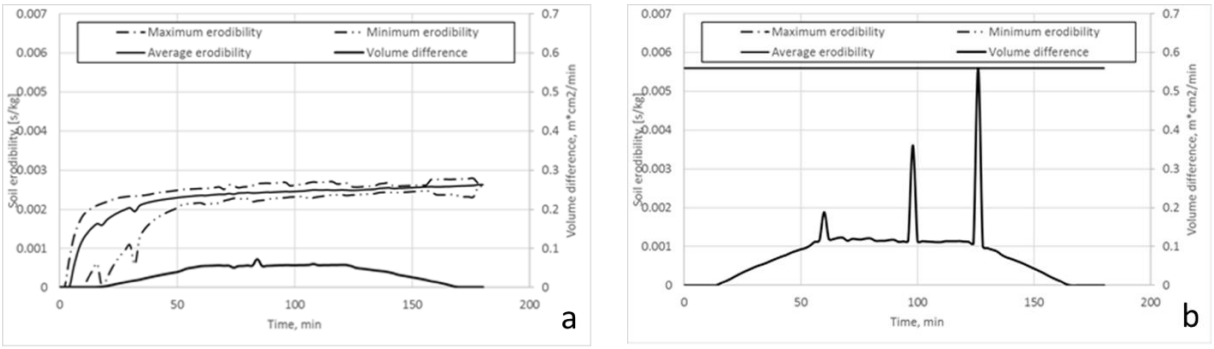


**Figure 5.6 Soil erodibility and difference in the eroded volume in time for the VEP (a) and CEP (b) models.**

## Results

Four modeling case studies were conducted and used to investigate the influence of four factors: (1) soil type, (2) the initial soil saturation, (3) groundwater depth, and (4) soil heterogeneity in the form of different layering – on channel erosion by varying permeability and the top soil depth. This investigation used the model, which was described above, and considered effects of subsurface fluxes. Where it is applicable, all scenarios have the same domain geometry, initial and boundary conditions, surface runoff in the channel, and initial soil moisture content.

### Study 1: Impact of Soil Type

Soils are very diverse material; they change their texture and structure based geographic locations, agricultural practices, biodiversity, and weather patterns. All soils have different responses to any runoff erosion. While the soil type is considered in erosion models, the effect of subsurface fluxes on soil particle detachment is not included. This is because it is expected that different soils will respond differently to the effect of variable subsurface fluxes.

To study these effects, a series of numerical experiments was performed for six soils. In addition to the Clark-Ost clay loam soil which was considered for the base case scenario. These six soils (Figure 5.7) were compared to study the erosion process sensitivity to the soil type with the respect to variable critical shear stress and soil erodibility due to the changes in hydraulic pressure gradient.

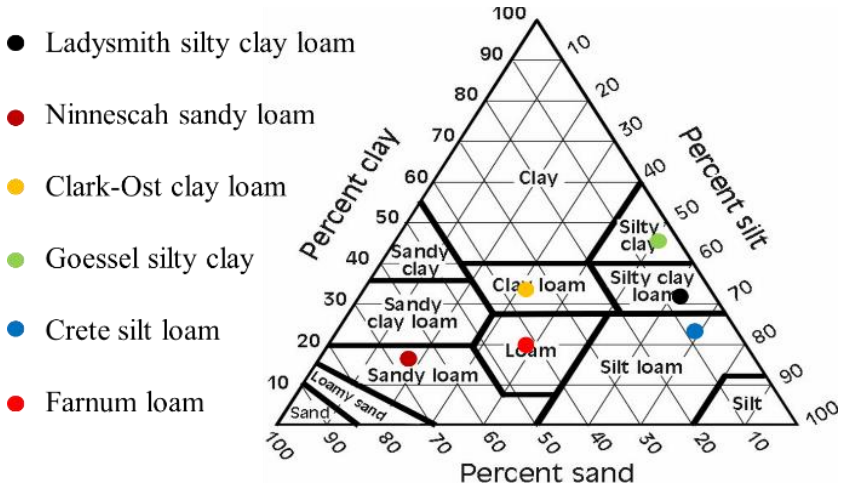


**Figure 5.7 Six selected soils for numerical experiment.**

For the baseline scenario, the hydraulic properties were computed based on the texture data from SSURGO database (KDASC, 2013) were applied to the ROSETTA model (Schaap et al., 2001) and are presented in Table 5.1.

For this study, the results are presented in Figure 5.8 in the form of a cumulative change of channel cross-section in time for the VEP and CEP models. Figure 5.8 shows a clear distinction between two groups of soils: (1) Crete, Ladysmith and Goessel; and (2) Farnum, Clark-Ost, and Ninnescah. The difference can be explained by the differences in the reference critical shear stress caused by low sand content for the group of Crete, Ladysmith and Goessel soils. Within that group, for the CEP model, the erosion rates are higher for Crete and lower for Goessel. This difference is expected due to variations in reference soil erodibility coefficient

(Table 5.1). Interestingly, if the VEP model is used, the erosion rates of these soils change their order to the opposite one, regardless of having the same reference soil erodibility values. Such behavior can be explained by different effects of subsurface flows on soil cohesion at the channel boundary. The Goessel silty clay will more likely develop higher pressure gradients than will Crete silt loam.

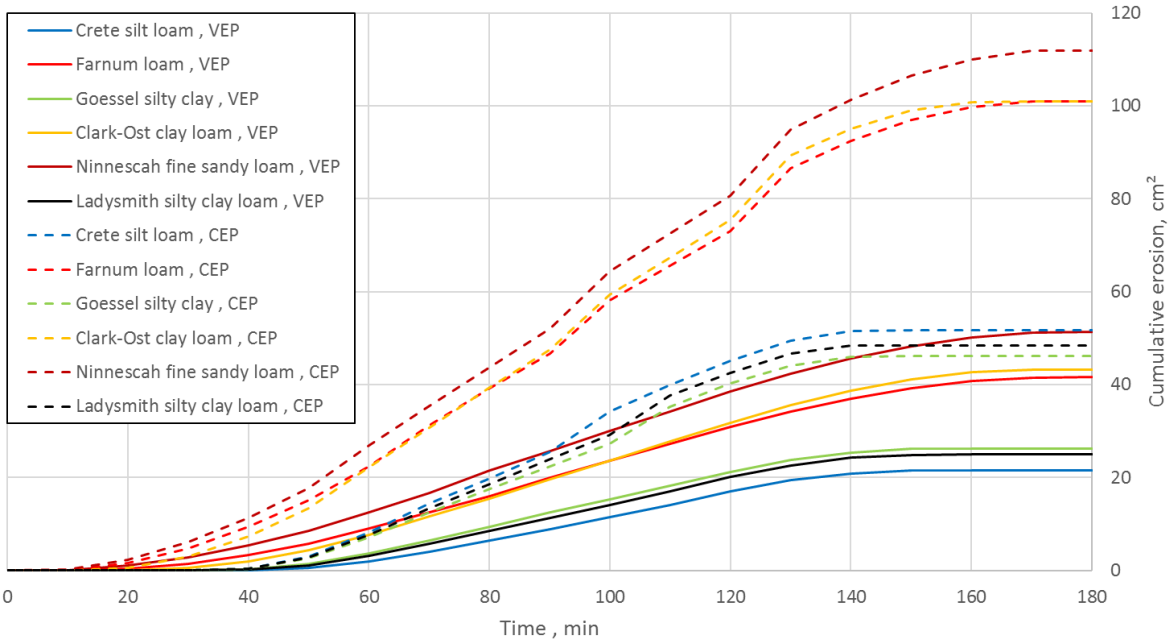


**Figure 5.8 Cumulative erosion for six selected soils in time.**

## Study 2: Impact of Initial Saturation

Models of soil erosion rarely account for the effects of antecedent soil moisture condition on soil cohesion and soil particle detachment; even if they do, it is only in the form of a decrease or an increase in the amount of surface runoff. The soil moisture effect on the erosion model parameters is accounted for only in conceptual models (i.e., A. Al-Madhhachi et al., 2014). Thus, it is interesting to investigate the effect of the initial soil moisture conditions on the erosion process with the VEP model.

Furthermore, based on the results of the study of six soils, Farnum loam, Goessel silty clay and Crete silt loam were selected with the aim of investigating the effect of the initial soil moisture condition on the erosion process. For this study, the boundary of no flux conditions were used as the same for the baseline scenario except the initial saturation took values of 40%, 60%, 80%, 90% and 95%. According to Equation 5.5, initial saturation was converted to the uniform initial soil pressure. It must, however, be noted that the effect of the initial saturation on runoff from the catchment and the hydrograph was not taken into account. This assumption was made to investigate the local effect of initial saturation on the erosion process within the channel independently.

Figure 5.9 depicts the total eroded area of the channel cross-section of a unit long channel for three soils at various initial saturations.

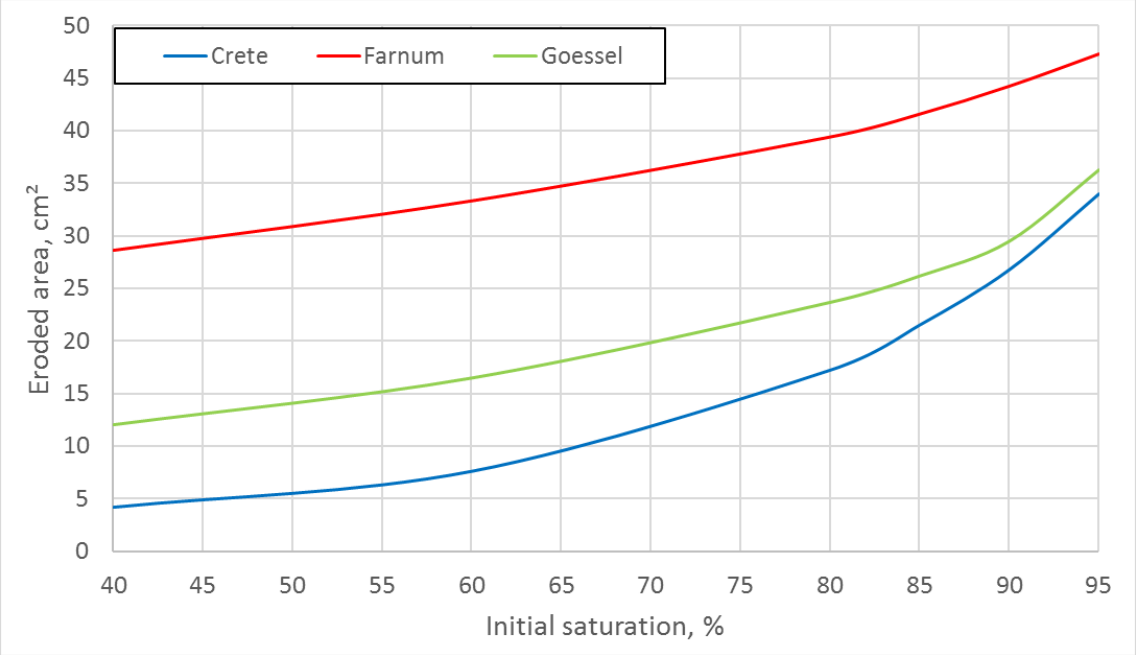


**Figure 5.9 Eroded area for three soils and variable initial saturation.**

For all three soils, the more the eroded area increases, the more the initial saturation increases. This trend may be explained by higher drainage gradients for soils under near

saturation condition. When the whole soil profile is wet, the water flux within the profile decreases. This corresponds to higher drainage (negative) gradients, which decrease soil erosion according to the change of erosion parameters defined by the VEP model.

On the other hand, the relatively dry condition of the soil profile causes a significantly higher influx of water into the soil from the channel which corresponds to low (high in magnitude, but negative) pressure gradients. Lower gradients increase the critical shear stress and decrease soil erodibility, thus resulting in an overall decrease in the total soil erosion rate.

The overall effect of the initial saturation on total soil erosion can be assessed with the percentage of the increase in total eroded area for 40% versus 95% saturation. In this case, Farnum loam had a 65% increase in the erosion rates, Goessel silty clay had 200 % increase, and Crete silt loam over 700% increase. Crete silt loam also shows a strong nonlinear relationship compared to other two types of soil. Therefore, it can be concluded that the higher percentage of silt in Crete silt loam was more susceptible to the effect of the initial saturation than were the other two soils.

### Study 3: Impact of Groundwater Depth

Similar to the case of initial saturation, high groundwater levels are rarely accounted in the erosion models. Nonetheless, it is known that a higher water table may significantly alter the erosion process (Tebebu et al., 2010; R. Wells et al., 2009). Thus, the effect of various groundwater levels on the erosion was studied with the VEP model.

The same three soils, utilized for the study of impacts of initial saturation, were used to study the effect of groundwater. Boundary conditions and channel fluxes were kept the same as in the baseline scenario. However, the initial pressure condition was changed to accommodate

the saturated soil within the layered domain. The groundwater was also modeled in the form of zero soil pressure at a depth of the groundwater table. The linear pressure change with depth was assumed for the rest of the profile with the system being in the hydrostatic equilibrium. Also modeled were the depths of groundwater table from 10 to 150 cm, and the cumulative erosion was calculated. Similar to the study on initial saturation, the effect of groundwater on the change of the runoff and peak discharge was implicitly ignored to investigate only the effect on soil erosion of groundwater level.

Figure 5.10 presents the total eroded area for a range of groundwater depths for three soils. As shown below, all the soil types showed similar results. The more their groundwater depth, the more their eroded area decreased. For Farnum loam and Crete silt loam soils, there was no increase in eroded area when the groundwater depth was between 10 and 40 cm.

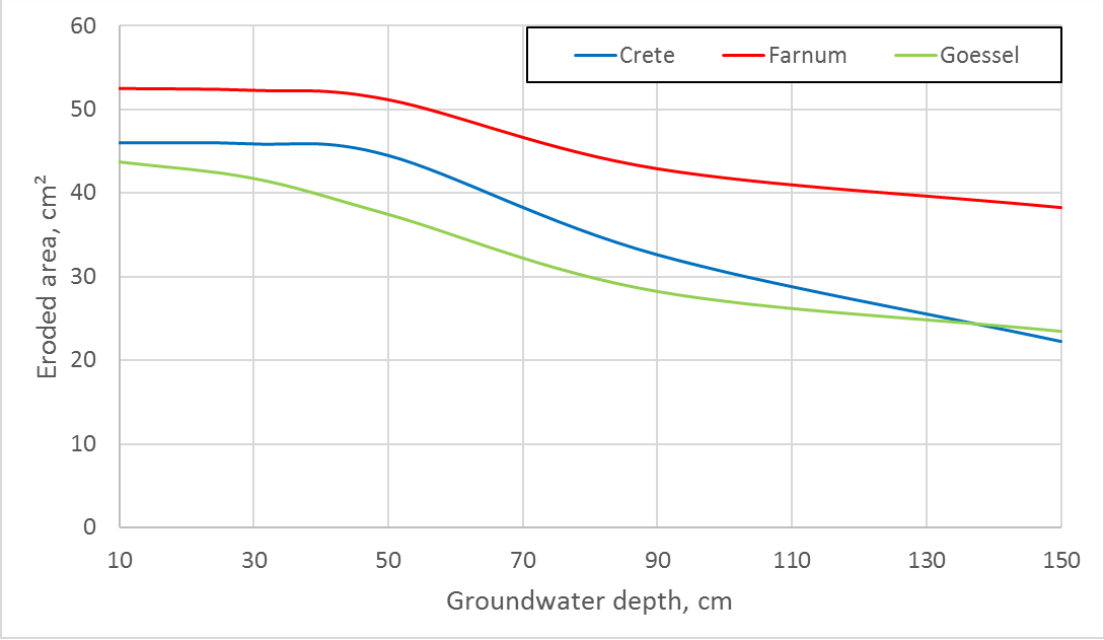


**Figure 5.10 Eroded area for three soils and variable groundwater depth.**

Interestingly, for shallow groundwater (up to 40 cm depth), the eroded area was within 10 cm² for three soils; as for the case of 85% initial saturation, the difference in the area was about

20 cm². A similar conclusion can be drawn for shallow groundwater depth (less than 40 cm) compared to the deeper groundwater level (more than 120 cm). This finding can be explained by the influence of the hydraulic pressure gradients which, in the case of a close proximity of the full saturation (shallow groundwater) causes, reduced critical shear stress and higher erosion rates. Also, the difference in total erosion for shallow versus deep groundwater level for Crete silt loam is higher (23.8 cm²) than that of Farnum loam (14.3 cm²). To say it another way, the Crete silt loam is more sensitive to the effect of hydraulic gradient on the erosion parameters than Farnum loam.

The form of the erosion curves in Figure 5.10 is similar to the form of the water retention curve for the same soils. Their similarity may be explained by the fact that the level of groundwater relates to the zero pore water pressure. In this case, the lower groundwater level would change the initial pressure and the pressure gradient towards the higher drainage, including the lower erosion rates.

### Study 4: Impact of Soil Layers

The soil is a heterogeneous porous medium. Even in the laboratory settings, it is difficult to consistently replicate the same experiment on a soil and obtain the same outcome. Moreover, under field conditions, the soil structure is even more complex with plant roots, biota activity, management practices, and the present geologic features. Such complex soil heterogeneity can be mimicked by introducing soil layering structure with different retention parameters. In the most detailed U.S.-wide soil database, SSURGO database (KDASC, 2013), soil layers below the surface often have a saturated hydraulic conductivity of one order or sometimes two orders of magnitude lower than in the top soil layer. Such layers can be called clay pans. Another possible

case of the saturated hydraulic conductivity reduction with depth can be explained by the presence of excessive traffic causing the formation of compacted soil layers called plough pans. In this study, a reduced saturated hydraulic conductivity of the second soil layer at the depths of 15 cm (denoted as "D15" in Figure 5.11) and 30 cm (as "Base" in Figure 5.11) was applied and studied.

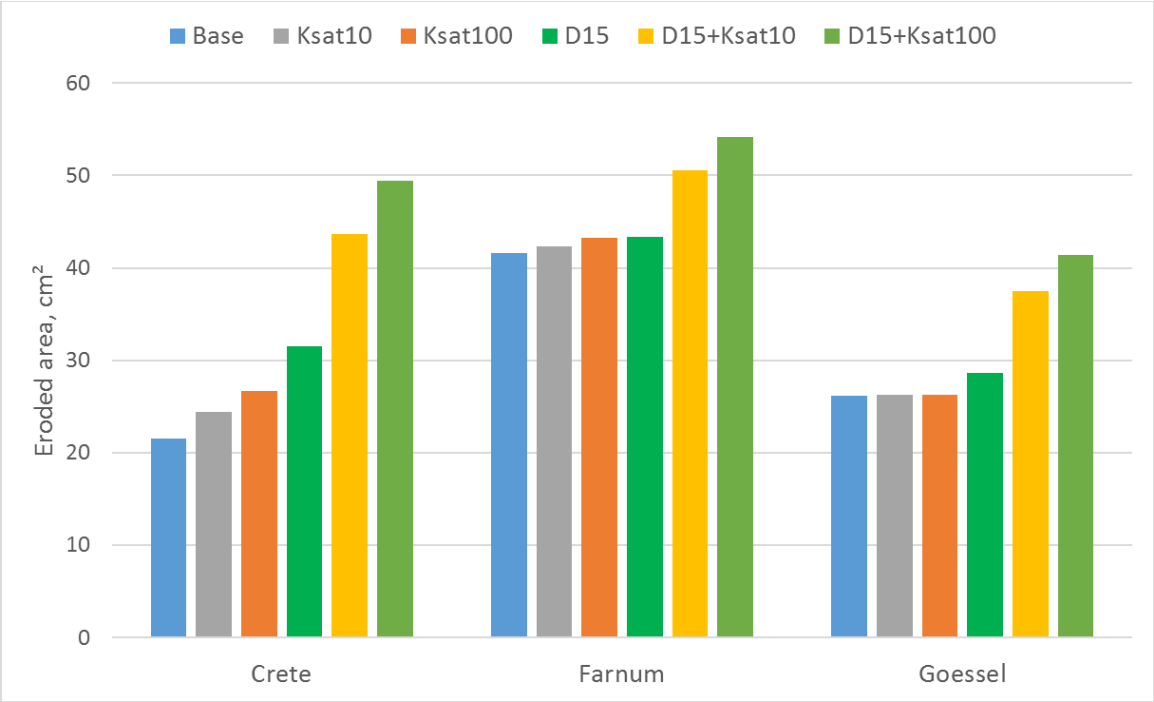


**Figure 5.11 The eroded area for three soils and various layering conditions: Base is the baseline scenario, Ksat10 and Ksat100 is the scenarios with the 10 and 100 times lower saturated hydraulic conductivity consequentially, D15 is the scenario with the depth of top soil of 15 cm, and D15+Ksat10 and D15+Ksat100 are the combinations of the scenarios.**

Crete silt loam, Farnum loam, and Goessel silty clay soils were used for this study. All model parameters – such as boundary and initial conditions and channel and rainfall fluxes – were used as the baseline scenario, while the two parameters related to soil layering were adjusted for this study. The first parameter is the saturated hydraulic conductivity of the second soil layer below the top soil layer. Also used were additional values of 0.1 and 0.01 as

multiplications of the original value (denoted as “Ksat10” and “Ksat100” in Figure 5.11), which were calculated based on the ROSETTA model (Schaap et al., 2001). Two depths of the second layer were considered for all values of saturated hydraulic conductivity (“D15+Ksat10” and “D15+Ksat100”).

All three soils showed a significant dependence on the reduced saturated hydraulic conductivity for the 15 cm depth of the second layer (Figure 5.11). Such behavior can be explained by the effect of pressure propagation in the soil profile. Pressure buildup in the shallow soil layers is possible only if both conditions are met: the relatively shallow depth and the reduced hydraulic conductivity. If the conductivity is changed, then there may not be enough time for water during the rainfall event to reach the second layer and allow the pressure buildup. On the other hand, if only the depth is decreased, then the saturated hydraulic conductivity may be sufficiently high and not allow a pressure buildup.

When the influence of pressure is present, erosion rates are expectedly higher for the lower saturated hydraulic conductivity for all three soils. This observation is also explained by the sooner relative pressure buildup for the lower conductivity. What’s more, only Crete silt loam showed a significant dependence on the saturated hydraulic conductivity for the 30 cm depth of the second layer. This result shows that the subsurface condition in Crete silt loam allows the sooner relative pressure buildup even with the 30 cm deep soil second layer. In short, the Crete silt loam soil showed higher susceptibility to the effect of the pressure gradient.

# Discussion

## Influence of Subsurface Fluxes

The influence of the initial conditions on the erosion process was investigated in two modes: a study of the influence of the initial saturation profile and a study of the influence of the groundwater depth. Both studies had one common condition that was investigated: the amount of pore water in the soil domain at the beginning of the numerical experiment. Expectedly, both experiment sets showed the same trend of the increased erosion rates for higher initial water content. This finding is explained by a buildup of higher hydraulic pressure gradients for a higher antecedent water content. By comparing Figure 5.9 and Figure 5.10, it may be concluded that the curve of the total eroded area versus initial saturation can be a part of the curve of total eroded area versus the groundwater depth. This conclusion can be explained by the different initial saturation of the top layer corresponding to the different groundwater depth. For example, as groundwater depth increases, the overall saturation of the soil profile decreases. Then, the variable initial saturation would define the differences in the pressure gradients and differences in erosion rates. Moreover, if the system reaches equilibrium, the soil moisture distribution should mimic the distribution of the water retention curve. This means that the function of soil saturation versus the depth would be the same as the water retention curve with the soil water content versus pressure heads. On the other hand, if the system is not in the equilibrium, the water retention curve is satisfied. This also means that the distribution of the soil moisture with the depth is different. This effect can also explain the shape of the curves in Figure 5.10 where an increase of groundwater depth relates to the initial condition of the moisture in the soil profile formulated in terms of pressure.

## Soil Erosion and Management

One of the benefits of using the VEP model is that it makes it possible to model the effect of agricultural field management and soil layering for the stage of channel erosion before the channel depth reaches the non-erodible layer. Non-erodible layers usually have low permeability, which creates strong differences in hydraulic pressure gradients due to differences in the layers' hydraulic conductivities. In addition, the use of the VEP model allows differentiating model runs with various initial and interior conditions. The use of the proposed modification to the erosion equation significantly reduced the overall erosion rates compared to the CEP model. This means that for the selected acting shear stress (as demanded by channel geometry and flow depth), hydraulic gradients caused drainage conditions of water moving into the soil, thus providing stabilizing effects to the soil material and reducing erosion rates. If strong seepage gradients are present with water exfiltrating from the soil domain, then the increase in the erosion rates is expected. For the selected and presented channel flow (initial and boundary conditions), the reduction in erosion rates may be explained by the significant (up to 45%) decrease in soil erodibility coefficient within the VEP model. If other parameters of the VEP model were used with the same computed gradients and the acting shear stress, the critical shear stress and soil erodibility coefficient might have resulted in strong seepage conditions. Because of this, such parameters need to be detetermined from experimental studies. Conducting such experiments is a complicated task since the control and measurement of channel flow and seepage conditions are needed for various levels of flows and pressure gradients, in addition to common soil properties. Although parameters used in this study were determined from the experiment for clay loam soil, more cross-check experimental studies are still necessary for other soil types.

## Possible Channel Shapes

An advantage of the use of the VEP model is that it may be used to investigate the effect of hydraulic pressure gradients on the shape of the channel. In some cases, initial and boundary conditions can cause relatively higher hydraulic gradients in the horizontal direction which causes a faster widening of the channel. Alternatively, the conditions can be created for the formation of the W-shaped channels (Figure 4.4). To showcase this effect, one scenario was calculated for the Crete soil with the following initial and boundary conditions: a groundwater depth of 20 cm, a depth of the second layer of 30 cm, no rainfall during the simulation, the same channel flow and a side flux into the domain at AE boundary of 0.04 cm/h (Figure 4.2). This scenario may represent the case of the channel erosion process at the end of the rainfall event and close to catchment outlet when runoff is present and infiltrated water percolates into the domain as a lateral subsurface flow. The high groundwater table was caused by the series of antecedent rainfall events. Figure 5.12 depicts how the depth of W-shape channel varies with time.

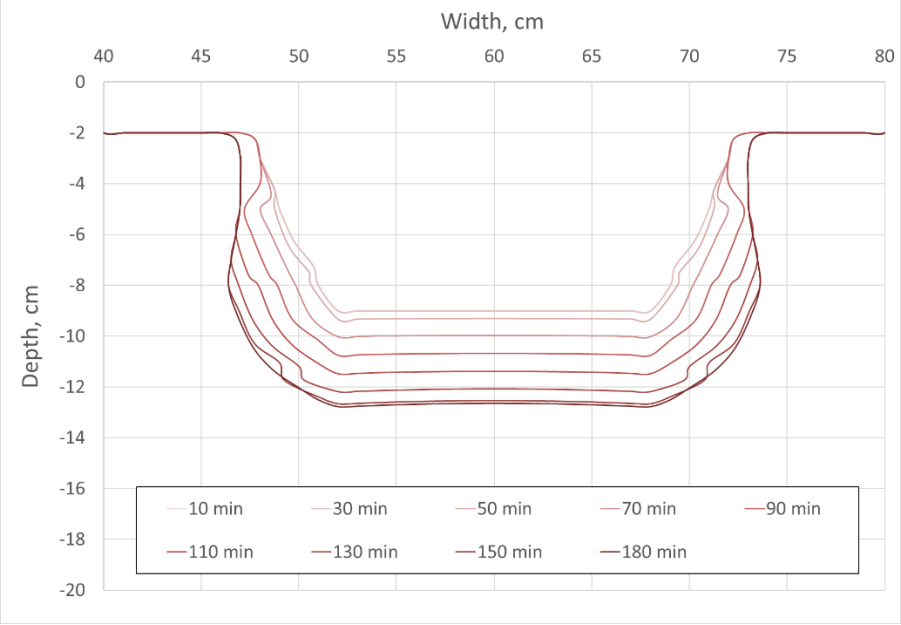


**Figure 5.12 W-shape channel cross sections in time.**

As shown above, the cross sections for different times channel has higher erosion rates at the corners. Such behavior can only be explained by the differences in hydraulic pressure gradients, a behavior that is allowed only with the VEP model. On the other hand, the CEP model would only allow a uniform channel development (Figure 5.4.b) with a shape that is controlled by the channel flow and the initial shape.

The total eroded area for this scenario was 62.1 $cm^2$, which is significantly higher than the erosion for other VEP model scenarios of Crete silt loam; it is even higher than the total eroded area of the CEP model run. This result proves that the VEP model incorporates the results of a CEP model as a special case. In this way, the VEP model can be used to simulate a much wider range of channel erosion problems.

Equally important is that the use of the suggested VEP model requires significant computing power, and such model can only be suggested for research studies. However, with the introduction of certain simplifications, it may be used in the other already developed soil erosion models. One of the suggested simplification is the use of global pressure gradients in the horizontal and vertical directions for rectangular-shaped channels. In that case, channel propagation will only be allowed for the rectangular shape where widening would be adjusted due to the lateral flow, and the deepening would be adjusted due to the infiltration rate. Global hydraulic pressure gradients may also be assessed from the flow in the soil and known saturated hydraulic conductivity via Darcy's equation or by a solution of the Richards's equation.

## Summary

This study considered the impacts of subsurface fluxes on the process of soil erosion due to concentrated flows. A previously described two-dimensional model (see Chapter 4) for

channel erosion allowed numerical calculations of subsurface fluxes, while the modified excess shear stress equation with the VEP model allowed one to account for the influence on channel bed retreat rates. The baseline scenario presented the difference in the VEP model and the CEP model, as well as concluding that the erosion process could be affected by seepage/drainage forces.

Furthermore, four numerical experiment studies were conducted to investigate different effects on the erosion process. The first study consisted of computations of erosion for six different soils. Findings showed that all soils had similar behavior when the VEP model was used instead of the CEP model. The second study consisted of the computations for different initial soil moisture contents. Apart from the influence of the possible increase in the runoff, the effect of subsurface fluxes was considered. Results of the second research showed that the initially dried soil is less susceptible to erosion than saturated soil. The third study was similar to the second one and considered the groundwater depth. Results of this third research showed the erosion process dependence on the proximity of the groundwater depth. Conclusions were made on the similarity of the groundwater depth and the soil moisture content. Finally, the fourth study consisted of the computation of soil erosion for soils with introduced heterogeneity in the form of layering. Results showed that introducing an impervious layer significantly increases soil erosion. In addition, all the four studies showed that silt loam is the most sensitive to the subsurface flux soil type. Finally, the application of the VEP model significantly changes erosion rates compared to the rates computed with the CEP model. The VEP model also allows one to account for more parameters, thus allowing one to investigate the performance of best management practices in greater detail.

# Chapter 6 - Integrated Process-Based Modeling of Channelized Flow and Soil Erosion in Small Watersheds

## Introduction

It is a fact that a growing population of the world demands more food and clean water. Almost all the available arable land in the U.S. has been used for food production. Nonetheless, for sustainable agriculture, this land must be used responsibly considering all environmental, societal, and economic factors that have impacts on human subsistence. One of the most important agricultural and environmental issues is the loss of productive soil as a result of soil erosion. This insidious situation is getting worse with changing climate because of the amplifying fluctuations between droughts and excessive rainfall events causing a change in both the precipitation amounts and the soil moisture conditions. Hence, a better understanding of benefits of best management practices is needed in order to manage agricultural land more efficiently, preserve the U.S. soils, increase food production, and make water cleaner by keeping reservoirs from sedimentation and algal bloom. Thankfully, soil erosion processes have been extensively studied, and there is now a better understanding of the major factors that contribute to soil erosion.

Ephemeral gully erosion is well known as a significant source of topsoil loss from agricultural fields (A. Capra, 2013; J. Poesen et al., 2003). A number of soil erosion models account for the ephemeral gully contribution in different ways. Most of the models, however, use the approach of Foster and Lane (1983) or its simplified version. This approach assumes constant flux and computes erosion rates for the whole event. Based on the assumption of the acting shear

stress distribution over the wetted perimeter, this model can be used to determine the equilibrium width at which the channel erodes downward up to a non-erodible layer. Apart from that, the model employs excess shear stress equation (Equation 6.1) to determine the deepening rates.

$$E = K_e \cdot (\tau - \tau_{cr})^a \tag{6.1}$$

where $E$ is the erosion rate in (kg/s/m$^2$), $K_e$ is the soil erodibility (s/m), $a$ is the dimensionless parameter usually taken as 1, and $\tau$ is the acting shear stress (Pa). Once the non-erodible layer is reached, the expansion from the equilibrium width to the final width happens at a decreasing rate up to the total duration of the effective runoff.

Well-known Ephemeral Gully Erosion Model (Merkel et al., 1989) computes ephemeral gully erosion rates for the whole gully. It also has an event-based temporal scale. And erosion is calculated as a total ephemeral gully erosion for the whole event. It uses an empirical equation simplified from the approach of Foster and Lane to determine the equilibrium width. Another approach was used by S. M. Dabney et al. (2014). They used raster-based computed hydrograph fluxes and determined channel shape on the event basis with the help of Foster and Lane model (1983). The Erosion Model for Dynamic Rill Networks (Storm et al., 1990) also uses Foster and Lane model; however, in this model, the hydrograph is being treated as the series of flows of short duration with a constant flux. To accommodate such approach, the model adopts a variable in time two-tier channel shape. The CHANNEL model (Fogle & Barfield, 1992) also uses principles from the Erosion Model for Dynamic Rill Networks (Storm et al., 1990), the acting shear stress distribution from Foster and Lane (1983), and the jet impingement theory to account for the headwall propagation and the development of scour holes along the channel. This approach can also be used to depict the development of the variable channel cross-section shape, which is represented by the series of the segments. The Water Erosion Prediction Project (WEPP) model (D. C. Flanagan, 2012) has a watershed version which may compute channel

erosion for ten segments of the channel using the Foster and Lane approach, and the erosion for the channel segments is still being computed on the event basis. Even though the WEPP model produces dynamic hydrograph, it only uses the effective flat hydrograph of peak runoff rate with an effective duration. The European Soil Erosion Model (Morgan et al., 1998), unlike WEPP model, produces dynamic hydrograph and sediment graph and uses them for the dynamic spatially distributed computation of channel erosion. However, the channel geometry is the same through the channel, and it is simplified to the trapezoidal shape with the erosion process occurring uniformly over the contact area. Spatial and temporal distributions and the channel geometry options of described models are presented in Table 6.1.

**Table 6.1 Comparison of the physically based ephemeral gully erosion models**

| Model | Channel Geometry | Hydrograph and Sediment Graph | Spatially Distributed |
|---|---|---|---|
| EGEM | simplified Foster and Lane | flat | single channel |
| EphGEE | simplified Foster and Lane | flat | raster based |
| Dynamic Rill Network | modified Foster and Lane | dynamic | single channel |
| CHANNEL | complex | dynamic | distributed |
| WEPP | simplified Foster and Lane | flat | distributed |
| EUROSEM | trapezoidal | dynamic | distributed |
| Proposed | modified Foster and Lane | dynamic | distributed |

All models use basic erosion principle at different temporal and spatial scales and various complexity of the channel shape from the erosion with a single shape for the event as a whole to the distribution of the hydrograph and complex channel shape. However, there is still a need for an approach with high-resolution temporal and spatial scale but with the simple yet representative channel geometry so that it can be robustly applied to the large areas with numerous small watersheds. The new approach can additionally benefit from the incorporation of the interaction of concentrated flows with subsurface hydrological processes to account for the

effect of changing erodibility parameters due to seepage/drainage conditions and the antecedent soil moisture content.

The main goal of this study was to evaluate conditions and rates of ephemeral gully erosion on agricultural fields. The specific objectives were to develop an integrated process-based model of soil erosion from ephemeral gullies and to evaluate the performance of several best management practices, such as no-till (NT) and conversion to prairie (P), compared with a practice of conventional tillage (T). For the first objective, the developed integrated model should connect surface runoff from a contributing catchment with soil hydrological regime through soil moisture dependent erosion parameters.

## Mathematical Model

A physically-based mathematical model was developed. It uses a dynamic integration of runoff hydrograph from contributing catchments and channel routing algorithms to compute spatially distributed soil erosion from the ephemeral gully in soil with the non-erodible layer. The model consists of several modules, inputs, and outputs that are schematically shown in Figure 6.1. The input parameters for the WEPP model (described later) consist of the soil type, the rainfall amount and distribution, and the management practices. The WEPP model then produces an output hydrograph, soil erodibility parameters, and a total sediment loss which is then used to determine the sediment graph. The soil roughness and channel slopes are used to rout hydrograph in the channel and obtain the estimate hydrograph of channel flow which is used to determine seepage/drainage gradient and adjust soil erodibility parameters. Once the final soil erodibility is known, the final channel flow is calculated. The calculated value is used to determine the potential erosion which is then adjusted to the actual erosion/deposition rates due

to the transport capacity calculated based on the soil type and computed acting shear stresses. All processes are described in detail below.

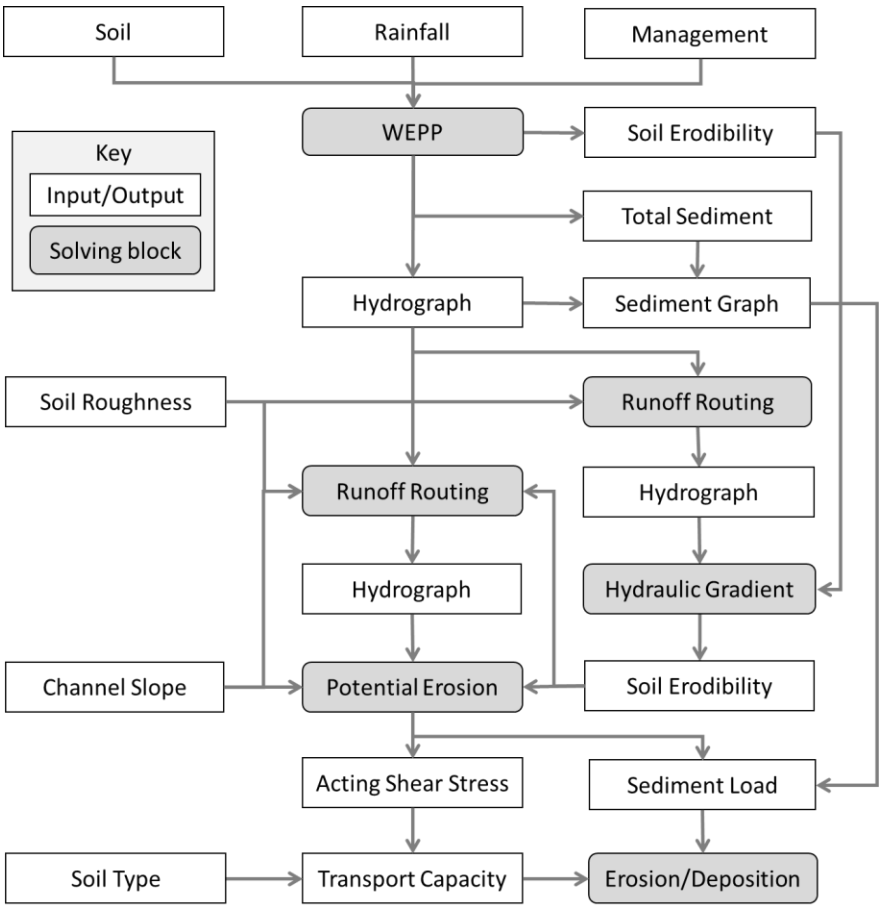


**Figure 6.1 Flowchart of the proposed model.**

## Ephemeral Gully Representation

An ephemeral gully is represented by a channel divided into segments of equal lengths (Figure 6.2). Each channel segment has a constant depth, width, and slope within each segment. Overall, the rectangular shape with the parabolic bottom (described later) stays the same for any segment. The flow into the channel is provided by surface runoff from either a single gully headcut catchment (point A) or channel segment side catchments (B and C).

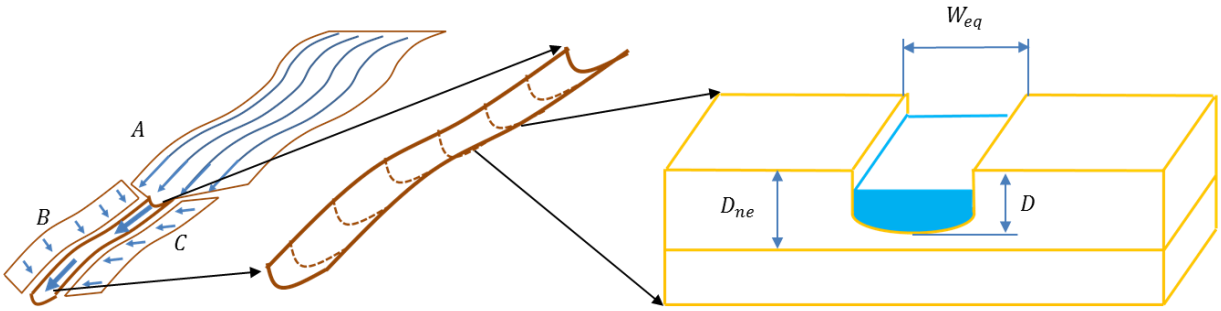


**Figure 6.2 Geometrical representation of the ephemeral gully.**

## Catchment Hydrograph

The catchment hydrograph was determined with the use of a WEPP model (D. C. Flanagan et al., 1998). It utilizes a simplified one-dimensional kinematic wave approach to rout the hydrograph through the rectangular representation of the catchment. The WEPP model can be used to account for management practices by changing the parameters of the soil such as infiltration and roughness depending on the type and the time since the last tillage operation. The WEPP model also computes sheet and rill erosion along the representative slope and produces a total sediment loss for the event. Although it produces a distributed hydrograph, only an effective hydrograph is used to compute soil erosion. An effective hydrograph is the hydrograph with the constant water flow of a peak rate and with the duration weighted to this peak rate so that the total runoff is the same. The distributed hydrograph was used as the output hydrograph from the catchment.

## Hydrograph and Routing

Both headcut and side catchments are modelled with the WEPP model (described above). Specific parameters for the WEPP models were based on the characteristics of individual catchment areas such as soil, topography, area, vegetation, surface roughness, and management.

Also, time intervals within the output hydrograph were strictly defined by the WEPP model output. Similar to the approach used in the Dynamic Rill Network (Storm et al., 1990), the model hydrographs are represented as a step-wise function with a constant flux during each time step (Figure 6.3). Such approach, unlike the approach of effective hydrograph (described above), allows the possible sediment deposition during each time. A sediment graph is determined based on the simulated hydrograph and a combined sediment load from headcut and side catchments. An assumption of constant sediment concentration is used for sediment graph calculations.

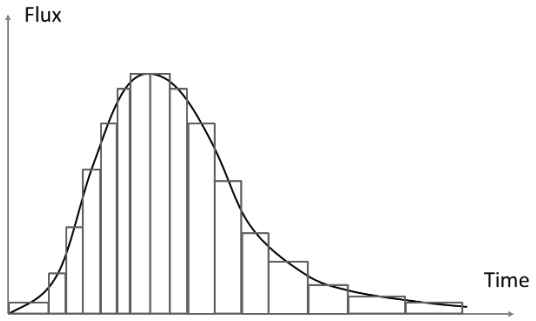


**Figure 6.3. Hydrograph discretization in time.**

Input fluxes from headcut and side catchments are routed through the ephemeral channel by solving the kinematic wave equation:

$$\frac{\partial Q}{\partial x} + \frac{\partial A}{\partial t} = q \tag{6.2}$$

where Q is the channel flux ($m^3$/sec), A is the area of the channel cross-section ($m^2$), q is the distributed side flux ($m^2$/sec), x is the distance (m), and t is the time (sec). The cross-sectional area of the channel segment is determined with an assumption that the channel is always at its equilibrium width determined from the Foster and Lane model (1983), described in the "Erosion" section as a function of the critical shear stress and water flow rate. This makes the Equation 6.2 non-linear. For numerical modeling, the discretized form of Equation 6.2 requires being linearized within the iterative solution of the discretized equation. A finite difference

numerical method is used to solve the kinematic wave equation (Equation 6.3) representing a one-dimensional channel:

$$\frac{Q_{i+1}^{n+1}}{2\cdot\Delta x}-\frac{Q_{i-1}^{n+1}}{2\cdot\Delta x}+\frac{A_i^{n+1}}{\Delta t}-\frac{A_i^{n}}{\Delta t}=q_i^n \tag{6.3}$$

where superscript *n* denotes a time step, and subscript *i* represents the channel segment.

A cross-sectional area of each channel segment is determined by the Manning's equation for current (n+1) and previous (n) time steps:

$$A_i^{n+1}=\frac{Q_i^{n+1}\cdot n_M}{\sqrt{S_i}\cdot\left(R_i^{n+1}\right)^{2/3}} \tag{6.4}$$

$$A_i^{n}=\frac{Q_i^{n}\cdot n_M}{\sqrt{S_i}\cdot\left(R_i^{n}\right)^{2/3}} \tag{6.5}$$

where R is the hydraulic radius determined by Foster and Lane model (1983) (m), S is the local slope of the channel segment (m/m), and $n_M$ is the Manning's roughness coefficient ($m^{1/6}$).

Substituting Equations 6.4 and 6.5 into Equation 6.3 results in the discretized form of the kinematic wave equation that is solved for the flux *Q*:

$$\frac{Q_{i+1}^{n+1}}{2\cdot\Delta x}-\frac{Q_{i-1}^{n+1}}{2\cdot\Delta x}+\frac{Q_i^{n+1}\cdot n_M}{\sqrt{S_i}\cdot\left(R_i^{n+1}\right)^{2/3}\cdot\Delta t}-\frac{Q_i^{n}\cdot n_M}{\sqrt{S_i}\cdot\left(R_i^{n}\right)^{2/3}\cdot\Delta t}=q_i^n \tag{6.6}$$

The backward-implicit scheme is used for the discretization in time. The iterative Picard method (Lapidus, 1982) is used to improve the solution for the unknown equilibrium width. Hence, Equation 6.6 is solved numerically to approximate the width from the previous time step and then solved again in the same form for an improved estimate of the width for the current time step. Time steps, which were ranging from 1 minute to 5 minutes, were determined by the timestep of the WEPP output. The flux boundary condition is used at the top with the flux determined from the hydrograph for the headcut catchment with WEPP ($x=0$: $Q_1=Q_{WEPP}$), and the uniform slope and channel shape ($x=L$: $Q_N=Q_{N+1}$) conditions are used at the bottom of the domain.

## Erosion

Changes in the channel cross-section occur due to soil erosion along the channel boundary and sediment deposition to the channel bed. Several erosion scenarios are possible for each channel segment depending on multiple factors such as the current flow rate, sheet and rill sediment delivery rate from the headcut and side catchments, and erosion from the upstream channel segments. These conditions regulate the amount of soil leaving each channel segment for each time step. When the transport capacity is exceeded, soil deposition occurs. In the proposed model, the soil erosion is computed based on the calculation of the maximum available (potential) erosion and adjustments according to sediment transport capacity.

The potential erosion is computed based on the modified Foster and Lane model (Foster & Lane, 1983) with an assumption of the infinite transport capacity. The widening and deepening rates are also determined with the classical Foster and Lane model (1983). This model assumes the distribution of the acting shear stress over the wetted perimeter of the channel. The linear coordinate of the wetted perimeter, where the acting shear stress equals to the critical shear stress, determines the equilibrium width of the downward movement of the channel bottom. Once the channel reaches the non-erodible layer, it starts to widen at a decreasing rate. Rates of the downward movement and widening are being determined with Equation 6.1, which accounts for the distribution of the acting shear stress.

The actual erosion and deposition are adjusted based on the calculated sediment load and actual transport capacity within the channel. The erosion and deposition in each segment of the channel are computed for each time step. Although in the Foster and Lane model, the virtual channel shape has a parabolic profile at the bottom (see Figure 6.2), the channel width and channel depth are introduced as the two main factors representing the channel cross-sectional

profile. Therefore, a rectangular representation of the channel is adopted in the model where the depth of the rectangle is the lowest point of the channel, and the channel width is determined by the equilibrium width. If the equilibrium width is higher than the equilibrium width from the previous time step, a new width is adopted. At that step, the channel depth is also adjusted such that the total area of the channel stays the same (Figure 6.4). This approach, unlike the one from the Dynamic Rill Network model (described in the Introduction), assumes more physical channel shape reconfiguration as the channel walls collapse and deposit sediment at the bottom of the channel.

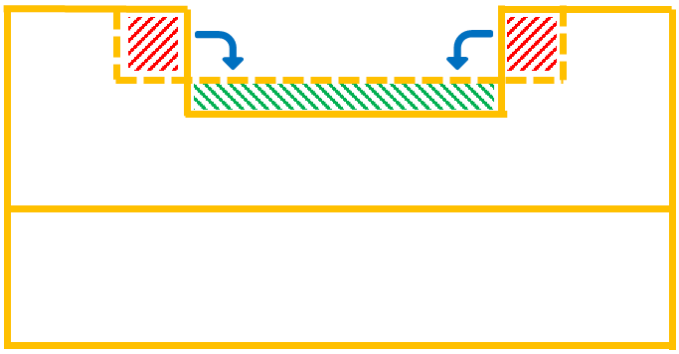

**Figure 6.4. Scheme of the sidewalls failure for higher equilibrium widths: red – failed material, green – deposited material.**

Foster and Lane's model assumes a constant flow during the runoff event for determining a shape of the channel cross-section. In the case of time-dependent channel flow rates, a modified approach is introduced. The channel shape re-configuration scheme (see Figure 6.5) shows the process of computing potential erosion with the modified approach of Foster and Lane model to allow channel erosion driven by hydrograph with a variable erosion rate. The differences are noticeable in the adjustment of the initial width and depth, compared to the previous time step, and the channel reshaping after the current time step if two-tier channel shape was used (see below).

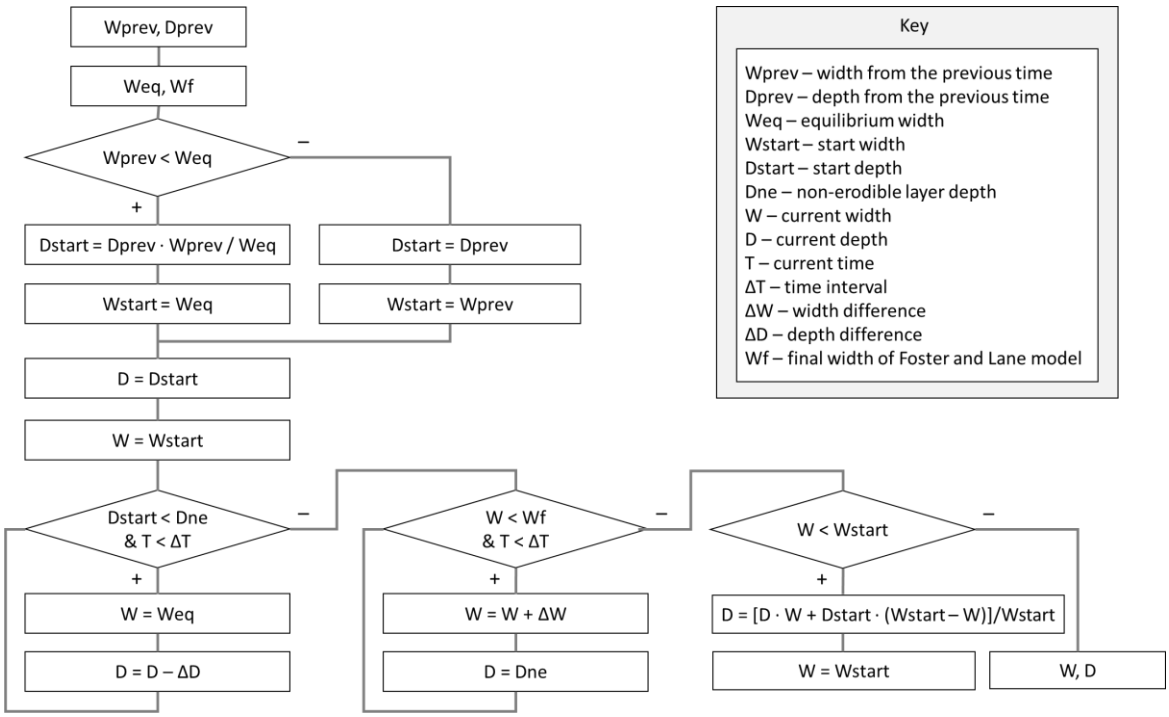


**Figure 6.5 Modified scheme of widening and deepening of the channel.**

For the case when the equilibrium width is smaller than the current width of the channel from the previous step, a two-tier channel is used for the application of the classical Foster and Lane approach (Figure 6.6). In this case, if the channel reaches non-erodible layer, the depth of the bank is lower for the widening stage until it reaches the width from the previous time stage. The current depth is being adjusted when the current width is lower than the width at the beginning of the current time step.

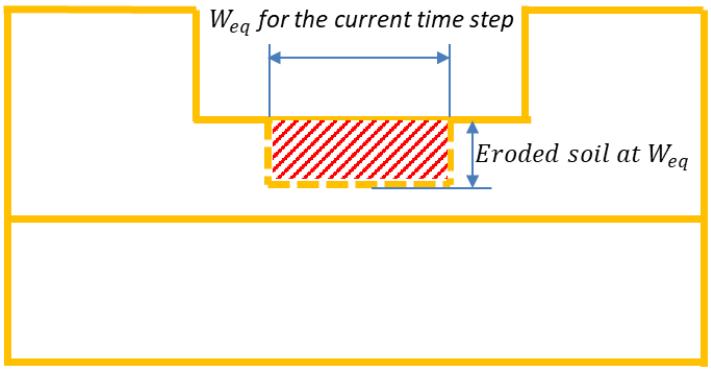


**Figure 6.6 Temporary two-tier channel shape.**

The increase of the equilibrium width occurs on the rising part of the hydrograph. On the declining part, the equilibrium width is lower than the width from the previous time step (Figure 6.6). In this case, the erosion rate is computed for the equilibrium width, but the final width is adopted from the previous time step. However, the eroded depth is reduced to ensure the same eroded volume. Also for any time step, it is possible that the channel reaches a non-erodible layer; in any case, both the final depth and the width are taken into account in computing the eroded volume.

Erosion/deposition is determined by the solution of the quasi-steady-state sediment continuity equation (Equation 6.7) for each time step and the whole channel.

$$\frac{dG}{dx} = D_f + D_s \tag{6.7}$$

where $G$ is the sediment load (kg/m/sec), $D_f$ is the erosion/deposition rate from the channel (kg/m²/sec), and $D_s$ is the sediment income from the side catchment (kg/m²/sec).

The erosion rate is computed with Equation 6.4:

$$D_f = D_c \cdot \left(1 - \frac{G}{T_c}\right) \tag{6.8}$$

where $D_c$ is the potential erosion rate from the channel (kg/m²/sec), and $T_c$ is the transport capacity (kg/m/sec) which is determined with the Equation 6.5 (Finkner, Nearing, Foster, & Gilley, 1989):

$$T_c = K_f \, \tau_{act}^{3/2} \tag{6.9}$$

where $K_f$ is the transport capacity coefficient (kg/m/sec/ $Pa^{3/2}$) which can be used as a calibration parameter and a control of erosion/deposition process threshold, and $\tau_{act}$ is the acting shear stress (Pa).

Sediment load is computed for current time step for each channel segment

$$\frac{G_i - G_{i-1}}{L_i} = D_{c\,i} \cdot \left(1 - \frac{G_i}{T_{c\,i}}\right) + D_{s\,i} \tag{6.10}$$

where subscript $i$ denotes the channel segment.

When multiplied by $L_i$ Equation 6.10 gives:

$$G_i - G_{i-1} = D_{c\,i} \cdot L_i - G_i \frac{D_{c\,i} \cdot L_i}{T_{c\,i}} + D_s \cdot L_i \tag{6.11}$$

From which the sediment load for the channel segment can be expressed:

$$G_i = \frac{D_{c\,i} \cdot L_i + D_{s\,i} \cdot L_i + G_{i-1}}{1 + \frac{D_{c\,i} \cdot L_i}{T_{c\,i}}} \tag{6.12}$$

On the other hand, the potential erosion rate can be expressed through the volume of the eroded material by computing the difference in shapes from the previous and current time steps.

$$D_c = \frac{M_{potential\,i}}{W_{eq\,i} \cdot L_i \cdot \Delta t} = \frac{\rho_b \cdot V_{potential\,i}}{W_{eq\,i} \cdot L_i \cdot \Delta t} = \frac{\rho_b \cdot (W_{final\,i} \cdot D_{potential\,i} - W_{initial\,i} \cdot D_{initial\,i}) \cdot L_i}{W_{eq\,i} \cdot L_i \cdot \Delta t} \tag{6.13}$$

The side sediment load can be computed as a rate of sediment delivery supplied by the side expressed through the mass of sediment during the time step from the side slope length corresponding to the channel segment.

$$D_s = \frac{M_{side\,i}}{W_{eq\,i} \cdot L_i \cdot \Delta t} \tag{6.14}$$

Once the transport capacity and the sediment load are computed, the next condition should be checked to determine whether sediment load is less than a transport capacity for erosion to occur:

$$G_i < T_{c\,i} \tag{6.15}$$

In the case of erosion, its rate can be determined from the volumetric change of the channel due to change in the shape:

$$D_f = \frac{\rho_b \cdot (W_{final\,i} \cdot D_{final\,i} - W_{initial\,i} \cdot D_{initial\,i}) \cdot L_i}{W_{eq\,i} \cdot L_i \cdot \Delta t} \tag{6.16}$$

The assumption is made that the channel has the same width as from the potential erosion, and only eroded depth should then be adjusted to account for the actual rates. After knowing the change of the channel cross-section from the potential erosion and the transport capacity and sediment load, the actual erosion rate can be expressed by the following equation:

$$\frac{\rho_b \cdot \left(W_{final\,i} \cdot D_{final\,i} - W_{initial\,i} \cdot D_{initial\,i}\right) \cdot L_i}{W_{eq\,i} \cdot L_i \cdot \Delta t} =$$

$$= \frac{\rho_b \cdot (W_{final\,i} \cdot D_{potential\,i} - W_{initial\,i} \cdot D_{initial\,i}) \cdot L_i}{W_{eq\,i} \cdot L_i \cdot \Delta t} \cdot \left(1 - \frac{G_i}{T_{c\,i}}\right) \quad (6.17)$$

Cancelling out the same denominators, expression for the adjusted depth would be:

$$(W_{final\,i} \cdot D_{final\,i} - W_{initial\,i} \cdot D_{initial\,i}) = (W_{final\,i} \cdot D_{potential\,i} - W_{initial\,i} \cdot D_{initial\,i}) \cdot \left(1 - \frac{G_i}{T_{c\,i}}\right) \quad (6.18)$$

Then the actual final depth of the channel can be expressed by the Equation 6.19:

$$D_{final\,i} = \frac{(W_{final\,i} \cdot D_{potential\,i} - W_{initial\,i} \cdot D_{initial\,i}) \cdot \left(1 - \frac{G_i}{T_{c\,i}}\right) + W_{initial\,i} \cdot D_{initial\,i}}{W_{final\,i}} \quad (6.19)$$

## Deposition

After computing the potential erosion rates, the sediment load was determined from Equation 6.12 and then compared to the transport capacity (Equation 6.9) for each segment of the channel. If the sediment load was greater than the transport capacity, then sediment deposition occurred. The deposition rates were computed with Equation 6.20:

$$D_f = 2 \cdot \frac{\beta \cdot v_f}{q} \cdot (T_c - G) \quad (6.20)$$

where $\beta$ is the raindrop-induced turbulence coefficient (non-dimensional), $v_f$ is the effective fall velocity for the sediment (m/sec), and $q$ is the flow discharge per unit width (m²/sec). In the model computation, only one sediment fraction was used – small aggregates. It accounted for half of the deposited sediment (Haan, Johnson, & Brakensiek, 1982); hence, Equation 6.20 was multiplied by two to account for all sediment fractions.

On the other hand, the deposition can be estimated by accounting for the deposited volume:

$$2 \cdot \frac{\beta \cdot v_f}{q_i} \cdot (T_{c\,i} - G_i) = \frac{\rho_b \cdot (W_{initial\,i} \cdot D_{initial\,i} - W_{final\,i} \cdot D_{final\,i}) \cdot L_i}{W_{eq\,i} \cdot L_i \cdot \Delta t} \quad (6.21)$$

In contrast to the case of erosion with the increase of channel depth and width, the deposition process accumulates sediment on the channel bottom at the initial channel width from current time step or a final width from the previous time step, which are the same. Thus:

$$W_{final\ i} = W_{initial\ i} \tag{6.22}$$

and the final depth of the channel after deposition can be expressed from Equations 6.21 and 6.22:

$$D_{final\ i} = D_{initial\ i} - 2 \cdot \frac{\beta \cdot v_f \cdot \Delta t \cdot (T_{c\,i} - G_i)}{q_i \cdot \rho_b} \frac{W_{eq\ i}}{W_{initial\ i}} \tag{6.23}$$

## Adjustment of the Soil Erodibility Parameters

The effect of soil hydrological regime was accounted by introducing soil erodibility and critical shear stress coefficients as functions of the soil hydraulic gradient, *I*:

$$E = K_e(I) \cdot \left(\tau_{act} - \tau_{cr}(I)\right)^a \tag{6.24}$$

$$K_e = K_e^{ref} \cdot \eta \cdot (1 + k_K \cdot I) \tag{6.25}$$

$$\tau_{cr} = \tau_{cr}^{ref} \cdot \varepsilon \cdot e^{-kI} \tag{6.26}$$

where $E$ is the erosion rate (kg/s/m$^2$), $K_e$ is the soil erodibility (s/m), $\tau_{cr}$ is the critical shear stress (Pa), $I$ is the soil hydraulic gradient (cm/cm), $K_e^{ref}$ is the reference soil erodibility determined from the WEPP model (s/m), $\tau_{cr}^{ref}$ is the reference critical shear stress determined from the WEPP model (Pa), and $\eta, k_K, \varepsilon, k$ – are model parameters obtained from the experiment or using other mechanistic models (see Chapter 4 for more details).

The hydraulic gradient was assumed to be positive for the stage of channel deepening, while it was set to zero for the stage of channel widening. The vertical hydraulic gradient represented the subsurface hydrologic regime of the channel and was obtained for one channel segment corresponding to the center of the channel. Computing the hydraulic gradient for each

channel segment could be beneficial to improve the solution; nevertheless, it would significantly increase the computational time.

To determine the soil pore pressure hydraulic gradient, a finite difference method was used to solve the Richards equation (Equation 6.27) in a one-dimensional vertical domain and three-layered soil with varying boundary conditions:

$$\frac{\partial \theta}{\partial t} = \frac{\partial}{\partial z}\left[K(h)\frac{dh}{dz}\right] - \frac{\partial K(h)}{\partial z} \tag{6.27}$$

where $\theta$ is the volumetric water content, $h$ is the matric potential, $K$ is the hydraulic conductivity as a function of matric potential, $z$ is the vertical coordinate, and $t$ – time

The mass conservative mixed head and soil water content numerical scheme was applied to improve model performance (Celia & Bouloutas, 1990). The backward-implicit scheme is used for discretizing the temporal term with Picard iteration for nonlinear parts of the equation. Equation 6.28 presents the discretized version of the Equation 6.27:

$$\frac{\theta_i^{n+1} - \theta_i^n}{\Delta t} = \frac{K_{i+\frac{1}{2}}^{n+1}}{\Delta z}\left[\frac{h_{i+1}^{n+1} - h_i^{n+1}}{\Delta z} - 1\right] - \frac{K_{i-\frac{1}{2}}^{n+1}}{\Delta z}\left[\frac{h_i^{n+1} - h_{i-1}^{n+1}}{\Delta z} - 1\right] \tag{6.28}$$

where $n$ is a superscript denoted to discretization in time, and $i$ is the subscript denoted for the discretization in space.

The numerical model handled saturated condition automatically, while infiltration fluxes were calculated at each time step. The top boundary condition was based on the head which was determined by the depth of water within the channel. A unit gradient boundary condition was assumed at the bottom boundary. The ROSETTA (Schaap et al., 2001) model was used to determine soil hydraulic parameters based on soil textural data. The greater details of the used parameters were presented in Chapter 4.

After the hydraulic gradient and the critical shear stress were updated for the current step, the channel flow routing was re-computed to adjust the channel flow hydrograph with the change of the channel equilibrium width that corresponded to the updated critical shear stress values.

## Model Validation

A field experiment was conducted during a growing season in 2014. The precipitation, soil water content and gully erosion cross sections were recorded. A total of 7 survey campaigns were conducted, and 18 significant rainfall events occurred during the growing season. All rainfalls were simulated with the model, and 7 values of eroded/deposited volumes were compared for the model and the experiment. The selected value of the Manning's roughness coefficient was 0.25 for natural streams (Huffman, 2013). The critical shear stress and soil erodibility parameters were selected as baseline values from the WEPP model for the Crete silt loam (see Chapter 3 for the detailed description of the experiment). Only one parameter, $K_f$, was adjusted to ensure a good fit. A value of 0.001 was selected to favor the deposition processes as 4 points resulted in the sediment deposition in the channel and 1 point did not have any erosion/deposition. The selected value of the $K_f$ produced the Nash-Sutcliffe Efficiency statistic of 0.72 (Figure 6.7), which is considered a good fit in the field of surface runoff and erosion modeling (Moriasi et al., 2007).

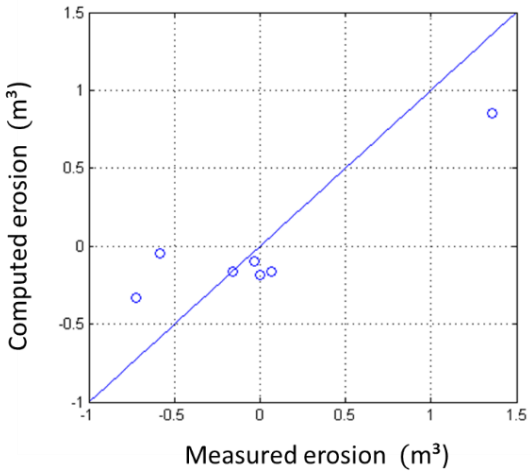


**Figure 6.7 Computed versus measured volumes of eroded soil.**

# Results

## Scenarios

The model was tested on 42 scenarios applied to the ephemeral gully observed during the field experiment in Chapter 3. Seven rainfall events with return periods of 1, 2, 5, 10, 25, 50, and 100 years were simulated with the model. These rainfalls were simulated with a WEPP built-in weather component for a simulation of a single rainfall event. All rainfalls had a duration of 4 hours, maximum rainfall intensity of 307.3 (mm/hr), time to peak of 30%, and precipitation amount of 70, 82, 102, 119, 145, 166, and 188 mm respective to the corresponding return periods of 1, 2, 5, 10, 25, 50, and 100 years.

Each rainfall simulation had applied three best management practices: tillage, no-tillage and conversion to the prairie. Parameters used for the WEPP input file are presented in Table 6.2. Two levels of antecedent soil moisture contents were simulated for each rainfall and each management practice. Dry soil condition was assumed to have 70% of soil saturation, while the soil saturation was taken at 95% for wet soil condition.

**Table 6.2. Input parameters to the WEPP model for three management practices.**

| Parameter | units | Practice | | |
|---|---|---|---|---|
| | | Till | No-till | Prairie |
| Initial Plant | - | Corn | Corn | Bluestem Prairie |
| Bulk density after last tillage | (g/cub. cm) | 1.3 | 1.3 | 1.3 |
| Initial canopy cover (0-100%) | % | 90 | 90 | 90 |
| Days since last tillage | days | 60 | 420 | 20000 |
| Days since the last harvest | days | 270 | 720 | 20000 |
| Initial frost depth | cm | 0 | 0 | 0 |
| Initial interrill cover (0-100%) | % | 50 | 90 | 56 |
| Initial residue cropping system | - | Fallow | Annual | Perennial |
| Cumulative rainfall since last tillage | mm | 150 | 1700 | 50000 |
| Initial ridge height after last tillage | cm | 2 | 2 | 1.7 |
| Initial rill cover (0-100%) | % | 50 | 90 | 61 |
| Initial roughness after last tillage | cm | 2 | 2 | 0.8 |
| Rill spacing | cm | 0 | 0 | 0 |
| Rill width type | - | Temporary | Permanent | Permanent |
| Initial snow depth | cm | 0 | 0 | 0 |
| Initial depth of thaw | cm | 0 | 0 | 0 |
| Depth of secondary tillage layer | cm | 10 | 10 | 10 |
| Depth of primary tillage layer | cm | 20 | 20 | 20 |
| Initial rill width | cm | 0 | 0 | 0 |
| Initial total dead root mass | kg/sq.m | 0.5 | 0.4 | 0.2 |
| Initial total submerged residue mass | kg/sq.m | 0.2 | 0.1 | 0 |

## Detailed Example of the Selected Scenario

A single scenario was selected with the aim of representing model capabilities and various outputs. This scenario was based on the 82 mm 2-year return period rain storm. The management practice was converted to prairie, and antecedent soil moisture content was 95%.

The described above approach of hydrograph simulation within a channel allows one to know the water flux for each channel segment at any moment in time. Figure 6.8 shows a surface plot of a channel flux as a function of time and distance from the channel headcut. For the selected scenario, Figure 6.8 shows the gradual appearance of two peaks closer to the outlet of the channel. These peaks can be explained by the inflow from the side catchment which was introduced to the model as a separate slope. Unlike modeled hydrograph, true hydrograph have smoother peaks. Such a behavior of the model may be easily corrected by introducing several side catchments along the channel.

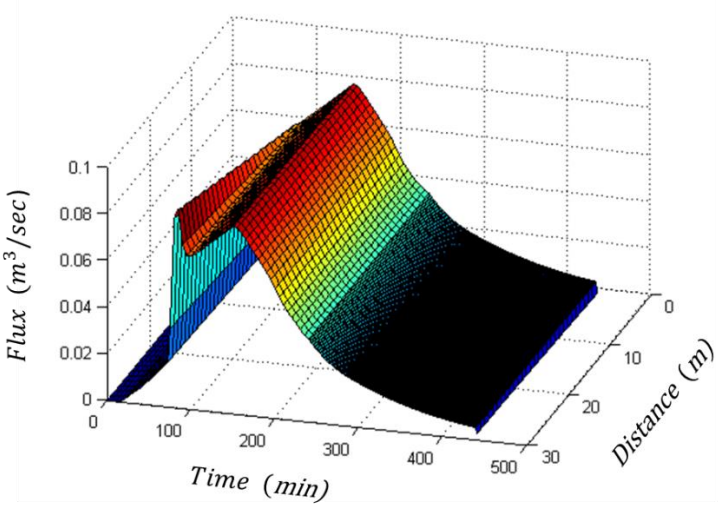


**Figure 6.8 Channel flow in space and time.**

Similar to the flux in the channel, the depth of the eroded soil in the channel can be plotted as a surface plot. Figure 6.9 shows an eroded depth on the plane of time and space in the form of a channel distance. A rapid deposition of the material (channel depth decreased from 10 cm to 2 cm) is seen for the rising part of the hydrograph (from 1$^{st}$ to 100$^{th}$ minute), and gradual erosion (the channel depth increased from 2 cm to 5 cm) is seen for the falling part of the hydrograph in the last 8 meters of the channel.

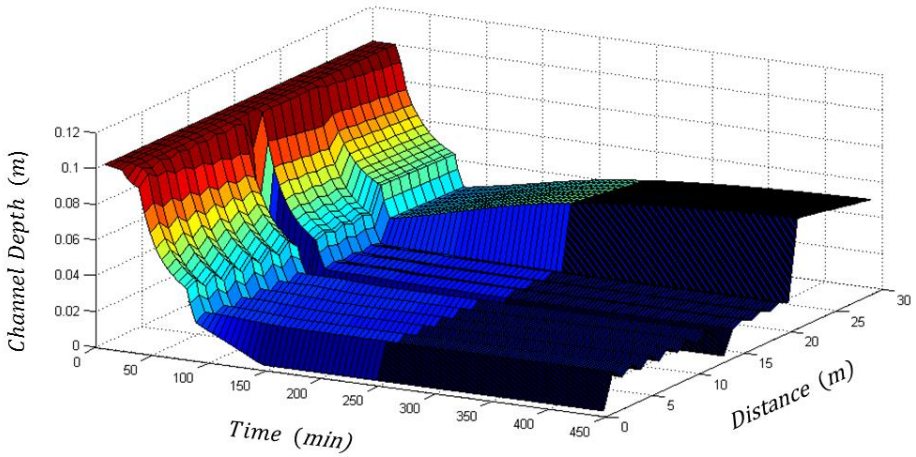


**Figure 6.9 Channel depth in space and time.**

The rapid deposition in the channel occurs due to the reshaping of the initial channel cross according to the flux and the increase of the equilibrium width from 10 cm to 40 cm (Figure 6.5) due to the increase in the water flow on the rising part of the hydrograph. It is also clearly noticeable in the surface plot of the channel width on the plane of time and channel distance (Figure 6.10). Once the channel reaches the maximum width, there is no further widening; only deepening is possible if sediment transport capacity allows it.

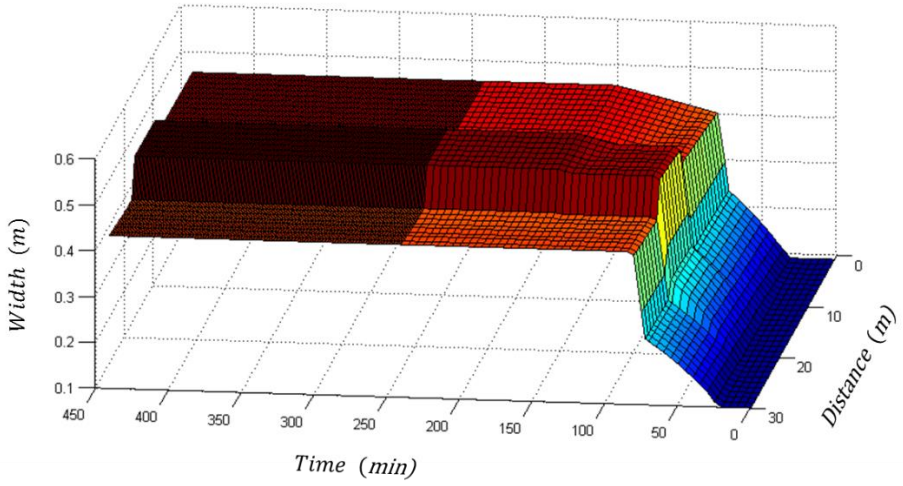


**Figure 6.10 Channel width in space and time.**

The local channel slope influences different channel widths along the channel distance. Three sections of relatively constant width are depicted in Figure 6.10. These sections (from 0 to 12 m, from 12 to 22 meters and from 22 to 30 m) correspond to sections of the channel with different slopes. There is also a minor change in the channel width within each section due to the increased distance channel flow.

## Results for All Scenarios

The modeling results are presented in the form of the total soil loss from the catchment as a combination of sheet-and-rill erosion and ephemeral gully erosion. The total sediment load is

plotted in Figure 6.11 versus the precipitation amount for three types of management and two antecedent soil moisture conditions.

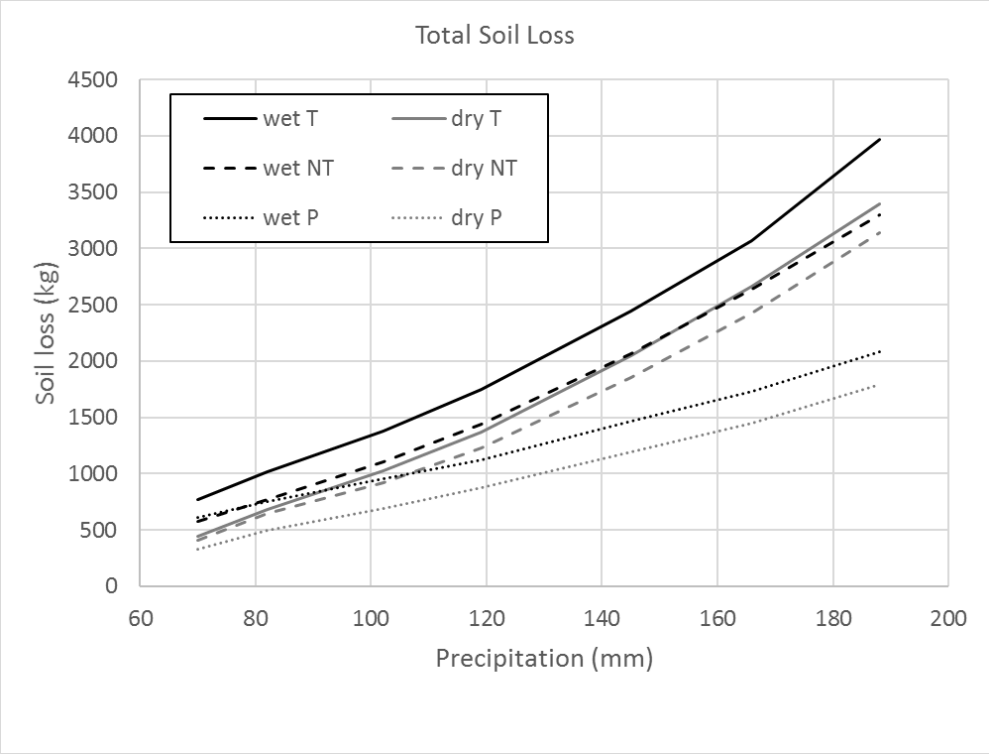


**Figure 6.11. Total soil loss for three practices and two antecedent conditions.**

The results show an increase in soil loss with the increase of precipitation. For all types of management and rainfall, the dry condition produced less erosion than the wet condition. As expected, the application of no-tillage and conversion to prairie significantly (from 12 to 50% for no-till and 50% for conversion to prairie) reduced the erosion rates compared to the tillage operation. Interestingly, the conversion to prairie has a larger impact for larger precipitation events than the effect of no-tillage scenario.

The plot of sediment load from the ephemeral gully versus precipitation amount is presented in the Figure 6.12.

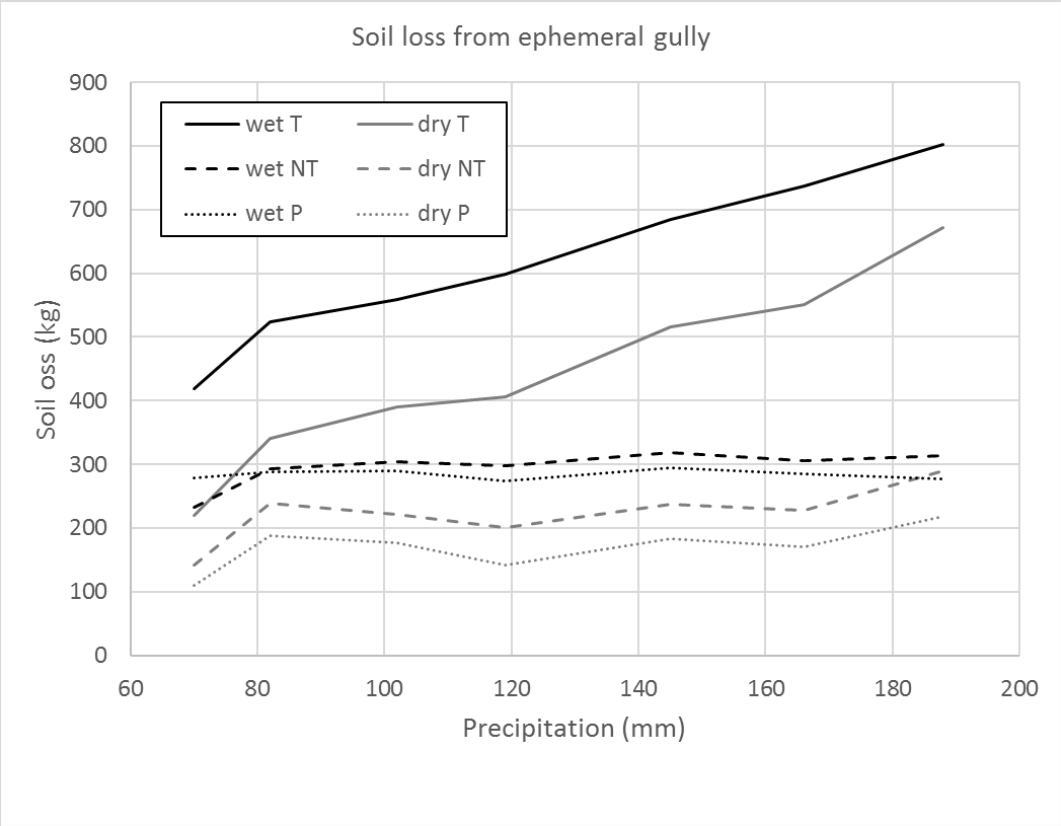


**Figure 6.12. Ephemeral gully erosion for three practices and two antecedent conditions.**

Similar to the total sediment loss, soil erosion from the ephemeral gully for the tillage operation increases with the growth of the precipitation amount. Also, dry antecedent soil moisture condition produces less erosion than does the wet condition. Moreover, ephemeral gully erosion for no-tillage and conversion to prairie scenarios levels off at a certain erosion rate of 300 kg/event, and it does not depend on the amount of precipitation for both dry and wet conditions.

## Discussion

The percent reduction in the total soil loss from sheet-rill and ephemeral gully erosion is presented in Figure 6.13 for 28 scenarios of two management practices aimed at soil

conservation. Best management practices efficiency was calculated based on the tillage operation, as a base scenario.

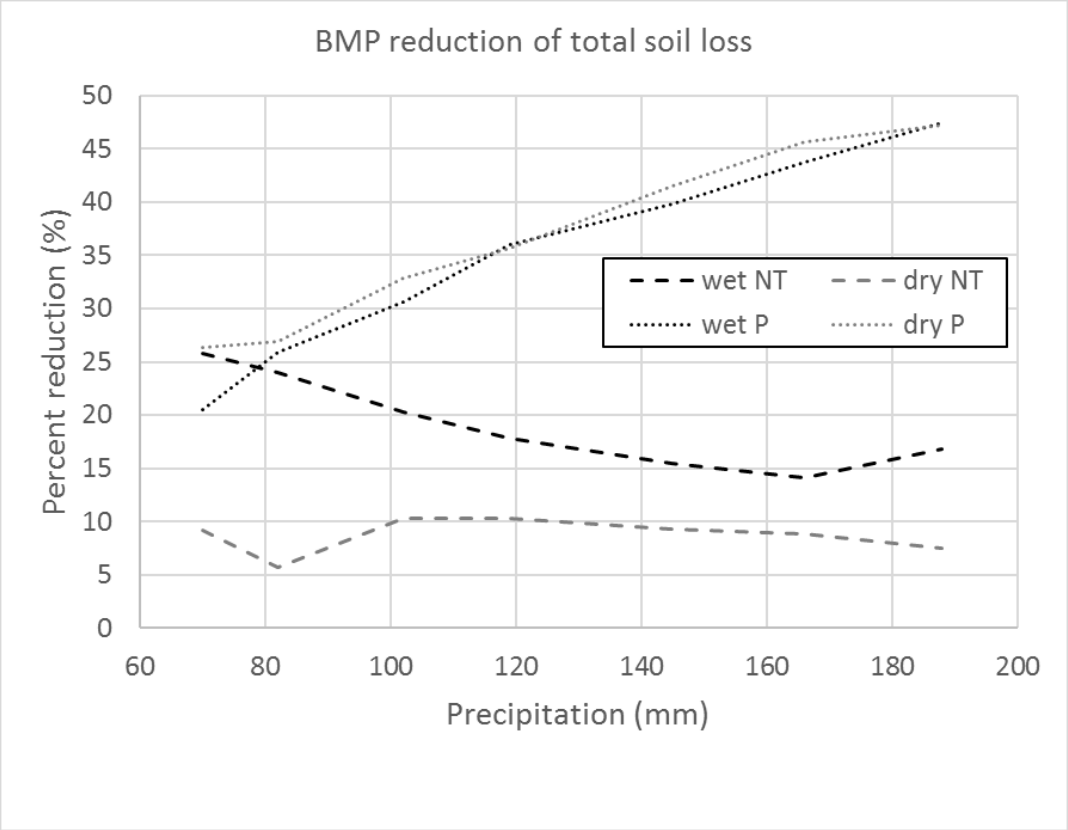


**Figure 6.13. Performance of two practices with two antecedent conditions on the reduction of the total soil loss.**

It was observed that the reduction rate for no-tillage operation decreases is inversely proportional to precipitation, while it increases to convert to a prairie scenario. Such behavior of the erosion rate can be explained by the fact that no-till operation was modeled, and it does not take into account long-term improvements in both soil hydraulic conductivity and soil erodibility which depend on the number of days and the total precipitation from the last tillage (Table 6.2). In addition, the reduction rates for conversion to prairie scenario do not depend on the antecedent soil moisture condition.

Furthermore, ephemeral gully erosion reduction rates show reverse behavior with no-till operations efficiency as it is not dependent on the antecedent soil moisture condition and the conversion to the prairie having difference for wet and dry conditions (Figure 6.14). Both of these practices also produced similar reduction rates of erosion for the ephemeral gully. That is, the conversion to the prairie performed slightly better than no-till operation did.

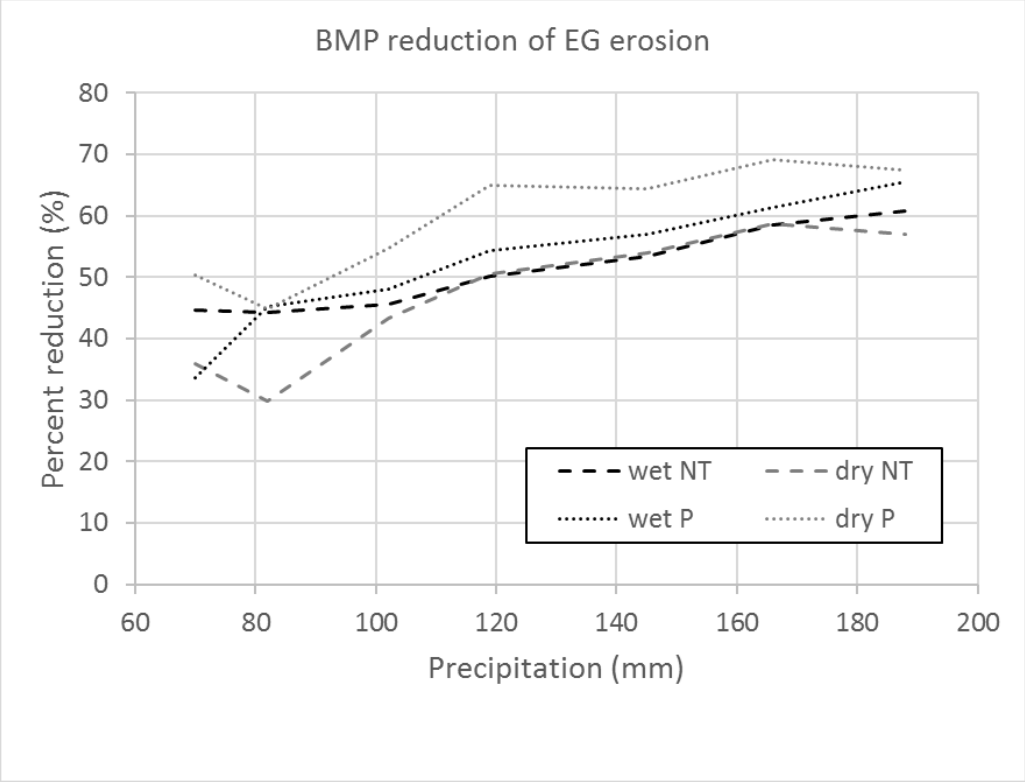


**Figure 6.14. Performance of two practices with two antecedent conditions on a reduction of ephemeral gully erosion.**

Cover crops, double cropping system and combinations of practices can be recommended as additional scenarios to be considered and modeled in future research. Another interesting research recommendation is the modeling of the long-term effects of best management practices, which will require modifying the model significantly in order to account for the gradual change in all necessary soil parameters.

# Conclusions

This study resulted in the development of a new process-based ephemeral gully erosion model, which allows one to use dynamic hydrograph and sediment graph and compute spatially distributed erosion along the ephemeral gully channel. The model incorporated the functional dependence of the soil erodibility and critical shear stress from the soil subsurface regime. The performance of the model was evaluated by comparing the experimental data, an evaluation that resulted in an acceptable NSE value of 0.72. Three management practices were modeled for seven precipitation amounts, and two antecedent soil moisture conditions resulting in 42 scenarios. Results showed that conversion to the prairie has the better reduction rates of total soil loss for larger precipitation amount, while a no-tillage operation decreases its efficiency when the precipitation amount increases. Both no-tillage operation and conversion to the prairie increase their efficiency for the erosion from the ephemeral gully. Another interesting finding is that there is little or no difference in the reduction rate of the total soil loss between wet and dry conditions for the conversion to the prairie. It was also noted that there is no difference in the reduction rate of ephemeral gully erosion between wet and dry conditions for the no-tillage operation.

Nevertheless, the presented model has a number of assumptions and limitations. Multitude factors are known to have an effect on soil erosion. This work did not consider factors including and not limited to: (1) the change of the soil texture with time at the catchment and the channel, (2) the biological activity which increases soil hydraulic conductivity and affects soil stability on the surface, (3) the effect of the fertilizers, pesticides and other possible chemicals which may influence soil stability and hydraulic conductivity, (4) the effect of the temperature and its daily and seasonal variations, (5) the soil swelling/shrinking, (6) the soil crusting between

events and seasons, (7) micro-topography, and (8) the channel side slopes stability. Some of these factors can be relatively easily implemented in the model; for example, the soil crusting between events was accounted for in the WEPP model where it affected soil erodibility.

It is recommended that the following model improvements can be explored in future studies. The tRIBS model (Francipane et al., 2012) can be used to represent the hydrograph and the spatial distribution of both catchments and the channel itself. The erosion/deposition of all sediment fractions can be done separately for each fraction rather than using a lumped approach. Different sediment characteristics for different soil layers, as well as deposited and newly eroded soil, will also allow better modeling of the long-term effect of the no-tillage operation. Horizontal pressure gradients can be used to improve the estimation of widening rates. Finally, the dynamic wave equation can be used to account for possible situations with a backflow at the channel outlet.

# Chapter 7 - Summary

As the world population continues to increase every day, there would be more demand for quality food and clean drinking water across the globe. This continuous demand would also compel farmers, government agencies, and other stakeholders to provide sustainable agriculture. Nevertheless, it would be very difficult to achieve sustainable agriculture if there is no reliable solution to mitigate the effects of topsoil losses. One of the most significant contributors to total soil losses is ephemeral gully erosion, a type of erosion in which concentrated runoff water slowly washes away the topsoil. Even though researchers have studied ephemeral gully erosion and developed models to estimate the associated soil loss in the last few decades, some physical processes of channel erosion and concentrated flow are yet to be well-understood and accounted for in the models. Thus, there is a need to have a better understanding of ephemeral gully erosion, as well as finding workable solutions to help reduce soil loss from ephemeral gullies. This goal can be achieved by determining the best management practice that would fit the field conditions, including precipitation patterns and hydrological regimes.

The purpose of this research work is to study channel erosion affected by the hydrological regime, the soil moisture condition and the dynamic change during the erosive event. An experimental study, mathematical model and applications, and a simplified model development were conducted to understand the influences of subsurface water fluxes and seepage, including the drainage regimes on the ephemeral gully erosion. Consisting of a field experiment (see Chapter 3), the study explored the influence of hydrological regime on channel erosion. This research work also produced an experimental data to validate the model developed in Chapter 6. Based on the results obtained from Chapter 3 and the literature review from Chapter 2, a 2-dimensional model was developed. This model included the function of soil

erodibility parameters, which depended on the hydrological gradients. This model was further applied to study the effect of various parameters on channel erosion (see Chapter 5). To apply the newly developed approach described in Chapter 4 to a larger scale project and to compare management practices, a one-dimensional watershed scale model was developed and tested (see Chapter 6).

The first study (see Chapter 3) was a two-year field experiment set up in a cultivated field in Central Kansas. A weather station with rainfall, soil moisture content, temperature, and flow discharge was instrumented around the ephemeral gully channel. In addition, the ephemeral gully was surveyed 15 times during two growing seasons. The runoff was modeled and validated on discharge readings, and the acting shear stresses were computed for 12 selected runoff events. These stresses resulted in conditions favorable to channel development according to the excess shear stress equation. However, the development of the gully was caused by events during three survey periods. All these events had different magnitudes, and no critical threshold was established to reduce erosion events by the magnitude of runoff peak or according to the acting shear stresses. A new threshold function was proposed for the acting shear stress, which depended on the changes in soil moisture content from its antecedent condition to the time of highest runoff intensity. The introduction of this function allowed events to be separated, on a threshold basis, into erosion events and no erosion events. It was concluded that the runoff amount and peak runoff rate were not the only major factors influencing ephemeral gully erosion and that the soil moisture conditions and subsurface flow regime should be accounted for.

The second study (see Chapter 4) focused on developing a mathematical model that would account for subsurface soil water fluxes. The model assumed that the critical shear stress function depended on soil water pore pressure gradient in such a way that positive gradients

(seepage) helped detach soil particles and decreased critical shear stress, whereas negative gradients (drainage) increased the cohesiveness in the soil structure and increased critical shear stress. The aim of developing the two-dimensional model was to compute soil pore pressure gradients by the numerical solution of the Richards equation with the backward implicit scheme. These gradients were consequently used to compute a propagation of the channel boundary. The model was tested on two experiments reported in the literature, and acceptable results were produced. Based on the differences in computed and measured erosion rates, a functional dependence of the soil erodibility coefficient on the hydraulic gradient was proposed. The proposed excess shear stress function was tested on one reported experiment, and the results were congruent with those obtained from experimental data. The use of this function was proposed to account for subsurface fluxes during the dynamic process of channel erosion.

Furthermore, the function described above was applied to a series of numerical experiments in the third study (see Chapter 5) to evaluate the influence of a number of parameters on channel erosion while accounting for the subsurface water regime. To achieve this objective, six types of soil were tested with the same initial conditions of the channel geometry and channel flow. Crete silt loam soil was found to be more susceptible to hydraulic gradient impacts. Also, three soils were tested for the initial soil moisture condition, groundwater depth, and heterogeneity in soil layering. Findings showed that the initial high saturation of the soil, the high groundwater levels, and the presence of impervious layers produced elevated erosion rates compared to the lower initial saturation, low level of groundwater and no impervious layer, respectively. All computations were made with the conventional excess shear stress model which produced higher erosion rates than the proposed modified excess shear stress equation model. What's more, the conducted studies can be used to understand the influence of various soil

factors on the erosion process, and they can be adapted to other simpler models which are applicable to larger scale problems. One possible application is to test the selected best management practices and estimate their efficiency under various soil and climatic conditions.

The model described in Chapter 4 is complex, and it requires relatively high computation power. Thus, it is less likely to apply to large-scale studies. To overcome this problem, a new spatially and temporally process-based model for estimating ephemeral gully erosion at the field scale was proposed and developed as the fourth study (see Chapter 6). This model was based on the approach proposed by Foster and Lane (1983) with a modification to account for variable channel flows. The channel was divided into segments of a uniform slope and a specific cross-sectional shape. A kinematic wave equation was solved to route the water flow within the channel. Also calculated with the WEPP model is the water inflow from the uphill catchment. The soil hydrologic condition was accounted for with the model proposed in Chapter 4 only in the vertical direction; a Richards equation was also solved numerically in one-dimension. The developed model was tested on the dataset from the experiment described in Chapter 3, and it produced acceptable results with an NSE of 0.71. In addition to that, three best management practices – tillage, no-tillage, and conversion to prairie – were tested with the model on a set of rainfall events with seven different return periods (1 year, 2 years, 5 years, 10 years, 25 years, 50 years, and 100 years) and two different antecedent soil moisture conditions: wet (saturation of 70%) and dry (saturation of 95%). Results indicated that the wet initial condition caused higher erosion rates, thus identifying a substantial contribution from ephemeral gully to a total soil loss.

Nevertheless, this research work has some limitations, and several assumptions were made in order to simplify the experimental process. For instance, the experimental study described in Chapter 3 was conducted on just one field; therefore, results cannot be translated

into all ephemeral gullies. Regardless of this limitation, this study can be used to understand the process, and it is believed that new data from potential future studies can help provide more statistically significant models. Apart from that, Chapter 2 described a model that has a scale of short channel cross-section. While this model can be used as a research tool, it would be very difficult to apply this model to large-scale projects. Besides, the model described in Chapter 6 is still limited to one catchment even though it is applicable to larger scale projects. All studies did not also take into account the following parameters described in Chapter 6 :(1) the change of the soil texture, (2) the biological activity, (3) the effect of the fertilizers, pesticides and other possible chemicals, (4) the effect of the temperature and its daily and seasonal variations, (5) the soil swelling/shrinking, (6) the soil crusting, (7) the microtopography, and (8) the channel side slopes stability.

In sum, the results presented in this dissertation show the importance of model development based on physical principles such as accounting for subsurface dynamic conditions of the soil. This research work also indicates that an integration of subsurface fluxes in ephemeral gully erosion process can have substantial impacts on the results of erosion models. Moreover, this study can be used to investigate other types of soil erosion such as permanent streams, classical gullies, and rills. However, due to the different scale and a lag of subsurface flows compared to the surface processes, rills may slightly depend on this subsurface effect. Nevertheless, an integration of the modified excess shear stress equation can be implemented in other existing models. This integration can be leveraged to account for a wider range of problems such as the joint effects of the subsurface hydrologic regime and nutrient transport and the study of the long-term differences in best management practice efficiency due to climate change. The result of this dissertation can also be used to understand processes of soil erosion from ephemeral

gullies. For instance, the developed models can be used to consider the effects of subsurface soil hydrology in predicting soil erosion for different best management practices. However, more accurate and complex estimation of the efficiency of best management practices can be employed in finding the most suitable ones for certain soils and conditions of the field. This appropriate selection of practices will also help in controlling anthropogenically induced erosion process and maintaining sustainable agriculture.

# References

Al-Madhhachi, A., Fox, G. A., Hanson, G. J., Tyagi, A. K., & Bulut, R. (2014). Mechanistic detachment rate model to predict soil erodibility due to fluvial and seepage forces.(report). *Journal of Hydraulic Engineering, 140*(5), 04014010.

Al-Madhhachi, A., Fox, G., Hanson, G., Tyagi, A., & Bulut, R. (2013). Mechanistic detachment rate model to predict soil erodibility due to fluvial and seepage forces. *Journal of Hydraulic Engineering, 140*(5), 04014010.

Alonso, C. V., Bennett, S. J., & Stein, O. R. (2002). Predicting head cut erosion and migration in concentrated flows typical of upland areas. *Water Resources Research, 38*(12), - 1303. doi:10.1029/2001WR001173

Bennett, S. J., Casalí, J., Robinson, K. M., & Kadavy, K. C. (2000). Characteristics of actively eroding ephemeral gullies in an experimental channel. *Transactions of the American Society of Agricultural Engineers, 43*(3), 641-649.

Betts, H. D., & DeRose, R. C. (1999). Digital elevation models as a tool for monitoring and measuring gully erosion. *International Journal of Applied Earth Observation and Geoinformation, 1999*(2), 91-101.

Bingner, R. L., Wells, R. R., Momm, H. G., Rigby, J. R., & Theurer, F. D. (2016). Ephemeral gully channel width and erosion simulation technology. *Natural Hazards, 80*(3), 1949-1966. doi:10.1007/s11069-015-2053-7

Brooks, A. P., J G Shellberg, J Knight, & J Spencer. (2009). Alluvial gully erosion: An example from the mitchell fluvial megafan, queensland, australia. *Earth Surface Processes and Landforms, 34*(14), 1951-1969. doi:10.1002/esp.1883

Bryan, R., Hawke, R., & Rockwell, D. (1998). The influence of subsurface moisture on rill system evolution. *Earth Surface Processes and Landforms, 23*(9), 773-789.

Capra, A., P Porto, & B Scicolone. (2009). Relationships between rainfall characteristics and ephemeral gully erosion in a cultivated catchment in Sicily (Italy). *Soil & Tillage Research, 105*(1), 77-87. doi:10.1016/j.still.2009.05.009

Capra, A., Di Stefano, C., Ferro, V., & Scicolone, B. (2009). Similarity between morphological characteristics of rills and ephemeral gullies in Sicily, Italy. *Hydrological Processes, 23*(23), 3334-3341.

Capra, A., Mazzara, L. M., & Scicolone, B. (2005). Application of the EGEM model to predict ephemeral gully erosion in Sicily, Italy. *Catena, 59*(2), 133-146. doi:10.1016/j.catena.2004.07.001

Capra, A. (2013). *Ephemeral gully and gully erosion in cultivated land: A review*

Carnicelli, S., Benvenuti, M., Ferrari, G., & Sagri, M. (2009). Dynamics and driving factors of late Holocene gullying in the main Ethiopian rift (MER). *Geomorphology, 103*(4), 541-554. doi:http://dx.doi.org/10.1016/j.geomorph.2008.07.019

Casali, J., Bennett, S. J., & Robinson, K. M. (2000). Processes of ephemeral gully erosion. *International Journal of Sediment Research, 15*(1), 31-41.

Casalí, J., Rafael Giménez, & Sean Bennett. (2009). Gully erosion processes: Monitoring and modelling. *Earth Surface Processes and Landforms, 34*(14), 1839-1840. doi:10.1002/esp.1867

Casali, J., Loizu, J., Campo, M. A., De Santisteban, L. M., & Alvarez-Mozos, J. (2006). Accuracy of methods for field assessment of rill and ephemeral gully erosion. *Catena, 67*(2), 128-138. doi:10.1016/j.catena.2006.03.005

Casalí, J., López, J. J., & Giráldez, J. V. (1999). Ephemeral gully erosion in southern navarra (spain). *Catena, 36*(1-2), 65-84. doi:10.1016/S0341-8162(99)00013-2

Casalí, J., López, J. J., & Giráldez, J. V. (2003). A process-based model for channel degradation: Application to ephemeral gully erosion. *Catena, 50*(2–4), 435-447. doi:10.1016/S0341-8162(02)00127-3

Castillo, C., R Pérez, M R James, J N Quinton, E V Taguas, & J A Gómez. (2012). Comparing the accuracy of several field methods for measuring gully erosion. *Soil Science Society of America Journal, 76*(4), 1319. doi:10.2136/sssaj2011.0390

Celia, M. A., & Bouloutas, E. T. (1990). A general mass- conservative numerical solution for the unsaturated flow equation. *Water Resources Research, 26*(7), 1483-1496. doi:10.1029/WR026i007p01483

Cheng, H., Xueyong Zou, Yongqiu Wu, Chunlai Zhang, Qiuhong Zheng, & Zhangyan Jiang. (2007). Morphology parameters of ephemeral gully in characteristics hillslopes on the loess plateau of china. *Soil & Tillage Research, 94*(1), 4-14. doi:10.1016/j.still.2006.06.007

Clark, L., & Wynn, T. (2007). Methods for determining streambank critical shear stress and soil erodibility: Implications for erosion rate predictions. *Transactions of the ASABE, 50*(1), 95-106.

Cobos, D., & Campbell, C. (2007). Correcting temperature sensitivity of ECH2O soil moisture sensors. *Appl.Note.Decagon Devices, Pullman, WA,*

Daba, S., Rieger, W., & Strauss, P. (2003). Assessment of gully erosion in Eastern Ethiopia using photogrammetric techniques. *Catena, 50*(2–4), 273-291. doi:http://dx.doi.org/10.1016/S0341-8162(02)00135-2

Dabney, S., Daniel Yoder, Dalmo A. N. Vieira, & Ronald Bingner. (2011). Enhancing RUSLE to include runoff-driven phenomena. *Hydrological Processes, 25*(9), 1373-1390. doi:10.1002/hyp.7897

Dabney, S. M. (2004). Erosion processes in gullies modified by establishing grass hedges. *Transactions of the ASAE, 47*(5), 1561. doi:10.13031/2013.17634

Dabney, S. M., Vieira, D. A. N., Yoder, D. C., Langendoen, E. J., Wells, R. R., & Ursic, M. E. (2014). Spatially distributed sheet, rill, and ephemeral gully erosion. *Journal of Hydrologic Engineering, ,* C4014009. doi:10.1061/(ASCE)HE.1943-5584.0001120

Daggupati, P., Douglas-Mankin, K. R., & Sheshukov, A. Y. (2013). Predicting ephemeral gully location and length using topographic index models. *Transactions of the ASABE, 56*(4), 1427-1440.

Daggupati, P., Sheshukov, A. Y., & Douglas-Mankin, K. R. (2014a). Evaluating ephemeral gullies with a process-based topographic index model. *Catena, 113*, 177-186. doi:http://dx.doi.org/10.1016/j.catena.2013.10.005

Daggupati, P., Sheshukov, A. Y., & Douglas-Mankin, K. R. (2014b). Evaluating ephemeral gullies with a process-based topographic index model. *Catena, 113*, 177-186. doi:http://dx.doi.org/10.1016/j.catena.2013.10.005

De Santisteban, L. M., J Casalí, J J López, J V Giráldez, J Poesen, & J Nachtergaele. (2005). Exploring the role of topography in small channel erosion. *Earth Surface Processes and Landforms, 30*(5), 591-599. doi:10.1002/esp.1160

Decagon. (2015). Decagon devices inc., pullman , WA, USA. Retrieved from http://www.decagon.com/

Desmet, P. J. J., & Covers, G. (1996). Comparison of routing algorithms for digital elevation models and their implications for predicting ephemeral gullies. *International Journal of Geographical Information Systems, 10*(3), 311-331.

Di Stefano, C., & Vito Ferro. (2011). Measurements of rill and gully erosion in Sicily. *Hydrological Processes, 25*(14), 2221-2227. doi:10.1002/hyp.7977

Dietrich, W. E., Wilson, C. J., Montgomery, D. R., & McKean, J. (1993). Analysis of erosion thresholds, channel networks, and landscape morphology using a digital terrain model. *The Journal of Geology, 101*(2, 100th Anniversary Symposium: Evolution of the Earth's Surface), 259-278.

Duan, J., & Pierre Julien. (2005). Numerical simulation of the inception of channel meandering. *Earth Surface Processes and Landforms, 30*(9), 1093-1110. doi:10.1002/esp.1264

Einstein, H. A. (. (1950). *The bed-load function for sediment transportation in open channel flows*. Washington: Washington : U.S. Dept. of Agriculture.

ESRI. (2015). ArcMap 10. Environmental systems resource institute, Redlands, California.

Eustace, A. H., M J Pringle, & R J Denham. (2011). A risk map for gully locations in central queensland, australia. *European Journal of Soil Science, 62*(3), 431-441. doi:10.1111/j.1365-2389.2011.01375.x

Finkner, S., Nearing, M., Foster, G., & Gilley, J. E. (1989). A simplified equation for modeling sediment transport capacity. *Trans.ASAE, 32*(5), 1545-1550.

Flanagan, D. C., Fu, H., Frankenberger, J. R., Livingston, S. J., & Meyer, C. R. (1998). A windows interface for the WEPP erosion model. *St. Joseph, Mich.: ASAE, ASAE Paper No. 982135*

Flanagan, D. C. (2012). WEPP: Model use, calibration, and validation. *Transactions of the ASABE, 55*(4), 1463. doi:10.13031/2013.42254

Flanagan, D. C., & Nearing, M. A. (1995). USDA-water erosion prediction project: Hillslope profile and watershed model documentation. *NSERL Report no.10,*

Flanagan, D. C., Gilley, J. E., & Franti, T. G. (2007). Water erosion prediction project ( WEPP): Development history, model capabilities, and future enhancements. *Transactions of the ASABE, 50*(5), 1603-1612.

Flores-Cervantes, J. H., Istanbulluoglu, E., & Bras, R. L. (2006). Development of gullies on the landscape: A model of headcut retreat resulting from plunge pool erosion. *Journal of Geophysical Research: Earth Surface, 111*(F1), - F01010. doi:10.1029/2004JF000226

Fogle, A., & Barfield, B. (1992). CHANNEL, a model of channel erosion by shear, scour and channel headwall propagation: Part 1. model development. *RR-186,, 1992, 100,*

Foster, G., & Lane, L. (1983). Erosion by concentrated flow in farm fields. *Proceedings of the DB Simons Symposium on Erosion and Sedimentation,* 9.65-9.82.

Fox, G., Sheshukov, A., Cruse, R., Kolar, R., Guertault, L., Gesch, K., & Dutnell, R. (2016). Reservoir sedimentation and upstream sediment sources: Perspectives and future research needs on streambank and gully erosion. *Environmental Management, 57*(5), 945-955.

Fox, G., & Wilson, G. V. (2010). The role of subsurface flow in hillslope and stream bank erosion: A review. *Soil Science Society of America Journal, 74*(3), 717. doi:10.2136/sssaj2009.0319

Francipane, A., Ivanov, V. Y., Noto, L. V., Istanbulluoglu, E., Arnone, E., & Bras, R. L. (2012). tRIBS-erosion: A parsimonious physically-based model for studying catchment hydro-geomorphic response. *Catena, 92*, 216-231.

Gabbard, D. S., Huang, C., Norton, L. D., & Steinhardt, G. C. (1998). Landscape position, surface hydraulic gradients and erosion processes. *Earth Surface Processes and Landforms, 23*(1), 83-93. doi:10.1002/(SICI)1096-9837(199801)23:1<83::AID-ESP825>3.0.CO;2-Q

Gao, X., Wu, P., Zhao, X., Shi, Y., Wang, J., & Zhang, B. (2011). Soil moisture variability along transects over a well-developed gully in the loess plateau, china. *Catena, 87*(3), 357-367.

Ghebreiyessus, Y. T., Gantzer, C. J., Alberts, E. E., & Lentz, R. W. (1994). *Soil erosion by concentrated flow: Shear stress and bulk density*

Gong, J. G., Y W Jia, Z H Zhou, Y Wang, W L Wang, & H Peng. (2011). An experimental study on dynamic processes of ephemeral gully erosion in loess landscapes. *Geomorphology, 125*(1), 203-213. doi:10.1016/j.geomorph.2010.09.016

Gordon, L. M., S J Bennett, C V Alonso, & R L Bingner. (2008). Modeling long-term soil losses on agricultural fields due to ephemeral gully erosion. *Journal of Soil and Water Conservation, 63*(4), 173-181. doi:10.2489/jswc.63.4.173

Gordon, L. M. (2007). Simulating ephemeral gully erosion in AnnAGNPS. *Transactions of the ASABE, 50*(3), 857. doi:10.13031/2013.23150

Graf, W. H. (1984). *Hydraulics of sediment transport* Water Resources Publication.

Gutiérrez, Á. G., Schnabel, S., & Contador, F. L. (2009). Gully erosion, land use and topographical thresholds during the last 60 years in a small rangeland catchment in SW spain. *Land Degradation & Development, 20*(5), 535-550. doi:10.1002/ldr.931

Haan, C. T., Johnson, H. P., & Brakensiek, D. L. (1982). *Hydrologic modeling of small watersheds* American Society of Agricultural Engineers.

Hancock, G. R., Coulthard, T. J., & Willgoose, G. R. (2011). Modeling erosion and channel movement - response to rainfall variability in south east australia. *19th International Congress on Modelling and Simulation - Sustaining our Future: Understanding and Living with Uncertainty, MODSIM2011, December 12, 2011 - December 16,* 1874-1880.

Hanson, G. (1990). Surface erodibility of earthen channels at high stresses part I-open channel testing. *Transactions of the ASAE, 33*(1), 127-0131.

Hanson, G. J., Robinson, K. M., & Cook, K. R. (2001). Prediction of headcut migration using a deterministic approach. *Transactions of the American Society of Agricultural Engineers, 44*(3), 525-531.

Hargrove, W. L., Johnson, D., Snethen, D., & Middendorf, J. (2010). From dust bowl to mud bowl: Sedimentation, conservation measures, and the future of reservoirs. *Journal of Soil and Water Conservation, 65*(1), 14A-17A.

Hirschi, M. C., & Barfield, B. J. (1988). KYERMO—A physically based research erosion model part I. model development. *Transactions of the ASAE, 31*(3), 804-0813.

Huang, C., Gascuel-Odoux, C., & Cros-Cayot, S. (2002). Hillslope topographic and hydrologic effects on overland flow and erosion. *Catena, 46*(2), 177-188.

Huang, C., & Laften, J. M. (1996). Seepage and soil erosion for a clay loam soil. *Soil Science Society of America Journal, 60*(2), 408-416.

Huffman, R. L. (2013). *Soil and water conservation engineering* American Society of Agricultural and Biological Engineers.

ISCO. (2013). Teledyne ISCO. Lincoln, NE,USA. Retrieved from http://www.isco.com/

Istanbulluoglu, E. (2005). Implications of bank failures and fluvial erosion for gully development: Field observations and modeling. *Journal of Geophysical Research, 110*(F1), F01014. doi:10.1029/2004JF000145

Julian, J. P., & Torres, R. (2006). Hydraulic erosion of cohesive riverbanks. *Geomorphology, 76*(1), 193-206.

Kabiri-Samani, A., Farshi, F., & Chamani, M. R. (2012). Boundary shear stress in smooth trapezoidal open channel flows. *Journal of Hydraulic Engineering, 139*(2), 205-212.

Karimov, V., Sheshukov, A., & Barnes, P. (2014). In situ field study of ephemeral gully propagation in a cultivated cropland. *2014 Montreal, Quebec Canada July 13–July 16, 2014*, 1.

Karimov, V., Sheshukov, A., & Barnes, P. (2015). Impact of precipitation and runoff on ephemeral gully development in cultivated croplands. *Proceedings of the International Association of Hydrological Sciences, 367*, 87.

KDASC. (2013). Kansas data access and support center, topeka, kan., USA. Retrieved from http://www.kansasgis.org/

Khatua, K. K., & Patra, K. C. (2007). Boundary shear stress distribution in compound open channel flow. *ISH Journal of Hydraulic Engineering, 13*(3), 39-54.

Kheir, R., John Wilson, & Yongxin Deng. (2007). Use of terrain variables for mapping gully erosion susceptibility in lebanon. *Earth Surface Processes and Landforms, 32*(12), 1770-1782. doi:10.1002/esp.1501

Khodashenas, S. R., Abderrezzak, K. E. K., & Paquier, A. (2008). Boundary shear stress in open channel flow: A comparison among six methods. *Journal of Hydraulic Research, 46*(5), 598-609.

Kirkby, M. J., & L J Bracken. (2009). Gully processes and gully dynamics. *Earth Surface Processes and Landforms, 34*(14), 1841-1851. doi:10.1002/esp.1866

Kirkby, M. J., L J Bull, J Poesen, J Nachtergaele, & L Vandekerckhove. (2003). Observed and modelled distributions of channel and gully heads—with examples from SE spain and belgium. *Catena, 50*(2), 415-434. doi:10.1016/S0341-8162(02)00128-5

Knapen, A., & J Poesen. (2009). Soil erosion resistance effects on rill and gully initiation points and dimensions. *Earth Surface Processes and Landforms, 35*(2), 217. doi:10.1002/esp.1911

Knapen, A., J Poesen, G Govers, & S De Baets. (2008). The effect of conservation tillage on runoff erosivity and soil erodibility during concentrated flow. *Hydrological Processes, 22*(10), 1497-1508. doi:10.1002/hyp.6702

Knapen, A., J Poesen, & S Debaets. (2007). Seasonal variations in soil erosion resistance during concentrated flow for a loess-derived soil under two contrasting tillage practices. *Soil & Tillage Research, 94*(2), 425-440. doi:10.1016/j.still.2006.09.005

Knapen, A., T Smets, & J Poesen. (2009). Flow-retarding effects of vegetation and geotextiles on soil detachment during concentrated flow. *Hydrological Processes, 23*(17), 2427-2437. doi:10.1002/hyp.7360

Knapen, A., Poesen, J., Govers, G., Gyssels, G., & Nachtergaele, J. (2007). Resistance of soils to concentrated flow erosion: A review. *Earth-Science Reviews, 80*(1), 75-109.

Knight, D. W., Demetriou, J. D., & Hamed, M. E. (1984). Boundary shear in smooth rectangular channels. *Journal of Hydraulic Engineering, 110*(4), 405-422.

Lapidus, L. (1982). In Pinder G. F. (Ed.), *Numerical solution of partial differential equations in science and engineering*. New York: New York : Wiley.

Lee, G., & Kim, J. -. (2010). Comparative analysis of geomorphologic characteristics of DEM-based drainage networks. *Journal of Hydrologic Engineering, 16*(2), 137-147.

Licciardello, F. (2007). Runoff and soil erosion evaluation by the AnnAGNPS model in a small mediterranean watershed. *Transactions of the ASABE, 50*(5), 1585. doi:10.13031/2013.23972

Liu, X., & Chiew, Y. (2012). Effect of seepage on initiation of cohesionless sediment transport. *Acta Geophysica, 60*(6), 1778-1796.

Liu, X., & Chiew, Y. (2014). Effect of upward seepage on bedload transport rate. *Water Science and Engineering, 7*(2), 208-217.

Lobkovsky, A. E., Jensen, B., Kudrolli, A., & Rothman, D. H. (2004). Threshold phenomena in erosion driven by subsurface flow. *Journal of Geophysical Research: Earth Surface, 109*(F4)

Mathworks Inc. (Natick, 2014). *MATLAB: R2014a*

.

Merkel, W. H., Woodward, D. E., & Clarke, C. D. (1989). Method to predict cropland ephemeral gully erosion. *Sediment Transport Modeling: Proceedings of the International Symposium,* New Orleans, LA, USA. 356-361.

Meyer, A., & Martínez-Casasnovas, J. A. (1999). Prediction of existing gully erosion in vineyard parcels of the NE spain: A logistic modelling approach. *Soil and Tillage Research, 50*(3-4), 319-331. doi:10.1016/S0167-1987(99)00020-3

Mirás-Avalos, J. M., Paz-González, A., Dafonte-Dafonte, J., Vidal-Vázquez, E., & Valcárcel-Armesto, M. (2009). Concentrated flow erosion as a main source of sediments in galicia, spain. *Earth Surface Processes and Landforms, 34*(15), 2087-2095.

Momm, H. G., Bingner, R. L., Wells, R. R., Rigby, J. R., & Dabney, S. M. (2013). Effect of topographic characteristics on compound topographic index for identification of gully channel initiation locations. *Transactions of the ASABE, 56*(2), 523-537.

Momm, H. G., Wells, R. R., & Bingner, R. L. (2015). GIS technology for spatiotemporal measurements of gully channel width evolution. *Natural Hazards,* doi:10.1007/s11069-015-1615-z

Montgomery, D. R. (1994). Road surface drainage, channel initiation, and slope instability. *Water Resources Research, 30*(6), 1925-1932. doi:10.1029/94WR00538

Montgomery, D. R., & Dietrich, W. E. (1994). Landscape dissection and drainage area-slope thresholds. *Process Models and Theoretical Geomorphology*, , 221-246.

Moore, I. D., & Burch, G. J. (1986). MODELLING EROSION AND DEPOSITION: TOPOGRAPHIC EFFECTS. *Transactions of the American Society of Agricultural Engineers, 29*(6), 1624-1630.

Moore, I. D., Burch, G. J., & Mackenzie, D. H. (1988). TOPOGRAPHIC EFFECTS ON THE DISTRIBUTION OF SURFACE SOIL WATER AND THE LOCATION OF EPHEMERAL GULLIES. *Transactions of the American Society of Agricultural Engineers, 31*(4), 1098-1107.

Morgan, R. P. C., Quinton, J. N., Smith, R. E., Govers, G., Poesen, J. W. A., Auerswald, K., . . . Styczen, M. E. (1998). The European soil erosion model (EUROSEM): A dynamic approach for predicting sediment transport from fields and small catchments. *Earth Surface Processes and Landforms, 23*(6), 527-544. doi:10.1002/(SICI)1096-9837(199806)23:6<527::AID-ESP868>3.0.CO;2-5

Moriasi, D. N., Arnold, J. G., Van Liew, M. W., Bingner, R. L., Harmel, R. D., & Veith, T. L. (2007). Model evaluation guidelines for systematic quantification of accuracy in watershed simulations. *Trans.Asabe, 50*(3), 885-900.

Nachtergaele, J., & Poesen, J. (1999). Assessment of soil losses by ephemeral gully erosion using high-altitude (stereo) aerial photographs. *Earth Surface Processes and Landforms, 24*(8), 693-706. doi:10.1002/(SICI)1096-9837(199908)24:8<693::AID-ESP992>3.0.CO;2-7

Nachtergaele, J., & Poesen, J. (2002). Spatial and temporal variations in resistance of loess-derived soils to ephemeral gully erosion. *European Journal of Soil Science, 53*(3), 449-463. doi:10.1046/j.1365-2389.2002.00443.x

Nachtergaele, J., Poesen, J., Sidorchuk, A., & Torri, D. (2002). Prediction of concentrated flow width in ephemeral gully channels. *Hydrological Processes, 16*(10), 1935-1953. doi:10.1002/hyp.392

Nachtergaele, J Poesen, L Vandekerckhove, D Oostwoud Wijdenes, & M Roxo. (2001). Testing the ephemeral gully erosion model (EGEM) for two mediterranean environments. *Earth Surface Processes and Landforms, 26*(1), 17-30. doi:10.1002/1096-9837(200101)26:1<17::AID-ESP149>3.0.CO;2-7

Nachtergaele, Jeroen Poesen, A Steegen, I Takken, L Beuselinck, L Vandekerckhove, & G Govers. (2001). The value of a physically based model versus an empirical approach in the prediction of ephemeral gully erosion for loess-derived soils. *Geomorphology, 40*(3), 237-252. doi:10.1016/S0169-555X(01)00046-0

National Research Council. (1986). *Soil conservation: An assessment of the national resources inventory* National Academies Press.

NOAA-NCEI. (2016). Climate-radar data inventories. Retrieved from https://www.ncdc.noaa.gov/

Nouwakpo, S. K., & Huang, C. (2012). A fluidized bed technique for estimating soil critical shear stress. *Soil Science Society of America Journal, 76*(4), 1192-1196.

Nouwakpo, S., & Chi-hua Huang. (2012). A fluidized bed technique for estimating soil critical shear stress. *Soil Science Society of America Journal, 76*(4), 1192. doi:10.2136/sssaj2012.0056

Nouwakpo, S. K., Huang, C., Bowling, L., & Owens, P. (2010). Impact of vertical hydraulic gradient on rill erodibility and critical shear stress. *Soil Science Society of America Journal, 74*(6), 1914-1921.

Nouwakpo, S., Chi-hua Huang, Laura Bowling, & Phillip Owens. (2010). Impact of vertical hydraulic gradient on rill erodibility and critical shear stress. *Soil Science Society of America Journal, 74*(6), 1914. doi:10.2136/sssaj2009.0096

Onset. (2013). Onset HOBO dataloggers. bourne, mass., USA. Retrieved from http://www.onsetcomp.com/

Orlandini, S., Paolo Tarolli, Giovanni Moretti, & Giancarlo Dalla Fontana. (2011). On the prediction of channel heads in a complex alpine terrain using gridded elevation data. *Water Resources Research, 47*(2) doi:10.1029/2010WR009648

Osmond, D., Meals, D., Hoag, D., Arabi, M., Luloff, A., Jennings, G., . . . Line, D. (2012). Improving conservation practices programming to protect water quality in agricultural watersheds: Lessons learned from the national institute of food and Agriculture–Conservation effects assessment project. *Journal of Soil and Water Conservation, 67*(5), 122A-127A.

Owoputi, L., & Stolte, W. (2001). The role of seepage in erodibility. *Hydrological Processes, 15*(1), 13-22.

Partheniades, E. (1965). Erosion and deposition of cohesive soils. *Journal of the Hydraulics Division, 91*(1), 105-139.

Poesen, J., Nachtergaele, G., Verstraeten, C., & Valentin. (2003). Gully erosion and environmental change: Importance and research needs. *Catena, 50*(2), 91-133. doi:10.1016/S0341-8162(02)00143-1

Poesen, J., Torri, D., & Vanwalleghem, T. (2010). *Gully erosion: Procedures to adopt when modelling soil erosion in landscapes affected by gullying* John Wiley & Sons: Chichester, UK.

Pollock, C., & Reeder, R. (2010). No-till--plenty of positives. *Resource Magazine, 17*(1), 4-7.

Regazzoni, P., Marot, D., & Nguyen, H. H. (2010). Surface erosion: Erodibility characterisation and physical parameters effects. *Scour and erosion* (pp. 182-191)

Robinson, K. M., & Bennett, S. (2000). Processes of headcut growth and migration in rills and gullies. *International Journal of Sediment Research, 15*(1), 69-82.

Robinson, K. M. (2002). Scour below an overfall: Part I. investigation. *Transactions of the ASAE, 45*(4), 949. doi:10.13031/2013.9947

Robinson, K. M., & Hanson, G. J. (1994). Deterministic headcut advance model. *Transactions of the ASAE, 37*(5), 1437-1437.

Robinson, K. M., & Hanson, G. J. (1996). Gully headcut advance. *Transactions of the American Society of Agricultural Engineers, 39*(1), 33-38.

Rockwell, D. (2002). The influence of groundwater on surface flow erosion processes during a rainstorm. *Earth Surface Processes and Landforms, 27*(5), 495-514.

Rodzik, J., Tomasz Furtak, & Wojciech Zglobicki. (2009). The impact of snowmelt and heavy rainfall runoff on erosion rates in a gully system, lublin upland, poland. *Earth Surface Processes and Landforms, 34*(14), 1938-1950. doi:10.1002/esp.1882

Schaap, M. G., Leij, F. J., & Van Genuchten, M. T. (2001). ROSETTA: A computer program for estimating soil hydraulic parameters with hierarchical pedotransfer functions. *Journal of Hydrology, 251*(3), 163-176.

Sheshukov, A. Y., Daggupati, P., & Douglas-Mankin, K. R. (2011). High spatial resolution soil data for watershed modeling: 2. assessing impacts on watershed hydrologic response. *Journal of Natural and Environmental Sciences, 2*(2), 32-41.

Sheshukov, A. Y., Daggupati, P., Douglas-Mankin, K. R., & Lee, M. (2011). High spatial resolution soil data for watershed modeling: 1. development of a SSURGO-ArcSWAT utility. *Journal of Natural and Environmental Sciences, 2*(2), 15-24.

Sidorchuk, A., & Sidorchuk, A. (1998). Model for estimating gully morphology. *Modelling Soil Erosion, Sediment Transport and Closely Related Hydrological Processes, ,* 333-343.

Sidorchuk, A. (2006). Stages in gully evolution and self-organized criticality. *Earth Surface Processes and Landforms, 31*(11), 1329-1344. doi:10.1002/esp.1334

Simon, A., Curini, A., Darby, S. E., & Langendoen, E. J. (2000). Bank and near-bank processes in an incised channel. *Geomorphology, 35*(3), 193-217.

Soane, B. D., Ball, J., Arvidsson, G., Basch, F., & Moreno, J. (2012). No-till in northern, western and south-western europe: A review of problems and opportunities for crop production and the environment. *Soil & Tillage Research, 118,* 66-87. doi:10.1016/j.still.2011.10.015

Soil Science Society of America. (2008). *Glossary of soil science terms 2008* ASA-CSSA-SSSA.

Souchère, V., Cerdan, O., Ludwig, B., Le Bissonnais, Y., Couturier, A., & Papy, F. (2003). Modelling ephemeral gully erosion in small cultivated catchments. *Catena, 50*(2–4), 489-505. doi:10.1016/S0341-8162(02)00124-8

Stein, O. R., & P Y Julien. (1993). Criterion delineating the mode of headcut migration. *Journal of Hydraulic Engineering, 119*(1), 37-50. doi:10.1061/(ASCE)0733-9429(1993)119:1(37)

Stolte, J., B Liu, C J Ritsema, H.G.M. van den Elsen, & R.Hessel. (2003). Modelling water flow and sediment processes in a small gully system on the loess plateau in china. *Catena, 54*(1), 117-130. doi:10.1016/S0341-8162(03)00060-2

Storm, D., Barfield, B., & Ormsbee, L. (1990). Hydrology and sedimentology of dynamic rill networks. volume I: Erosion model for dynamic rill networks, part A-introduction and overview, part B- erosion model development. *Available from National Technical Information Service, Springfield, VA 22161 as PB91-125351/AS.Price Codes: A07 in Paper Copy, A07 in Microfiche.Kentucky Water Resources Research Institute, Lexington, Research Report no.178, August 1990.121p, 29(TRUNCATED),* (178)

Svoray, T., & Markovitch, H. (2009). Catchment scale analysis of the effect of topography, tillage direction and unpaved roads on ephemeral gully incision. *Earth Surface Processes and Landforms, 34*(14), 1970-1984.

Taguas, E. V., Y Yuan, R L Bingner, & J A Gómez. (2012). Modeling the contribution of ephemeral gully erosion under different soil managements: A case study in an olive orchard microcatchment using the AnnAGNPS model. *Catena, 98*, 1-16. doi:10.1016/j.catena.2012.06.002

Taguas, E., Guzmán, E., Guzmán, G., Vanwalleghem, T., & Gómez, J. (2015). Characteristics and importance of rill and gully erosion: a case study in a small catchment of marginal olive grove. *Cuadernos De Investigación Geográfica, 41*(1)

Teasdale, G. N., & Barber, M. E. (2008). Aerial assessment of ephemeral gully erosion from agricultural regions in the pacific northwest. *Journal of Irrigation and Drainage Engineering, 134*(6), 807-814.

Tebebu, T. Y., Abiy, A. Z., Zegeye, A. D., Dahlke, H. E., Easton, Z. M., Tilahun, S. A., . . . Steenhuis, T. S. (2010). Surface and subsurface flow effect on permanent gully formation and upland erosion near lake tana in the northern highlands of ethiopia. *Hydrology and Earth System Sciences, 14*(11), 2207-2217.

Tekwa, I. J., Kundiri, A. M., & Chiroma, A. M. (2016). Efficiency test of modeled empirical equations in predicting soil loss from ephemeral gully erosion around mubi, northeast nigeria. *International Soil and Water Conservation Research, 4*(1), 12-19. doi:10.1016/j.iswcr.2016.02.002

Thomas, A. W., & Welch, R. (1988). Measurement of ephemeral gully erosion. *Transactions of the American Society of Agricultural Engineers, 31*(6), 1723-1728.

Thorne, C. R., Grissinger, E. H., & Murphey, J. B. (1984). Field study of ephemeral cropland gullies in northern mississippi. *1984 Winter Meeting - American Society of Agricultural*

*Engineers: Engineering the Future - Capitalizing on the New Technologies.* New Orleans, LA, USA.

USDA-NRCS. (2005). Soil survey geographic (SSURGO) database. USDA natural resources conservation service, washington, D.C. Retrieved from http://soildatamart.nrcs.usda.gov/default.aspx

Valcárcel, M., Taboada, M. T., Paz, A., & Dafonte, J. (2003). Ephemeral gully erosion in northwestern spain. *Catena, 50*(2–4), 199-216. doi:10.1016/S0341-8162(02)00139-X

Valentin, C., Poesen, J., & Li, Y. (2005). Gully erosion: Impacts, factors and control. *Catena, 63*(2–3), 132-153. doi:10.1016/j.catena.2005.06.001

Van Genuchten, M. T. (1980). A closed-form equation for predicting the hydraulic conductivity of unsaturated soils. *Soil Science Society of America Journal, 44*(5), 892-898.

Vanapalli, S., Fredlund, D., Pufahl, D., & Clifton, A. (1996). Model for the prediction of shear strength with respect to soil suction. *Canadian Geotechnical Journal, 33*(3), 379-392.

Vandaele, K., Poesen, J., Govers, G., & Van Wesemael, B. (1996). Geomorphic threshold conditions for ephemeral gully incision. *Geomorphology, 16*(2), 161-173. doi:10.1016/0169-555X(95)00141-Q

Vandekerckhove, L., Poesen, J., Oostwoud Wijdenes, D., & De Figueiredo, T. (1998). Topographical thresholds for ephemeral gully initiation in intensively cultivated areas of the mediterranean. *Catena, 33*(3-4), 271-292. doi:10.1016/S0341-8162(98)00068-X

Vandekerckhove, L., Poesen, J., Wijdenes, D. O., Nachtergaele, J., Kosmas, C., Roxo, M. J., & De Figueiredo, T. (2000). Thresholds for gully initiation and sedimentation in mediterranean europe. *Earth Surface Processes and Landforms, 25*(11), 1201-1220. doi:10.1002/1096-9837(200010)25:11<1201::AID-ESP131>3.0.CO;2-L

Vanwalleghem, T., Giráldez, J. V., Jiménez-Hornero, F. J., & Laguna, A. (2009). Evaluating a general sediment transport model for linear incisions under field conditions. *Earth Surface Processes and Landforms, 34*(14), 1852-1857.

Wells, R. R., Momm, H. G., Rigby, J. R., Bennett, S. J., Bingner, R. L., & Dabney, S. M. (2013). An empirical investigation of gully widening rates in upland concentrated flows. *Catena, 101*, 114-121.

Wells, R., Carlos Alonso, & Sean Bennett. (2009). Morphodynamics of headcut development and soil erosion in upland concentrated flows. *Soil Science Society of America Journal, 73*(2), 521. doi:10.2136/sssaj2008.0007

Wells, R., Henrique Momm, James Rigby, Sean Bennett, Ronald Bingner, & Seth Dabney. (2013). An empirical investigation of gully widening rates in upland concentrated flows. *Catena, 101*, 114-121. doi:10.1016/j.catena.2012.10.004

Wells, R., Sean Bennett, & Carlos Alonso. (2009). Effect of soil texture, tailwater height, and pore-water pressure on the morphodynamics of migrating headcuts in upland concentrated flows. *Earth Surface Processes and Landforms, 34*(14), 1867-1877. doi:10.1002/esp.1871

Wells, R. R., Momm, H. G., & Castillo, C. (2017). Quantifying uncertainty in high-resolution remotely sensed topographic surveys for ephemeral gully channel monitoring. *Earth Surface Dynamics, 5*, 347-367. doi:10.5194/esurf-5-347-2017

Wilson, B. (1993a). Development of a fundamentally based detachment model. *Transactions of the ASAE, 36*(4), 1105-1114.

Wilson, B. (1993b). Evaluation of a fundamentally based detachment model. *Transactions of the ASAE, 36*(4), 1115-1122.

Wilson, B. N., & Barfield, B. J. (1986). A detachment model for non-cohesive sediment. *Transactions of the ASAE, 29*(2), 445-0449.

Wilson, G. V., R F Cullum, & M.J.M.Römkens. (2008). Ephemeral gully erosion by preferential flow through a discontinuous soil-pipe. *Catena, 73*(1), 98-106. doi:10.1016/j.catena.2007.09.008

Wilson, G. V. W. (2009). Mechanisms of ephemeral gully erosion caused by constant flow through a continuous soil-pipe. *Earth Surface Processes and Landforms, 34*(14), 1858-1866. doi:10.1002/esp.1869

Wilson, G. (2011). Understanding soil-pipe flow and its role in ephemeral gully erosion. *Hydrological Processes, 25*(15), 2354-2364. doi:10.1002/hyp.7998

Wu, Y., Qiuhong Zheng, Yongguang Zhang, Baoyuan Liu, Hong Cheng, & Yanzai Wang. (2008). Development of gullies and sediment production in the black soil region of northeastern china. *Geomorphology, 101*(4), 683-691. doi:10.1016/j.geomorph.2008.03.008

Yan, L. J., X X Yu, T W Lei, Q W Zhang, & L Q Qu. (2008). Effects of transport capacity and erodibility on rill erosion processes: A model study using the finite element method. *Geoderma, 146*(1), 114-120. doi:10.1016/j.geoderma.2008.05.009

Yi, L., Zhang, W., & Yan, C. (2017). A modified topographic index that incorporates the hydraulic and physical properties of soil. *Hydrology Research, 48*(2), 370-383.

Zhang, Y., Youngqiu Wu, Baoyuan Liu, Qiuhong Zheng, & Jiayi Yin. (2007). Characteristics and factors controlling the development of ephemeral gullies in cultivated catchments of black soil region, northeast china. *Soil & Tillage Research, 96*(1), 28-41. doi:10.1016/j.still.2007.02.010

Zhang, Q., Dong, Y., Li, F., Zhang, A., & Lei, T. (2014). Quantifying detachment rate of eroding rill or ephemeral gully for WEPP with flume experiments. *Journal of Hydrology, 519*, 2012-2019. doi:10.1016/j.jhydrol.2014.09.040